

Material characterization of poly (vinylidene fluoride) : a thin film piezoelectric polymer
by Frank Conly Holloway

A thesis submitted in partial fulfillment of the requirements for the degree Of Master of Science in Mechanical Engineering
Montana State University
© Copyright by Frank Conly Holloway (1997)

Abstract:
Material properties of polyvinylidene fluoride are determined. It is shown that these properties are anisotropic and time dependent. The instantaneous elastic properties are found and compared to published results. A model describing the time dependent behavior of the material is then developed. It is shown that the theory of viscoelasticity can successfully accomplish this task, and the parameters describing this theory in the separate material directions are determined from dynamic mechanical testing and analysis. The results of these tests are then compared to results obtained from traditional creep tests. The piezoelectric coupling properties are also examined. It is shown that these coefficients are independent of studied parameters within measured ranges. The values of these coefficients are determined and compared to published results.

MATERIAL CHARACTERIZATION OF POLY(VINYLIDENE FLUORIDE): A THIN FILM PIEZOELECTRIC POLYMER

by

Frank Conly Holloway

A thesis submitted in partial fulfillment
of the requirements for the degree

of

Master of Science

in

Mechanical Engineering

MONTANA STATE UNIVERSITY-BOZEMAN
Bozeman, Montana

April 1997

N378
H72854

APPROVAL

of a thesis submitted by

Frank Conly Holloway

This thesis has been read by each member of the thesis committee and has been found to be satisfactory regarding content, English usage, format, citations, bibliographic style, and consistency, and is ready for submission to the College of Graduate Studies.

Aleksandra Vinogradov _____ (Signature) 4/17/97 Date

Approved for the Department of Mechanical and Industrial Engineering

Vic Cundy _____ (Signature) 4/17/97 Date

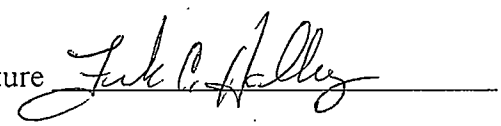
Approved for the College of Graduate Studies

Robert Brown _____ (Signature) 4/18/97 Date

STATEMENT OF PERMISSION TO USE

In presenting this thesis in partial fulfillment of the requirements for a master's degree at Montana State University - Bozeman, I agree that the Library shall make it available to borrowers under rules of the Library.

If I have indicated my intention to copyright this thesis by including a copyright notice page, copying is allowable only for scholarly purposes, consistent with "fair use" as prescribed in the U.S. Copyright Law. Requests for permission for extended quotation from or reproduction of this thesis in whole or in parts may be granted only by the copyright holder.

Signature 

Date 17 APRIL 97

TABLE OF CONTENTS

Page

1. INTRODUCTION 1

2. MICROSTRUCTURE AND PHYSICAL PROPERTIES OF PVDF 5

3. THEORETICAL BACKGROUND AND APPROACHES TO MATERIAL MODELING . 10

Piezoelectricity 10
Time Dependent Effects 15
Experimental Techniques 19

4. EXPERIMENTAL PROGRAM. 25

Main Objectives 25
Experimental Stages. 25
Stage 1 25
Stage 2 26
Stage 3 26
Stage 4 26

5. INSTANTANEOUS ELASTIC RESPONSE. 27

Parameters Considered. 27
Testing Apparatus 27
Set of Experiments 28
Results 29

6. SIGNIFICANCE OF TIME DEPENDENT EFFECTS 33

Parameters Considered. 33
Testing Apparatus 34
Set of Experiments 35
Results 36

7. VISCOELASTIC CONSTITUTIVE MODELING BASED ON DMTA 40

Parameters Considered. 40
Testing Apparatus 41
Set of Experiments 46
Data Reduction 49
Linear Results for Direction 1 53
Linear Results for Direction 2 58
Nonlinear Results for Direction 1 63

TABLE OF CONTENTS - Continued

Page

8. PIEZOELECTRIC STRAIN COEFFICIENTS 67

Parameters Considered 67
Testing Apparatus 67
Set of Experiments 68
Data Reduction 70
Results 72

9. DISCUSSION AND CONCLUSIONS 78

Instantaneous Elastic Properties 78
Significance of Time Dependent Effects 79
Viscoelastic Constitutive Modeling Based on DMTA 80
Piezoelectric Strain Coefficients 81
Future Work 82

REFERENCES 83

APPENDICES 85

Appendix A – Data Reduction Programs 86
Appendix B – Representative Set of Viscoelastic Function Plots 96
Appendix C – Curve Fit Results 105
Appendix D – Representative Set of Produced Voltage Plots 118

LIST OF TABLES

Table Page

2-1 Physical properties of 28 μm PVDF films 9

7-1 Test matrix for determination of viscoelastic properties form DMTA . . . 47

8-1 Test matrix for determination of piezoelectric strain coefficient properties. 69

9-1 Summary of instantaneous elastic properties of PVDF 79

9-2 Summary of results of viscoelastic characterization at room temperature. . 80

LIST OF FIGURES

Figure		Page
1-1	PVDF double bimorph actuator	2
2-1	Molecular structure of PVDF polymer before poling	6
2-2	Molecular structure of PVDF polymer after poling	7
2-3	Orientation of lamellae and dipole alignment after stretching and poling	8
3-1	Material coordinate axis	13
5-1	Stress-strain curve for material direction 1	29
5-2	Exploded view of stress-strain curve for material direction 1	30
5-3	Stress-strain curves for material direction 2	31
5-4	Exploded view of stress-strain curves for material direction 2	32
6-1	Adjustable thin film grips	34
6-2	Creep curves for tests conducted in the 1 direction	37
6-3	Normalized creep curves conducted in the 1 direction	37
6-4	Creep curves for tests conducted in the 2 direction	38
6-5	Normalized creep curves conducted in the 2 direction	39
7-1	Testing apparatus support frame	41
7-2	Photograph of experimental setup	43
7-3	Flow chart of experimental setup	44
7-4	Data reduction program flowchart	50
7-5	Complex modulus components in the 1 direction	54
7-6	Surface fit of storage modulus in the 1 direction	55
7-7	Master storage compliance curve in the 1 direction	56
7-8	Temperature dependent shift factor for the 1 direction	56
7-9	Master loss compliance curve in the 1 direction	57

LIST OF FIGURES - Continued

Figure Page

7-10 DMTA predicted creep compared with traditional creep measurements . . 58
7-11 Complex modulus components in the 2 direction.. 59
7-12 Surface fit of storage modulus in the 2 direction 60
7-13 Master storage compliance curve in the 2 direction 60
7-14 Temperature dependent shift factor for the 2 direction 61
7-15 Master loss compliance curve in the 2 direction 62
7-16 DMTA predicted creep compared with traditional creep measurements . . 63
7-17 Stress dependent shift factor for direction 1. 64
7-18 Comparison of linear and nonlinear DMTA results with creep tests 66
8-1 Sample produced voltage measuring circuit 71
8-2 Voltage produced from tests conducted in the 1 direction 74
8-3 Voltage produced from tests conducted in the 2 direction 74
8-4 Normalized voltage for various temperatures in the 1 direction 75
8-5 Average voltage for various pre-stress values in the 1 direction. 76
8-6 Voltage for various time values in the 1 direction 77
A-1 Program #1. 87
A-2 Program #2. 90
A-3 Program #3. 94
B-1 To B-8 Two of the complex functions in the 2 direction for the conditions shown. 97
C-1 Master storage compliance curve for material direction 1. 106
C-2 Master storage compliance curve for material direction 2. 107
C-3 Master loss compliance curve for material direction 1. 108

LIST OF FIGURES - Continued

Figure Page

C-4 Master loss compliance curve for material direction 2. 109

C-5 Master storage modulus curve for material direction 1. 110

C-6 Master storage modulus curve for material direction 2. 111

C-7 Master loss modulus curve for material direction 1. 112

C-8 Master loss modulus curve for material direction 2. 113

C-9 Creep compliance curve for material direction 1 114

C-10 Creep compliance curve for material direction 2 115

C-11 Relaxation modulus curve for material direction 1. 116

C-12 Relaxation modulus curve for material direction 2. 117

D-1 To D-8 Produced voltage during DMTA testing in the 2 direction for the conditions shown 119

NOMENCLATURE

Symbol	Description	Units
σ	Stress	Nm^{-2}
σ^{o}	Maximum stress amplitude	Nm^{-2}
σ_Y	Yield stress	Nm^{-2}
σ_U	Ultimate stress	Nm^{-2}
Y	Young's modulus	Nm^{-2}
ε	Strain	mm^{-1}
ε^{o}	Maximum strain amplitude	mm^{-1}
ε_Y	Yield strain	mm^{-1}
ε_U	Ultimate strain	mm^{-1}
η	Viscosity of dashpot	Pa sec
T_o	Reference temperature	C
a_T	Temperature dependent shift factor	
D(t)	Creep compliance	Pa^{-1}
$D'(\omega)$	Extension storage compliance	Pa^{-1}
$D''(\omega)$	Extension loss compliance	Pa^{-1}
$D^{*}(\omega)$	Extension complex compliance	Pa^{-1}
E(t)	Relaxation modulus	Pa
$E'(\omega)$	Extension storage modulus	Pa

NOMENCLATURE- Continued

Symbol	Description	Units
$E''(\omega)$	Extension loss modulus	Pa
$E^*(\omega)$	Extension complex modulus	Pa
δ	Phase angle between stress and strain	Degrees
$\Delta(t)$	Unit step function	
$\overline{D}$	Electric flux density	Cm^{-2}
e	Dielectric constant	Fm^{-1}
$\overline{E}$	Electric Field	Vm^{-1}
d	Piezoelectric coefficient	CN^{-1}
s	Elastic compliance coefficient	m^2N^{-1}
G	Shear modulus	m^2N^{-1}
ν	Poisson's ratio	
V_{act}	Actual voltage produced by sample	V
V_{osc}	Measured voltage produced by sample	V
$\overline{E}^{\circ}$	Maximum electric field amplitude	Vm^{-1}
ϕ	Phase angle between E_{act} and strain	degrees
z	Thickness	m

ABSTRACT

Material properties of polyvinylidene fluoride are determined. It is shown that these properties are anisotropic and time dependent. The instantaneous elastic properties are found and compared to published results. A model describing the time dependent behavior of the material is then developed. It is shown that the theory of viscoelasticity can successfully accomplish this task, and the parameters describing this theory in the separate material directions are determined from dynamic mechanical testing and analysis. The results of these tests are then compared to results obtained from traditional creep tests. The piezoelectric coupling properties are also examined. It is shown that these coefficients are independent of studied parameters within measured ranges. The values of these coefficients are determined and compared to published results.

CHAPTER 1

INTRODUCTION

The development of an active vibration suppression system specifically targeted for vibration control for experimental payloads aboard space vehicles has been underway at Montana State University since 1994. The project aims at using a low force, high displacement actuators in conjunction with sensors and control circuitry to minimize 3-D vibration accelerations from spacecraft mechanisms that can adversely affect sensitive experimental payloads.

Contributions to the project have been made by more than 16 individuals from both the physics and mechanical engineering departments. The efforts made toward this end can be divided into four main areas consisting of actuator design and development, feedback system analysis and optimization, accelerometer development, and electro-mechanical characterization.

The first area, actuator design and development, has focused on producing a low force, high displacement actuator capable of providing precise position control for the payload. The actuators have been constructed of piezoelectric polyvinylidene fluoride (PVDF or PVF_2) thin films (28μm thick) in a bellows configuration, as shown in Figure 1-1. This design has utilized two piezoelectric bimorphs glued together, creating the final form. Strategic application of electric fields to the electrodes of the bimorphs results in

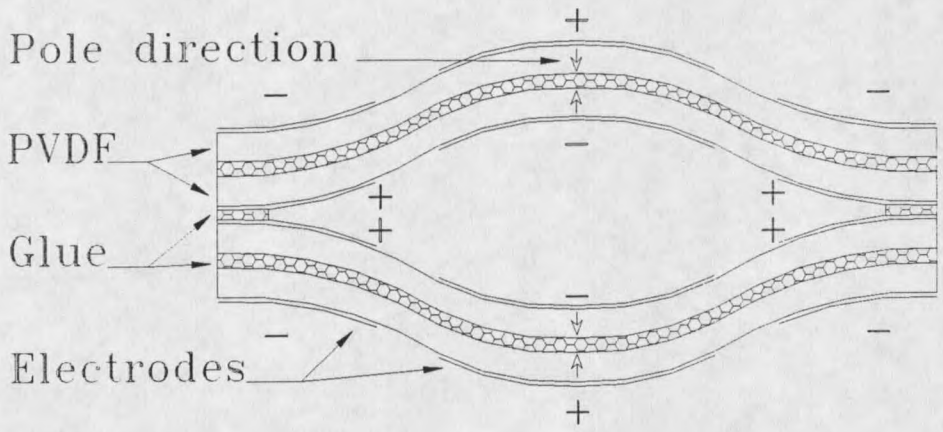


Figure 1-1. PVDF double bimorph actuator.

vertical displacement of the actuator in a known direction. Current actuator designs use voltages near 1000V and achieve vertical displacements of 1-3 mm over a range of frequencies from 0 to 25 Hz.

The next two areas of design effort focus on the electronic control of the actuators using feedback and feedforward signals from sensors. The control circuitry uses information from sensors perceiving the motion of the space vehicle and the payload as well as knowledge of actuator characteristics to produce an output signal which would then be used to control the actuators. Optimization of this system involves minimizing accelerations without allowing the payload to contact the walls of the payload enclosure. The objective thus involves providing minimal payload movement while ensuring that the payload properly "tracks" the space vehicle.

Design and development of both the actuator and the control system depends heavily on precise knowledge of the actuator's electro-mechanical properties. Without accurate description of the material response to a given set of conditions, the control system would be incapable of providing the corrective steps necessary to minimize accelerations. Also, the mechanical properties are critical in terms of describing the passive vibration response of the actuator. In addition, material properties are required to predict the usable conditions for the actuators, such as the operating temperature, load, and frequency range. Material characterization could also lead to future improvements of the actuator by tailoring it's design to the specific strengths of the material. For these reasons, the material properties of PVDF are necessary for the effective design of active control devices. The accurate characterization of these properties is the subject of this thesis.

Chapter 2 of this thesis provides a background into PVDF. This includes a description of the manufacturing processes that affects the microstructural form of the material. This is necessary for understanding the methodology behind the experimental program. Also, the known physical properties of PVDF are listed and discussed.

The third chapter contains a theoretical background of the constitutive laws describing the phenomena of piezoelectricity. A background is also given for the theory of viscoelasticity, which will be used to model the time dependent effects of the mechanical material response. The basis of an experimental technique developed to characterize these effects will then be given as a special case of this theory.

The fourth chapter describes the objectives and the components of the experimental program dedicated to determining the mechanical and electro-mechanical coupling properties of PVDF. Each of the separate tests conducted will be considered individually in chapters 5 to 8. This includes a list of the parameters that each test is aimed at characterizing, a description of each experimental setup, and the data reduction steps, and the results of the experiment.

Chapter 5 describes the testing methods used to determine the instantaneous elastic properties of PVDF. The sixth chapter outlines the tests aimed at determining the significance of time dependent effects on the mechanical response of the material. The characterization of the viscoelastic functions describing this time dependence from dynamic mechanical testing and analysis is described in chapter 7. The eighth chapter then illustrates the testing techniques used to determine the properties of the piezoelectric strain coefficients.

The final chapter is dedicated to a discussion of the experimental results and the conclusions that can be drawn from them.

CHAPTER 2

MICROSTRUCTURE AND PHYSICAL PROPERTIES OF PVDF

The material being characterized in this study is polyvinylidene fluoride (PVDF or PVF_2). The strong piezoelectric effect in PVDF was discovered in 1969 by Kawai [1]. Piezoelectric materials are those which exhibit a linear coupling between strain and electric field. Electric polarization of a material subjected to mechanical stress is known as the direct piezoelectric effect. Conversely, the straining of a material produced under the presence of an electric field is known as the converse piezoelectric effect. Some other materials that exhibit these characteristics include crystals such as $LiNbO_3$ and $LiTaO_3$, ceramics such as $BaTiO_3$, and polymers like PVF.

The piezoelectric response found in PVDF and its copolymers are among the largest of all polymers known [2]. This, combined with other beneficial characteristics of PVDF, such as its ease of shaping, low density, mechanical strength and flexibility, wide frequency response, high stability, and its availability in large dimensions at a relatively low cost, has generated considerable interest in the material. PVDF has been used in an ever increasing range of applications, including microphones, ultrasonic transducers, and strain gages [3].

PVDF is a semicrystalline polymer, $(-CH_2-CF_2-)_n$ as shown in Figure 2-1, that has crystallinity of 40-50%. From melt temperatures, PVDF forms lamellar crystals embedded

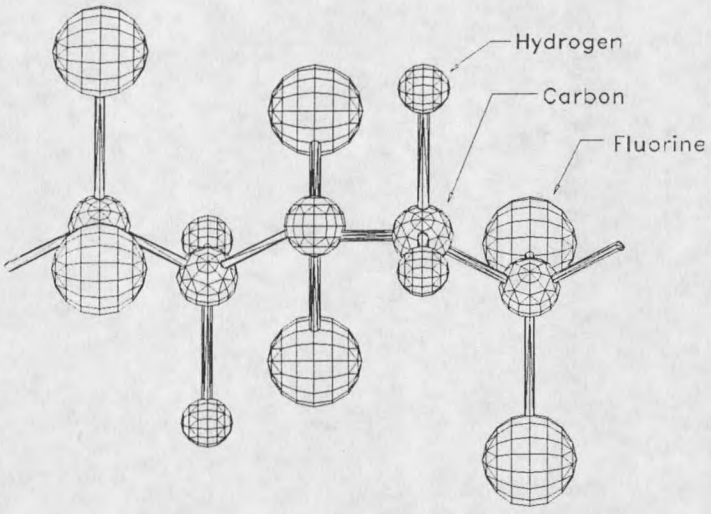


Figure 2-1. Molecular structure of PVDF polymer before poling.

in an amorphous background. The amorphous phase exhibits the behavior of a supercooled liquid having a liquid-glass transition at about -50 °C [1]. The polymer molecules are known to form four possible crystal structures termed α, α_p, β, and γ phases. The piezoelectric properties are believed to be mainly attributable to the β and α_p phases [1]. These crystal structures form from melt into spherulitic structures composed of crystalline lamella radiating from the center. These lamellae are made up of molecular chains that fold back upon themselves many times to form surfaces normal to the radii of the spherulites [4].

Because the hydrogen atoms are positively charged and the fluorine atoms are negatively charged with respect to the carbon atoms, PVDF is inherently polar. However, the molecular chains pack to form a polar cell in only two of the four possible crystal phases, β and α_p. These two forms therefore result in crystal lamellae that can have a net polarization. However, even the presence of polar crystallites does not yield

piezoelectricity in PVDF. This is due to the fact that the net polar moment of a region of the material is zero because of the random orientation of the individual crystallites [2]. For this reason, extruded sheets of PVDF are stretched and poled, thereby altering the molecular structure. Stretching serves to break up the spherulitic structures and orient the individual lamella so that the molecular axes are parallel to the stretch direction [2]. Poling of the stretched sheets is then achieved by holding them at temperatures above the glass transition so that the molecules are free to rotate as shown in Figure 2-2. In this process, PVDF is typically held at 130°C for up to 2 hours under an electric field of up to 100 kV mm^{-1} [5]. This field causes a rotation of molecular segments within the individual lamellae, thereby causing a net polarization. The material is then cooled to room temperature while maintaining the electric field, which permanently aligns the molecular dipoles thus giving the film piezoelectric properties. The orientation of the crystal

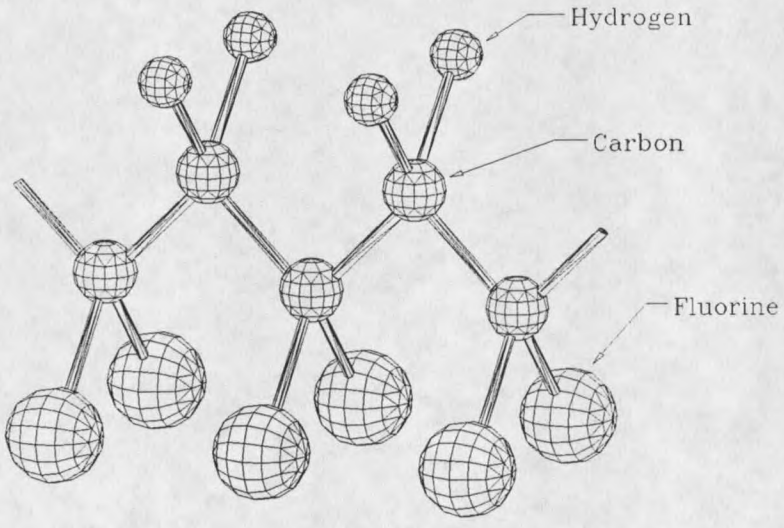


Figure 2-2. Molecular structure of PVDF polymer after poling.

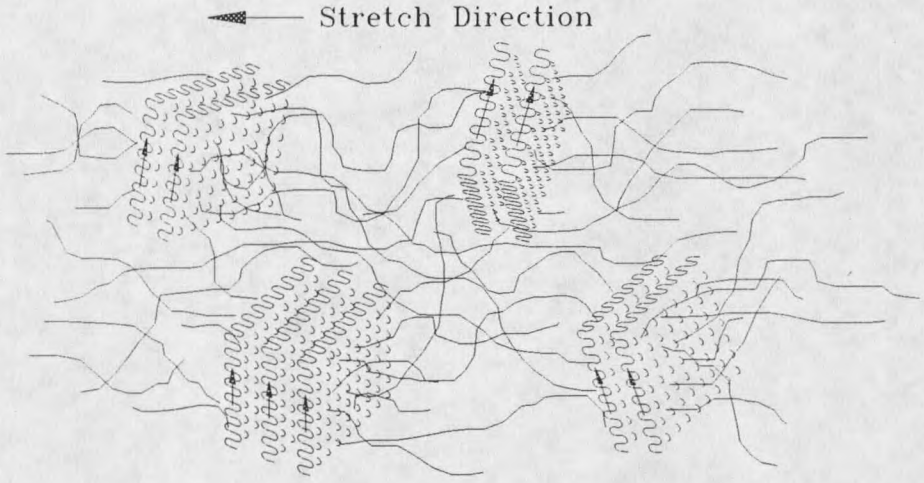


Figure 2-3. Orientation of lamellae and dipole alignment after stretching and poling. Polarization of lamellar crystal shown by arrows.

lamellae and the pole directions for stretched and poled PVDF is shown in Figure 2-3. This form, produced by the stretching and poling of PVDF thin sheets, exhibits the strong piezoelectric effect that makes the material particularly useful for sensor and actuator designs.

Many of the physical properties of stretched and poled PVDF have been provided by the manufacturer of the material currently being used for actuator development [3]. These properties are listed in Table 2-1. These values were all obtained from [3], with the exception of the Young's moduli and the mechanical loss tangent, which were obtained from [4]. These Young's moduli and mechanical loss tangent values were measured using a Rheovibron mechanical spectrometer and are believed to be more accurate than the values provided by AMP.

Table 2-1. Physical properties of 28 μm PVDF films.

Property	Symbol	Value	Units
Density	ρ	1.78×10^3	kg/m^3
Relative Permittivity	e/e_o	12-13	
Speed of Sound	v_1 v_3	1.5×10^3 2.2×10^3	m/s m/s
Capacitance	C	380	pF/cm^2 @ 1 kHz
Volume Resistivity	ρ_e	$>10^{13}$	Ωm
Temperature Range	T_{max} to T_{min}	80 to -40	°C
Maximum Operating Voltage	V_{max}	30	V/μm, DC @ 25°C
Breakdown Voltage	V_{BD}	80	V/μm, DC @ 25°C
Piezoelectric Strain Constant	d_{31} d_{32} d_{33}	23×10^{-12} 3×10^{-12} -33×10^{-12}	$(C/m^2)/(N/m^2)$ $(C/m^2)/(N/m^2)$ $(C/m^2)/(N/m^2)$
Electromechanical Coupling Factor	k_{31}	10	% @ 100 Hz
Young's Modulus	Y_{11} Y_{22}	2.56×10^9 2.61×10^9	Pa Pa
Mechanical Loss Tangent	tan(δ)	0.011	

CHAPTER 3

THEORETICAL BACKGROUND AND APPRACHES TO MATERIAL MODELING

Piezoelectricity

Although the properties of various piezoelectric materials have been studied in a number of publications [1,2,4,6], the origin of the piezoelectric phenomenon in polymers has not been completely identified [2]. A number of early models were developed to describe the piezoelectric behavior in some polymers. Most of these models are based on the presence of a dipole polarization in the crystalline regions embedded in amorphous material. These models, however, were able to account for only a portion of the observed effects, and were fragmentary and inconclusive [4]. This led to the development of more complex models that also incorporated the effects of trapped charges. Current models further take into account different thermal expansion coefficients and compressibilities for the crystalline and amorphous phases of piezoelectric polymers. Thus, a change in the thickness of a sample will cause a change in the electrode charge, or vice versa. These models can account for most of the observed piezoelectric activity, but are still considered to be incomplete [1].

It is clearly understood, however, that certain crystals that lack a center of

symmetry produce an electrical charge when mechanically deformed due to an induced dipole moment. This is caused by the non-symmetrical displacement of the centers of gravity of the positive and negative charges. Alternately, these materials develop a mechanical strain in the presence of an external field caused by a displacement of charges from electrostatic attraction or repulsion [2]. Typically, the mathematical description of this phenomenon consists of an interaction between a mechanical system in terms of stress and strain tensors, described by Hook's law, and an electrical system in terms of a linear relation between the electric flux density, electric field, and dielectric tensors.

The coupled system, in which there is energy conversion from the mechanical system to the electrical system (direct piezoelectric effect) or from the electrical system to the mechanical system (converse effect), is described by [7]

$$\varepsilon_{ij} = s_{ijkl}^{E}\sigma_{kl} + d_{mij}\overline{E}_{m} \tag{3-1}$$

$$\overline{D}_{n} = d_{nkl}\sigma_{kl} + e_{nm}^{\sigma}\overline{E}_{m} \tag{3-2}$$

where ε is strain (m/m), s^E is the elastic compliance coefficient under constant electric field (m^2N^{-1}) , σ is stress (Nm^{-2}), d is a piezoelectric coefficient (CN^{-1}), $\overline{D}$ is the electric flux density (Cm^{-2}), $\overline{E}$ is electric field (Vm^{-1}), and e^{σ} is the dielectric constant under constant stress (Fm^{-1}). The bars over the E and D variables are used in order to avoid confusion of these terms with the creep compliance and the relaxation modulus, introduced later. The d of Equation 3-1 represents strain per unit electric field and the d of Equation 3-2 represents electric flux density per unit electric field. The equality of these coefficients can be determined from conservation of energy [2].

The double index notations in Equations 3-1 and 3-2 are usually replaced by single

index notations such that

$$11 \rightarrow 1 \qquad 22 \rightarrow 2 \qquad 33 \rightarrow 3 \qquad 23 \rightarrow 4 \qquad 31 \rightarrow 5 \qquad 12 \rightarrow 6 \tag{3-3}$$

Respectively, Equations 3-1 and 3-2 in expanded for can be represented as

$$\begin{pmatrix} \varepsilon_1 \\ \varepsilon_2 \\ \varepsilon_3 \\ \varepsilon_4 \\ \varepsilon_5 \\ \varepsilon_6 \end{pmatrix} = \begin{bmatrix} s_{11} & s_{12} & s_{13} & s_{14} & s_{15} & s_{16} \\ s_{12} & s_{22} & s_{23} & s_{24} & s_{25} & s_{26} \\ s_{13} & s_{23} & s_{33} & s_{34} & s_{35} & s_{36} \\ s_{14} & s_{24} & s_{34} & s_{44} & s_{45} & s_{46} \\ s_{15} & s_{25} & s_{35} & s_{45} & s_{55} & s_{56} \\ s_{16} & s_{26} & s_{36} & s_{46} & s_{56} & s_{66} \end{bmatrix} \begin{bmatrix} \sigma_1 \\ \sigma_2 \\ \sigma_3 \\ \sigma_4 \\ \sigma_5 \\ \sigma_6 \end{bmatrix} + \begin{bmatrix} d_{11} & d_{21} & d_{31} \\ d_{12} & d_{22} & d_{32} \\ d_{13} & d_{23} & d_{33} \\ d_{14} & d_{24} & d_{34} \\ d_{15} & d_{25} & d_{35} \\ d_{16} & d_{26} & d_{36} \end{bmatrix} \begin{pmatrix} \overline{E}_1 \\ \overline{E}_2 \\ \overline{E}_3 \end{pmatrix} \tag{3-4}$$

$$\begin{pmatrix} \overline{D}_1 \\ \overline{D}_2 \\ \overline{D}_3 \end{pmatrix} = \begin{bmatrix} d_{11} & d_{12} & d_{13} & d_{14} & d_{15} & d_{16} \\ d_{21} & d_{22} & d_{23} & d_{24} & d_{25} & d_{26} \\ d_{11} & d_{22} & d_{33} & d_{34} & d_{35} & d_{36} \end{bmatrix} \begin{bmatrix} \sigma_1 \\ \sigma_2 \\ \sigma_3 \\ \sigma_4 \\ \sigma_5 \\ \sigma_5 \end{bmatrix} + \begin{bmatrix} e_{11} & e_{12} & e_{13} \\ e_{12} & e_{22} & e_{23} \\ e_{13} & e_{23} & e_{33} \end{bmatrix} \begin{pmatrix} \overline{E}_1 \\ \overline{E}_2 \\ \overline{E}_3 \end{pmatrix} \tag{3-5}$$

These equations describe the electro-mechanical coupling for a general, anisotropic material.

The compliance matrix of Equation 3-4 can be simplified if the material is assumed to be orthotropic, meaning that it has 3 planes of symmetry parallel to the coordinate directions shown in Figure 3-1. Also, the piezoelectric strain matrix of both equations can be simplified to the form given [7] for the crystal point group mm2, which applies to PVDF. The dielectric matrix of equation 3-5 is also reduced to the form for the orthogonal crystal class, which also applies to PVDF. Under these conditions, Equations 3-4 and 3-5 respectively become

$$\begin{pmatrix}\varepsilon_1\\ \varepsilon_2\\ \varepsilon_3\\ \varepsilon_4\\ \varepsilon_5\\ \varepsilon_6\end{pmatrix} = \begin{bmatrix} s_{11} & s_{12} & s_{13} & 0 & 0 & 0\\ s_{12} & s_{22} & s_{23} & 0 & 0 & 0\\ s_{13} & s_{23} & s_{33} & 0 & 0 & 0\\ 0 & 0 & 0 & s_{44} & 0 & 0\\ 0 & 0 & 0 & 0 & s_{55} & 0\\ 0 & 0 & 0 & 0 & 0 & s_{66}\end{bmatrix}\begin{bmatrix}\sigma_1\\ \sigma_2\\ \sigma_3\\ \sigma_4\\ \sigma_5\\ \sigma_6\end{bmatrix} + \begin{bmatrix} 0 & 0 & d_{31}\\ 0 & 0 & d_{32}\\ 0 & 0 & d_{33}\\ 0 & d_{24} & 0\\ d_{15} & 0 & 0\\ 0 & 0 & 0\end{bmatrix}\begin{pmatrix}\overline{E}_1\\ \overline{E}_2\\ \overline{E}_3\end{pmatrix} \tag{3-6}$$

$$\begin{pmatrix}\overline{D}_1\\ \overline{D}_2\\ \overline{D}_3\end{pmatrix} = \begin{bmatrix} 0 & 0 & 0 & 0 & d_{15} & 0\\ 0 & 0 & 0 & d_{24} & 0 & 0\\ d_{11} & d_{22} & d_{33} & 0 & 0 & 0\end{bmatrix}\begin{bmatrix}\sigma_1\\ \sigma_2\\ \sigma_3\\ \sigma_4\\ \sigma_5\\ \sigma_6\end{bmatrix} + \begin{bmatrix} e_{11} & 0 & 0\\ 0 & e_{22} & 0\\ 0 & 0 & e_{33}\end{bmatrix}\begin{pmatrix}\overline{E}_1\\ \overline{E}_2\\ \overline{E}_3\end{pmatrix} \tag{3-7}$$

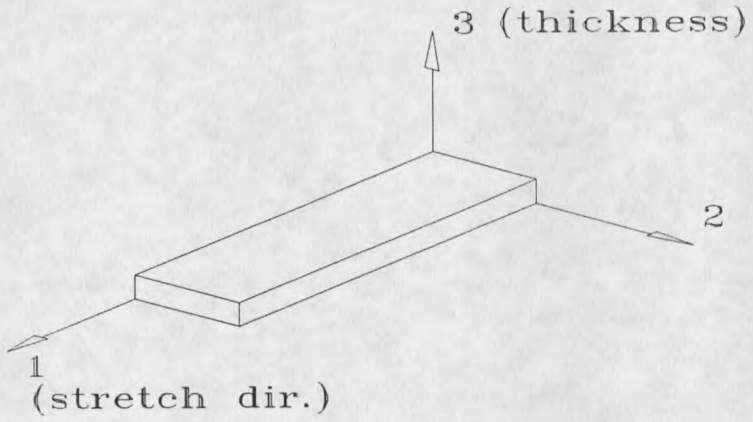


Figure 3-1. Material coordinate axis.

The PVDF samples being tested were thin films with a thickness of 28 μm electroded on the front and back faces. This configuration allowed simplification of Equations 3-4 and 3-5 with certain assumptions. Further, the material is assumed to be

under the condition of plane stress. This assumption is generally made for materials that have one dimension very much smaller than the other two [8]. The conditions of plane stress and single electrode direction are given by the relations

$$\sigma_3 = \sigma_{23} = \sigma_{31} = 0; \qquad \overline{E}_1 = \overline{E}_2 = 0; \tag{3-8}$$

These assumptions reduce Equations 3-6 and 3-7 to

$$\begin{pmatrix} \varepsilon_1 \\ \varepsilon_2 \\ \varepsilon_6 \end{pmatrix} = \begin{bmatrix} s_{11} & s_{12} & 0 \\ s_{21} & s_{22} & 0 \\ 0 & 0 & s_{66} \end{bmatrix} \begin{pmatrix} \sigma_1 \\ \sigma_2 \\ \sigma_6 \end{pmatrix} + \begin{bmatrix} 0 & 0 & d_{31} \\ 0 & 0 & d_{32} \\ 0 & 0 & 0 \end{bmatrix} \begin{pmatrix} 0 \\ 0 \\ \overline{E}_3 \end{pmatrix} \tag{3-9}$$

$$\overline{D}_3 = d_{31}\sigma_1 + d_{32}\sigma_2 + e_{33}\overline{E}_3 \tag{3-10}$$

Also, the strain in the third material direction can be found from the calculated strains in directions 1 and 2 from

$$\varepsilon_3 = \left\{ \frac{s_{31}s_{22} - s_{32}s_{12}}{s_{11}s_{22} - s_{12}^2} \right\} \varepsilon_1 + \left\{ \frac{s_{32}s_{11} - s_{31}s_{12}}{s_{11}s_{22} - s_{12}^2} \right\} \varepsilon_2 + d_{33}\overline{E}_3 \tag{3-11}$$

The elastic compliance terms can be rewritten in terms of Young's modulus, Poisson's ratio (ν), and a shear modulus (G) as

$$s_{11} = \frac{1}{Y_1} \qquad s_{22} = \frac{1}{Y_2} \qquad s_{12} = \frac{-\nu_1}{Y_1} = \frac{-\nu_2}{Y_2} = s_{21} \qquad s_{12(12)} = \frac{1}{G_{12}} \tag{3-12}$$

$$s_{31} = \frac{-\nu_3}{Y_3} \qquad s_{32} = \frac{-\nu_3}{Y_2} \tag{3-13}$$

These coefficients relate stress and strain for an elastic material. However, because PVDF thin films are known to be viscoelastic in nature, this description becomes inadequate for characterizing the piezoelectric interaction. In order to achieve an accurate

representation, Equations 3-9 and 3-10 would have to incorporate the time dependent behavior of PVDF. This would make the terms appearing in the compliance matrix of Equation 3-9 functions of time. The Poisson's ratios appearing in the s_{12} terms would be functions of time as well. However, Poisson's ratio as a function of time can be calculated from the instantaneous Poisson's ratio and knowledge of s_{11} and s_{22} as functions of time. This is accomplished by using a method outlined in reference 9 where it is assumed that the volume of a sample does not change with time and using the expression for s_{12} given by Equation 3-12.

Time Dependent Effects

Material behavior is often idealized in engineering practice as being elastic. An elastic material exhibits a one-to-one correspondence between stress and strain related by Hooke's law

$$\sigma = Y\varepsilon \tag{3-14}$$

where σ is the stress, Y is Young's modulus, and ε is the strain. However, actual materials show a very wide range of behavior than often deviates greatly from this idealization. Many materials, such as metals at high temperatures and plastics, demonstrate time dependence in both the rate of applied loading and the material's response [8]. These materials display creep, characterized by an increasing strain under a constant load. PVDF samples subjected to a constant stress have been shown to exhibit creep response [3]. Many materials that demonstrate time dependence can be modeled using the theory of viscoelasticity.

Two approaches can be used to achieve viscoelastic material modeling. The first approach makes use of elastic and viscous elements consisting of springs and viscous dashpots, respectively. These elements are arranged so that the relationship between stress and strain approximates the behavior of real materials. The spring element is linear-elastic and is characterized by Equation 3-14, where Y becomes the spring constant. In a viscous dashpot element, the stress is proportional to the time rate of strain

$$\sigma = \eta \dot{\varepsilon} \tag{3-15}$$

where η is the viscosity of the dashpot and the dot is used to designate the time derivative.

Viscoelastic models consist of combinations of these elements. For instance, the Maxwell model consists of a spring and dashpot in series. Realizing that this model has a total elongation equaling the sum of the elongation of each element, and using Equations 3-14 and 3-15, the equation describing the stress-strain relationship for this model written in standard form is

$$\sigma + p_1 \dot{\sigma} = q_1 \dot{\varepsilon} \tag{3-16}$$

The solution to this equation for a constant stress applied at $t = 0$ is found to be

$$\varepsilon = \frac{\sigma_o}{q_1}(p_1 + t) \tag{3-17}$$

This response shows an instantaneous strain at $t = 0$ and an unlimited strain with constant loading. For these reasons, this model is known as the Maxwell fluid.

Another elementary model is the Kelvin material, characterized by a spring and dashpot in parallel. Realizing that the elongation is the same in both elements for this model and utilizing Equations 3-14 and 3-15, the differential equation in standard form is

$$\sigma = q_o\varepsilon + q_1\dot{\varepsilon} \tag{3-18}$$

Again, the solution is found for a constant stress applied at time t = 0 to be

$$\varepsilon = \frac{\sigma_o}{q_o}(1 - e^{-\frac{q_o}{q_2}t}) \tag{3-17}$$

The response of this model to constant stress does not exhibit any instantaneous strain and slowly approaches a finite strain at extended time. Because of this behavior, this model is known as the Kelvin solid.

Actual viscoelastic, solid materials, however, do not exhibit the unlimited strain of the Maxwell model or the lack of instantaneous strain of the Kelvin model. More complex models are therefore made by the combination of springs, dashpots, Maxwell fluid, and Kelvin solid elements arranged in series or parallel. The expression relating stress and strain for a general model consisting of m springs and n dashpots is given as [11]

$$\sum_{0}^{m} p_k \frac{d^k\sigma}{dt^k} = \sum_{0}^{n} q_k \frac{d^k\varepsilon}{dt^k} \tag{3-20}$$

However, accurate models typically involve a large number of elements, making their use inconvenient and time consuming. Also, these models cannot be expanded to include three-dimensional loading.

The second approach used to achieve viscoelastic material modeling is based on the Boltzmann Superposition Principle. Suppose that D(t), the creep compliance which gives the strain to a constant, unit stress, is known. The strain resulting from a constant stress σ_o applied at time t=0 is then

$$\varepsilon(t) = \sigma_o D(t) \tag{3-21}$$

If an additional stress σ_1 is applied at time $t=t_1$, the Boltzmann Superposition Principle

states that the total strain response will be given by

$$\varepsilon(t) = \sigma_o D(t) + \sigma_1 D(t - t_1) \tag{3-22}$$

This response can be generalized for stress changing with infinitesimal steps from σ_o at infinitesimal steps in time from t=0. This behavior uses a hereditary integral to describe the stress strain relationship, which can be written in a three-dimensional form. The resulting strain caused by this stress history is then [12]

$$\varepsilon_{ij}(t) = \sigma_{kl_o} D_{ijkl}(t) + \int_0^t D_{ijkl}(t-\tau)\frac{d\sigma_{kl}}{d\tau}d\tau \tag{3-23}$$

The creep compliance, D(t), is different for each material and is determined by experiment, or from the differential equation of a viscoelastic model by letting $\sigma=\Delta(t)$ and $\varepsilon=D(t)$. Similarly, the stress corresponding to a strain history becomes

$$\sigma_{ij}(t) = \varepsilon_{kl_o} E_{ijkl}(t) + \int_0^t E_{ijkl}(t-\tau)\frac{d\varepsilon_{kl}}{d\tau}d\tau \tag{3-24}$$

where E(t) is the relaxation modulus, the stress per unit strain. The relaxation modulus is found in a manner analogous to the creep compliance. The creep compliance and the relaxation modulus are related by their Laplace transforms

$$\overline{E}(s)\overline{D}(s) = s^{-2} \tag{3-25}$$

Full viscoelastic modeling is therefore possible by determining the relaxation modulus or the creep compliance functions.

Experimental Techniques

Viscoelastic characterization of materials traditionally requires the use of long term static creep and relaxation tests to determine the creep compliance and the relaxation modulus needed for Equations 3-23 and 3-24. If these functions are to be determined over a range of temperatures or stress levels, the time required would be enormous. Dynamic characterization, however, allows the mapping of the creep compliance and the relaxation modulus from tests conducted in the frequency domain rather than the time domain, thus eliminating the need for long term testing. This is accomplished by calculating the complex parts of the viscoelastic functions from quantities measured in the frequency domain, and then transforming the complex functions into the time domain.

Dynamic testing for the purpose of determining the viscoelastic functions of a material has been shown to be an effective method for characterizing thin films [14, 15]. This method can be used to determine both linear and non-linear viscoelastic response [13]. These papers demonstrate that this method can successfully and accurately determine the viscoelastic functions of thin films in a fraction of the time required for traditional testing.

The equations used to calculate the viscoelastic functions from measurable quantities are derived from the constitutive equations of linear viscoelasticity. In the case of dynamic testing, a periodic oscillating strain (uniaxial, so that the subscripts may be dropped) is applied such that

$$\varepsilon = \varepsilon^{\circ} \sin(\omega t) \quad ; \quad \dot{\varepsilon} = \omega \varepsilon^{\circ} \cos(\omega t) \tag{3-26}$$

where ε° is the amplitude of strain and ω is the frequency of oscillation. Substitution of these equations in Equation 3-24 results in the stress response to the oscillatory strain loading as

$$\sigma(t) = \int_0^{\infty} E(s)\omega\varepsilon^{\circ} \cos\{\omega(t-s)\} ds \tag{3-27}$$

where $s = t-\tau$. From trigonometric relations, this equation can be rewritten as

$$\sigma(t) = \varepsilon^{\circ} \{\omega \int_0^{\infty} E(s) \sin(\omega s) ds\} \sin(\omega t) + \varepsilon^{\circ} \{\omega \int_0^{\infty} E(s) \cos(\omega s) ds\} \cos(\omega t) \tag{3-28}$$

Noting that the terms in brackets are functions of frequency only, we can rewrite this equation as

$$\sigma(t) = \varepsilon^{\circ} E'(\omega) \sin(\omega t) + \varepsilon^{\circ} E''(\omega) \cos(\omega t) \tag{3-29}$$

where $E'(\omega)$ is the storage modulus and $E''(\omega)$ is the loss modulus. Noting that the $E'(\omega)$ function replaced the term with $\sin(\omega t)$, it is in phase with the input strain and is directly proportional to the average energy stored in a cycle. The $E''(\omega)$ function replaced the term with $\cos(\omega t)$, which makes it 90° out of phase with the strain and is directly proportional to the average loss of energy as heat in a cycle. Therefore, the stress function of Equation 3-29 is periodic with, but out of phase with, the strain to a degree depending on the relative magnitudes of these terms.

From trigonometric relations, it can be shown that

$$E'(\omega) = \frac{\sigma^{\circ}}{\varepsilon^{\circ}} \cos\delta \quad ; \quad E''(\omega) = \frac{\sigma^{\circ}}{\varepsilon^{\circ}} \sin\delta \quad ; \quad \frac{E''(\omega)}{E'(\omega)} = \tan\delta \tag{3-30}$$

where δ is the phase angle between stress and strain and σ° is the maximum stress amplitude. As a result, the complex modulus is defined as

$$E^*(\omega) = E'(\omega) + iE''(\omega) \tag{3-31}$$

This equation immediately yields the complex compliance and its parts since

$$D^*(\omega) = \frac{1}{E^*(\omega)} = D'(\omega) + iD''(\omega) \tag{3-32}$$

$$D'(\omega) = \frac{1}{E'(\omega)(1+\tan^2\delta)} \quad ; \quad D''(\omega) = \frac{1}{E''(\omega)\{1+(\tan^2\delta)^{-1}\}} \tag{3-33}$$

where $D'(\omega)$ is the extension storage compliance and $D''(\omega)$ is the extension loss compliance. Thus, by measuring the ratio of maximum amplitude of stress to strain and the phase angle between stress and strain, we gain knowledge of the complex modulus and the complex compliance.

Once the complex moduli and compliances are known over a frequency range, they are converted by way of inverse Fourier transform to the time domain to obtain the creep compliance and the relaxation modulus. This method, however, requires integrals from 0 to ∞ to be performed numerically or graphically. These calculations can be tedious, sensitive to errors, or the known function may not be known over a wide enough range to give convergence. For these reasons, the approximate solution given by Ninomiya and Ferry [10] can be used if both of the components of the complex functions are known.

$$E(t) = E'(\omega) - 0.40E''(0.40\omega) + 0.014E''(10\omega)\Big|_{\omega=1/t} \tag{3-34}$$

$$D(t) = D'(\omega) + 0.40D''(0.40\omega) - 0.014D''(10\omega)\Big|_{\omega=1/t} \tag{3-35}$$

Knowledge of the creep compliance and the relaxation modulus completely characterizes

the linear material properties and can be used in Equations 3-23 and 3-24 to determine the current strain or stress from stress or strain histories, respectively. This description, however, is only accurate through the linear range of the material.

The range of frequencies over which the complex functions are known, and thus the time range over which the creep compliance and the relaxation modulus are known, can be expanded beyond the measured range. This is accomplished using the temperature-frequency correspondence principle, which states that an increase in temperature is nearly equivalent to a decrease in frequency [10]. Properties measured at one temperature and frequency correspond to properties at a different temperature and frequency through the temperature dependent shift factor a_T. Thus,

$$F(\omega, T) = F(\omega a_T, T_o) \tag{3-36}$$

where the function F represents the complex compliance or modulus or any component of these functions. Is has been experimentally shown that this principle is valid for a variety of materials, including thin film polymers [13]. This phenomenon can be seen not only in experiment, but also in theoretical relations describing viscoelastic behavior. This can easily be demonstrated by the Rouse theory for molecular viscoelastic behavior. This theory, also known as the bead-spring model with no hydrodynamic interaction among beads is given as [10]

$$E'(\omega) = cRT / M \sum_{p=1}^{N} \omega^2 \tau_p^2 / (1 + \omega^2 \tau_p^2) \tag{3-37}$$

where c is the concentration of (g polymer per cc solution), R is the gas constant, M is the molecular weight, T is temperature, N is the number of Gaussian submolecules, and τ is a function of the friction coefficient and temperature. The effect of changing the

temperature in this equation from T_o to T is to multiply the term outside of the summation by cT/c_oT_o and the to multiply each τ by some factor that is proportional to temperature, namely a_T. Because both ω and τ are squared and grouped together in both the numerator and denominator of the summation, the effect is the same as if ω were multiplied by a_T. Thus, measurements of a viscoelastic function taken at temperature T and frequency ω is equivalent to measurements taken at temperature T_o and frequency $a_T\omega$, except for the factor in front of the summation. Hence, measurements taken over a range of temperatures, when plotted as the measured function multiplied by T_o/T versus $\omega \cdot a_T$, will form a single composite curve corresponding to measurements at T_o since c_o/c differs from unity by only a very small amount due to thermal expansion [10]. This composite curve represents the frequency dependence of the function at a constant temperature over a greatly extended frequency range. Since not all materials exhibit a temperature-frequency correspondence, it is vital that the composite curve be composed of curves that superpose nearly exactly and that the same values of a_T are able to superpose all viscoelastic functions to ensure that the method is valid.

To increase the viscoelastic description beyond the linear stress range, a nonlinear viscoelastic theory developed by R. A. Shapery [14, 15] was used. This theory extends the approach of temperature-frequency superposition to stress-time superposition. Schapery describes nonlinear viscoelastic responses by introducing a reduced time variable, a_σ, which is dependent on the magnitude of stress [13]. Many nonlinear viscoelastic theories have been developed and tested, but studies have shown Schapery's

theory to be the most general and most adaptable of examined techniques [16]. For a uniaxial stress history, Schapery shows that the strain response is given by

$$\varepsilon(t) = g_o D_o \sigma(t) + g_1 \int_0^t \hat{D}(\Psi - \Psi') \frac{\partial g_2 \sigma(\tau)}{\partial \tau} d\tau \tag{3-38}$$

where D_o and $\hat{D}$ are the elastic and transient components of the creep compliance, D(t), and g_o,g_1, and g_2 are stress dependent parameters. The term g_o introduces nonlinear contributions to the elastic response, g_1 introduces nonlinear contributions to the transient response, and g_2 introduces nonlinear contributions to the rate of applied load. The terms Ψ and Ψ' are reduces time variables given by

$$\Psi = \Psi(t) = \int_0^t \frac{dt'}{a_\sigma} \tag{3-39}$$

$$\Psi' = \Psi'(\tau) = \int_0^\tau \frac{dt'}{a_\sigma} \tag{3-40}$$

The stress dependent shift factor, a_σ, is found by the superposition of creep curves measured at different stress levels in a manner similar to determining a_T for measurements taken at different temperatures. Similar to the master curves of the complex viscoelastic functions in the frequency domain, a master curve of the creep response is formed for a reference stress, which is the stress at which nonlinear behavior first begins.

CHAPTER 4

EXPERIMENTAL PROGRAM

Main Objectives

The goal of the experimental program was to determine the significance of the time dependent effects in the mechanical response of PVDF thin films and to provide accurate characterization of both the mechanical and piezoelectric properties of this material.

Experimental Stages

In order to achieve the goals of the main objective, several sets of tests, each with its own experimental setup, were conducted. This experimental program was broken into four individual stages in this thesis for clarity.

Stage 1

The first stage of the experimental program was directed at determining the instantaneous elastic material properties. Since PVDF is orthotropic, tests were conducted in the 1 and 2 material directions. These properties describe the instantaneous mechanical response of the material to loading conditions. The details of the experiments included in stage 1 are fully described in Chapter 5.

Stage 2

The second stage was directed at determining the significance of the time dependent effects on the mechanical response of the material in the 1 and 2 material directions. The results of these tests were used to determine if further time dependent characterization of the material was necessary. The details of the experiments conducted in this stage are fully described in Chapter 6.

Stage 3

Results from stage 2 tests indicated that there was significant material dependence on time. The sets of experiments in this stage were directed at modeling the time dependent effects with linear viscoelastic theory by determining the parameters of this model. Specifically, the creep compliance and the relaxation modulus for the 1 and 2 material directions were found using the method of dynamic mechanical testing and analysis. This stage also used the nonlinear viscoelastic theory described in Chapter 3 to model the material over a wider range of stress levels. The details of the experiments conducted in this stage are fully described in Chapter 7.

Stage 4

The final stage of the experimental program was directed at finding the properties of the piezoelectric strain coefficients. This included finding the effects of frequency, temperature, stress-levels, and time on the electro-mechanical coupling coefficient for both the 1 and 2 material directions. The details of the experiments conducted in this stage are fully described in Chapter 8.

CHAPTER 5

INSTANTANEOUS ELASTIC RESPONSE

Parameters Considered

The first step in characterizing the mechanical properties of PVDF thin films was to determine the instantaneous elastic properties. The parameters that were required to fully describe these properties consisted of Young's moduli in the 1 and 2 directions, Y_1 and Y_2, the yield stresses and strains in these same directions, σ_{Y1}, σ_{Y2}, ε_{Y1} and ε_{Y2}, the ultimate stresses and strain in the 1 and 2 directions, σ_{U1}, σ_{U2}, ε_{U1} and ε_{U2}, and the Poisson's ratios υ_{12} and υ_{21}. Since values of these parameters were previously known from publications [3, 4], these tests were conducted simply to verify the accuracy and repeatability of these values.

Testing Apparatus

To determine the above specified elastic characteristics, tests were conducted using an Instron model 4206-006 screw type testing machine in conjunction with a PC using Automated Materials Testing System -V. 5.25 software for test control and data acquisition via a GPIB (general purpose interface bus) card. Thus, the load and displacement were automatically recorded during testing. The Instron machine was

equipped with thin specimen, flat plate grips. Because of the rough surface of these grips, thin aluminum faceplates were used to sandwich the contact portions of the samples in the grips to insure even pressure distribution.

Set of Experiments

Three 7.62 cm (in the1 direction) by 2.54 cm (in the 2 direction) samples were tested to failure under a constant strain rate of 1.27 cm/min to produce stress-strain curves in the 1 direction. The produced set of stress-strain curves was then used to determine Y_1, σ_{Y1}, ε_{Y1}, σ_{U1}, and ε_{U1}. Similarly, three 7.62 cm (in the 2 direction) by 2.54 (in the 1 direction) samples were tested to failure under the same strain rate to obtain stress-strain curves in the 2 direction. The produced set of stress-strain curves was then used to determine Y_2, σ_{Y2}, ε_{Y2}, σ_{U2}, and ε_{U2}.

In addition, measurements were conducted to find the Poisson's ratios υ_{12} and υ_{21}. These were found by straining samples with the Instron in the 1 and 2 direction, respectively, and measuring the corresponding change in width. Several width strains were calculated for each sample at various prescribed extension strains up to yield. To find υ_{12}, a 8.82 cm (in the 1 direction) by 2.52 cm (in the 2 direction) sample was extended in the 1 direction and held at 8 evenly incremented strain levels up to yield. At each increment, the width of the sample (the 2 direction) was measured using a micrometer. Similarly, υ_{21} was found by extending a 8.82 cm (in the 2 direction) by 2.52 cm (in the 1 direction) sample in the 2 direction and holding at 8 evenly incremented strain levels up to yield. Again, the width (in the 1 direction) was measured at each increment.

Results

A Microsoft Excel spreadsheet was used to convert the recorded load and displacement data into stress and strain points for each of the six samples. Figure 5-1 shows the stress-strain curves for three samples tested in the 1 direction (for clarity, only every 15th data point is shown). This figure indicates that the yield point occurred early in the curves, at about 0.5×10^8 Pa. Figure 5-2 shows an expanded view of this area. The first 30 data points from each of the samples (note that only every 3rd data point is shown in this figure for clarity) was used to calculate an average initial slope of the curves. A

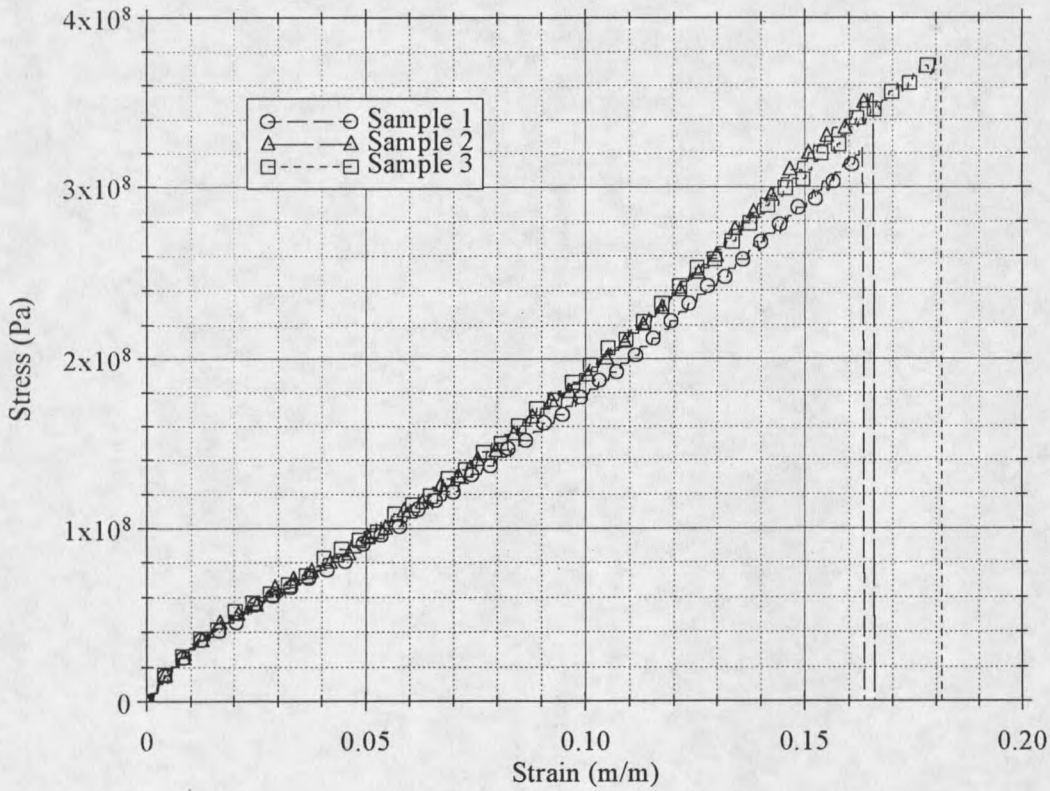


Figure 5-1. Stress-strain curve for material direction 1.

0.2% offset of this line was then used to determine the average yield point by determining where this line intersected the average stress-strain curve. This method resulted in a yield stress of 0.455×10^8 Pa and a yield strain of 1.82%. The ultimate stress and strain for the 1 direction were found by averaging the stress and strain values for the last non-failure data points from the three samples. These calculations resulted in an ultimate stress of 3.52×10^8 Pa and an ultimate strain of 16.99%.

The stress-strain curves for the three samples tested in the 2 direction are shown in Figure 5-3 (every 15th data point is shown for clarity). Unlike Figure 5-1, this graph does not exhibit steadily increasing stress until failure. Instead, the samples in the 2 direction

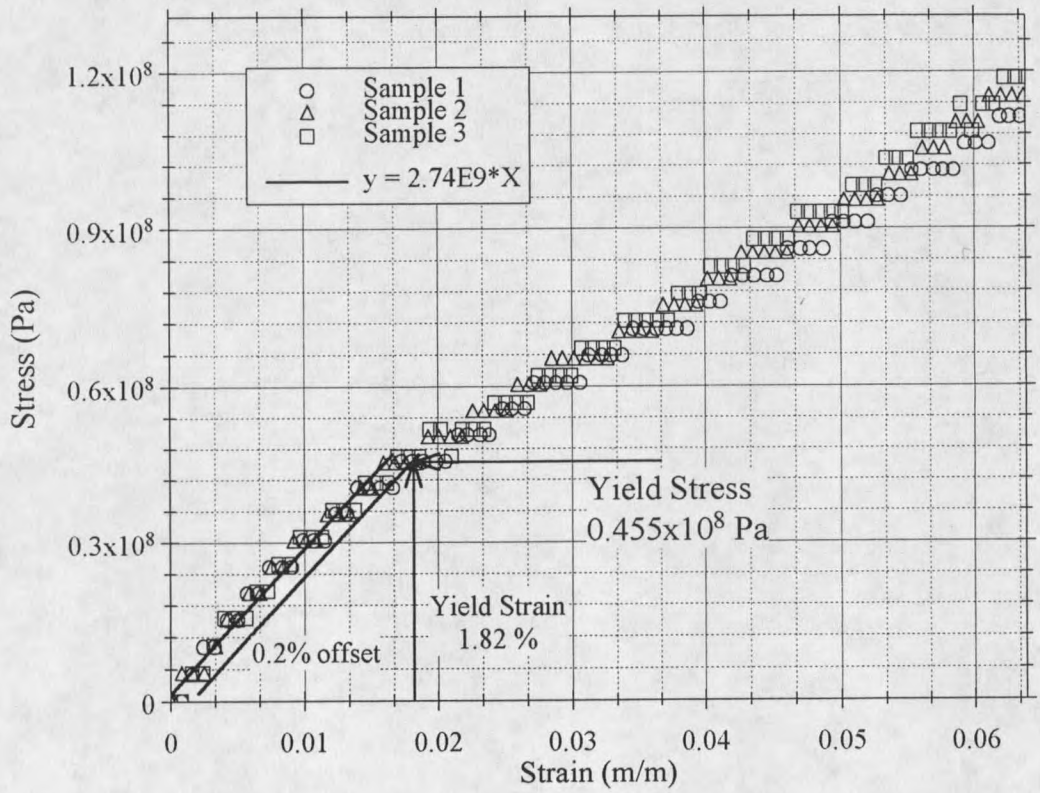


Figure 5-2. Exploded view of stress-strain curve for material direction 1.

began to neck just after yielding at about 4.0×10^7 Pa. Figure 5-4 shows an expanded view of this area. An average initial slope of these curves was calculated from the first 30 data points from each of the samples (note that only every 3rd data point is shown in this figure for clarity). A 0.2% offset of this line was then used to determine the average yield point by determining where this line intersected the average stress-strain curve. The yield stress and strain were found to be 0.396×10^8 Pa and 1.44%, respectively. The ultimate stress and strain for the 2 direction were found by averaging the maximum stress value and the associated strain from the three samples. These calculations resulted in an ultimate stress of 0.50×10^8 Pa at a strain of 2.54%.

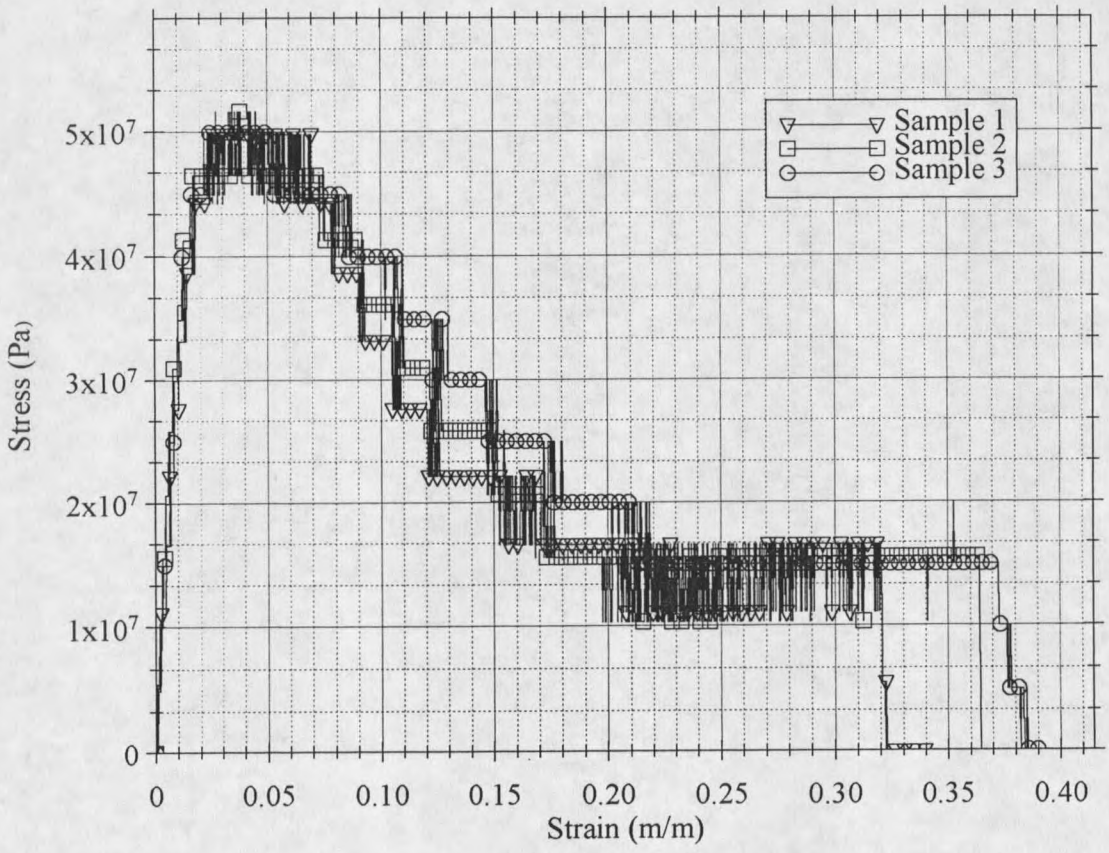


Figure 5-3. Stress-strain curves for material direction 2.

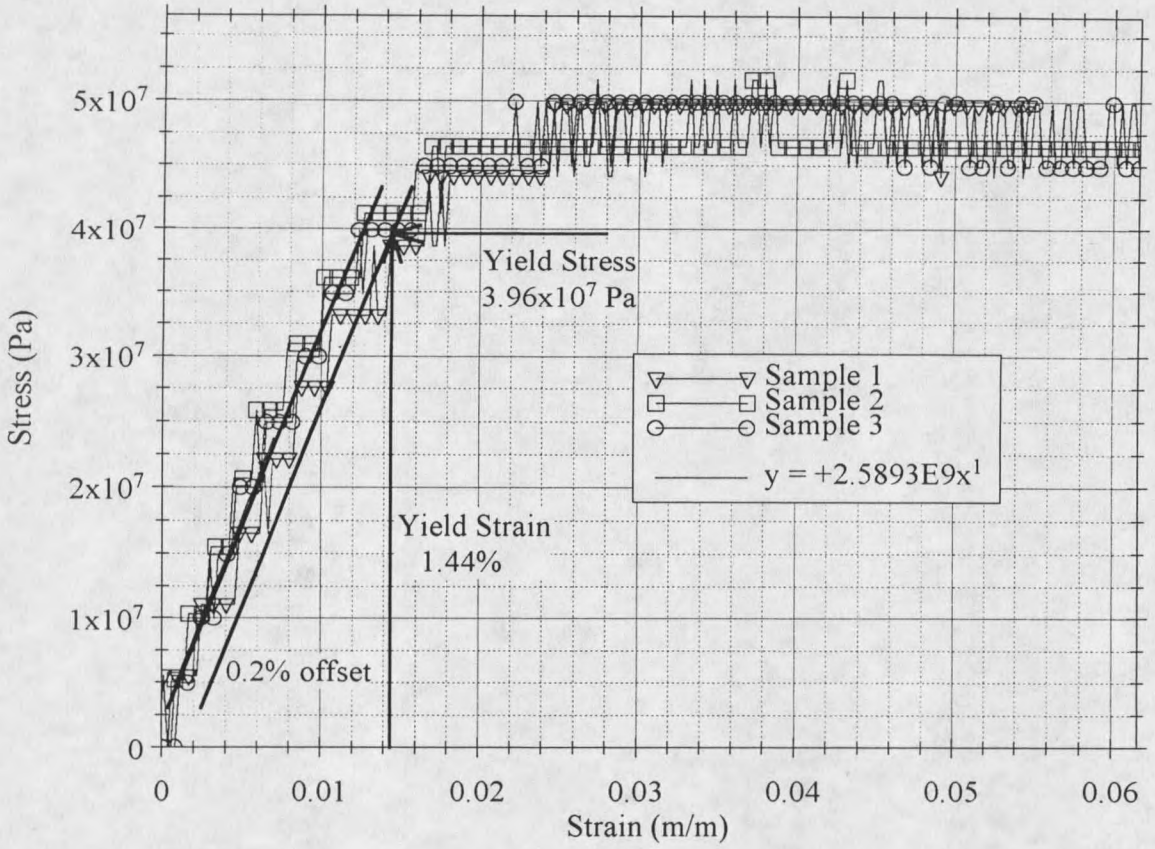


Figure 5-4. Exploded view of stress-strain curves for material direction 2.

Poisson's ratio was calculated as the negative of the ratio of width strain to extension strain. The resulting calculated Poisson's ratio, υ_{12}, varied from 0.423 to 0.486 with an average of 0.445. Similarly, υ_{21}, was found to vary from 0.425 to 0.475 with an average of 0.456.

CHAPTER 6

SIGNIFICANCE OF TIME DEPENDENT EFFECTS

Parameters Considered

Due to the fact that PVDF is a polymer and has been shown to exhibit time dependent properties [3], much of the characterization effort focused on describing the time dependent behavior of the film. This has been done in an effort to increase the accuracy of the mechanical properties of the material beyond the elastic compliance terms used in the piezoelectric constitutive laws. A recent literature review found only one paper concerning the time-dependent properties of PVDF, but it was concerned only with high-temperature stability of the material [6].

To address this issue, a series of creep tests were conducted to determine the extent of the time dependency of PVDF by finding the strain-time curves at various stress levels. These curves were found by subjecting samples to static stresses (dead loads). Therefore, the parameters considered in this set of experiments were the strains in the 1 and 2 material directions as functions of time. These tests resulted in knowledge of the significance of time dependent effects in the 1 and 2 directions. Also, as will be shown, the results provided the linearity range of the material in these directions.

Testing Apparatus

Creep tests require measurement of the time variation of strain of a sample when subjected to static stress. Placing thin film samples in uniform, unidirectional stress required grips that could facilitate both instrumentation and load attachment. Specially made grips that do not use knurled faces typically used for improved clamping of specimens were necessary. It was found that this type of clamp punctured the thin films and caused premature failure. Adjustable grips with flat, aluminum faceplates, as shown in Figure 6-1, were constructed for this purpose. A platform on which 200 gram masses could be stacked was attached to the lower grip, while the upper grip was secured to a stationary support structure.

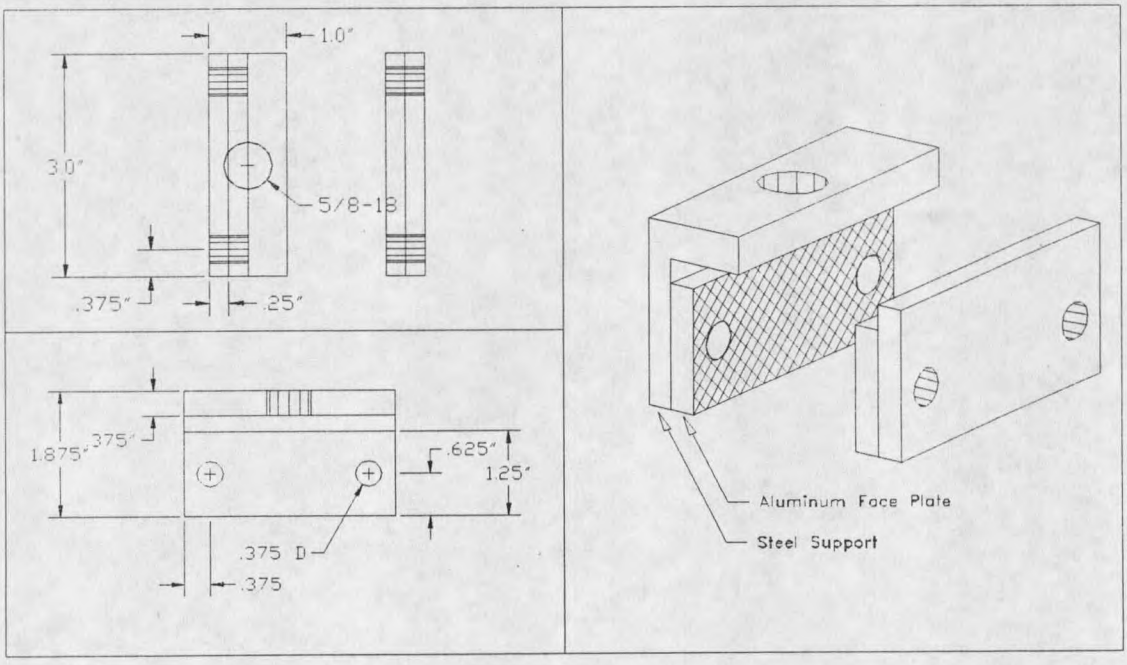


Figure 6-1. Adjustable thin film grips.

Measurement of strain during the test was achieved using a Data Instruments model Fastar 1000 (50 mm maximum displacement) LVDT. The instrument's output was a DC voltage proportional to the change in inductance caused by the LVDT's core movement. This output was measured and recorded with a Hewlett Packard model 54504A 400 MHz digitizing oscilloscope. The LVDT and processor combination had an absolute error less than ± 0.0452% of full scale.

A computer was used in this setup equipped with a National Instruments GPIB (General Purpose Interface Bus) communications card and NI-488.2 software for Windows 3.1 to communicate with the oscilloscope. The computer not only received and recorded data from the oscilloscope, but was also used to control its operations with BASIC command language programming. This arrangement allowed automating data acquisition and recording of strain during the creep tests.

Set of Experiments

For creep tests conducted in the 1 direction, 10 samples 2.54 cm (in the 2 direction) by 10.16 cm (in the 1 direction) were strained under 10 separate levels of constant stress for 2 hours at room temperature. The samples were positioned in the grips so that an average of 5.08 cm gage length was under uniform stress. The stress level was controlled by attaching 200 gram masses to the lower grip and ranged from 13.80% yield to 122.1% yield. Measurements of the LVDT output were made every 60 seconds for the first 12 minutes and every 12 minutes for the remaining test duration.

This set of experiments was repeated for creep measurements in the 2 direction with 6 samples 2.54 cm (in the 1 direction) by 10.16 cm (in the 2 direction). Static stress levels ranged from 15.71% yield to 91.57% yield. Unlike tests conducted in the 1 direction, stress levels in the 2 direction could not exceed the yield stress, as the samples would immediately neck resulting in unlimited strain.

Results

The strain vs. time curves for various stress levels in the 1 direction are shown in Figure 6-2. This graph clearly demonstrates the time dependency of PVDF, especially at higher stress levels. The initial strains after the application of the load are very close to the values predicted by Hooke's law, given in Equation 3-14. The strain then increases with time. These curves were then normalized with respect to their corresponding stress values in order to determine the linear range of viscoelastic behavior. Curves that superpose to form a single normalized curve are stress level independent and are therefore within the linear range of viscoelasticity. Normalized curves that lie outside of this curve exhibit stress dependent behavior and are therefore nonlinear.

The normalized strain vs. time curves are shown in Figure 6-3. This graph reveals that the viscoelastic response of the material is stress level dependent for stresses exceeding 56.9% yield.

Results of creep tests conducted in the 2 direction are given in Figure 6-4. These results also show a time dependency, but to a lesser degree than the response of the tests

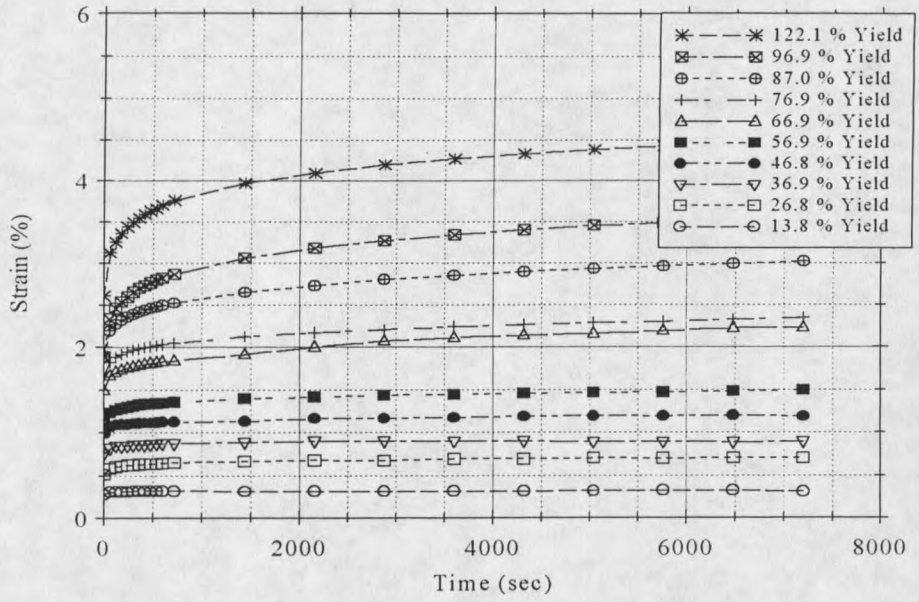


Figure 6-2. Creep curves for tests conducted in the 1 direction.

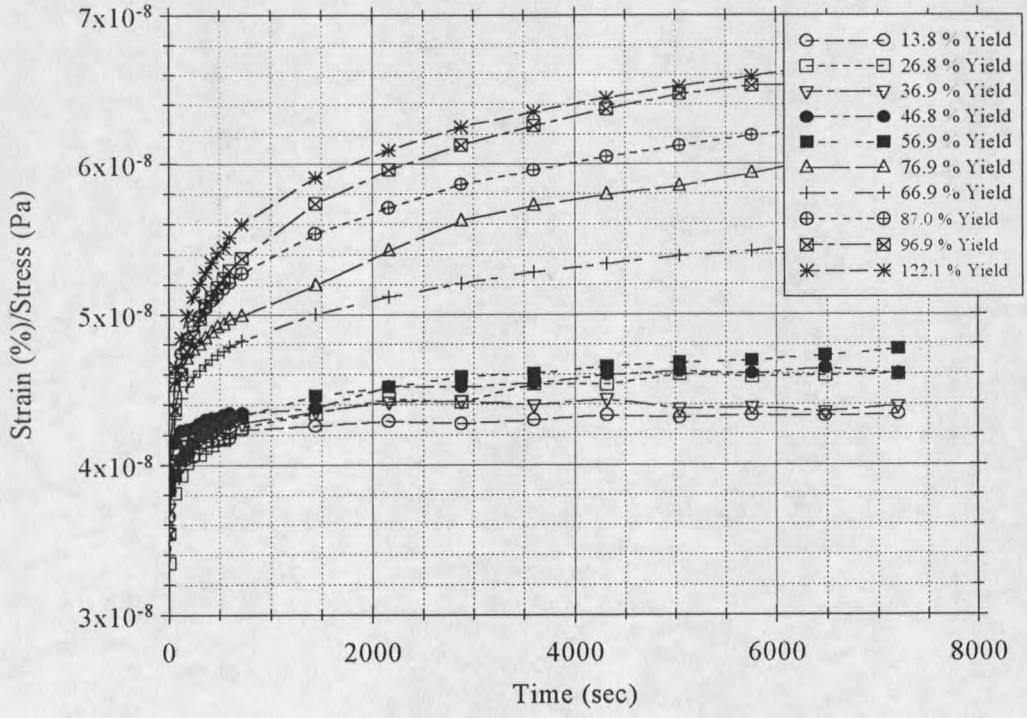


Figure 6-3. Normalized creep curves conducted in the 1 direction.

in the 1 direction. The creep strain over the 2 hour time period at any given stress level in the 2 direction is about half of the strain creep in the 1 direction. As an example, an increase of 0.1372% strain in the 1 direction occurred at 36.9% yield, while a 0.0774% strain increase occurred in the 2 direction at 33.77% yield, which is 56.40% of the strain increase in the 1 direction at approximately the same stress level. The strain increased 0.6991% in the 1 direction at 76.90% yield and only 51.0% of that, or 0.357% strain in the 2 direction at 76.29% yield.

The creep results in the 2 direction were also normalized to determine the range of linear viscoelasticity, as shown in Figure 6-5. The response in the 2 direction shows an increased range of stress independence, up to levels above 76.29% yield.

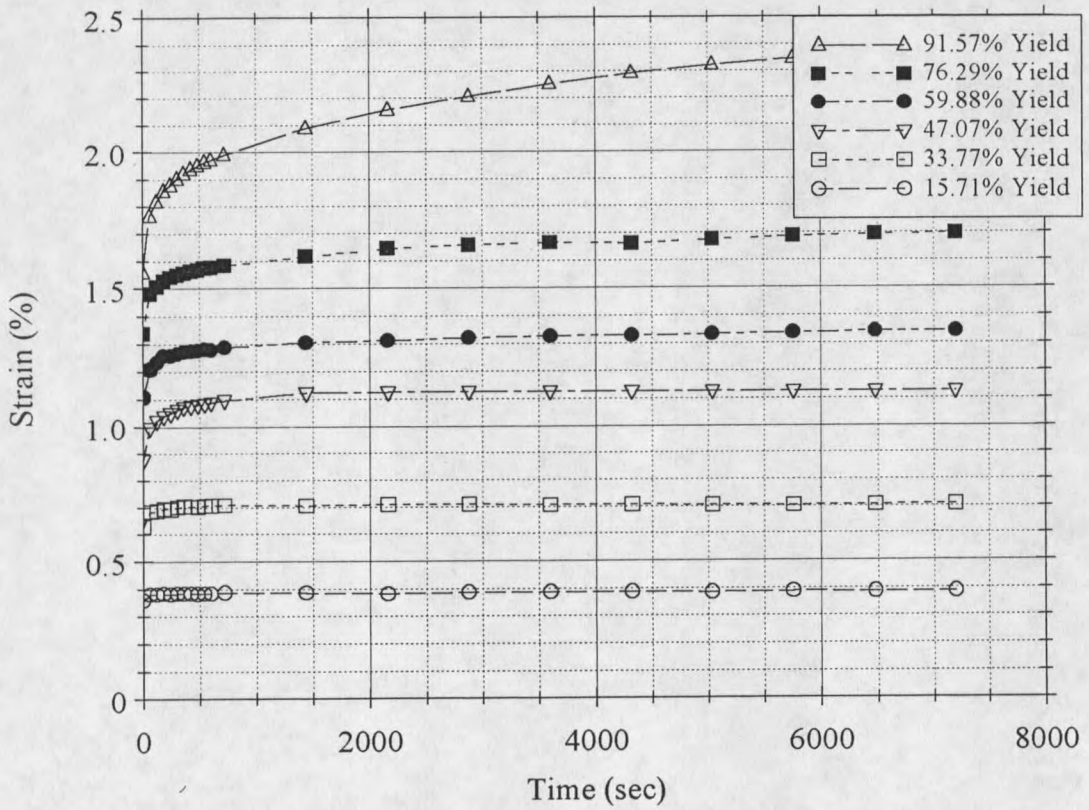


Figure 6-4. Creep curves for tests conducted in the 2 Direction.

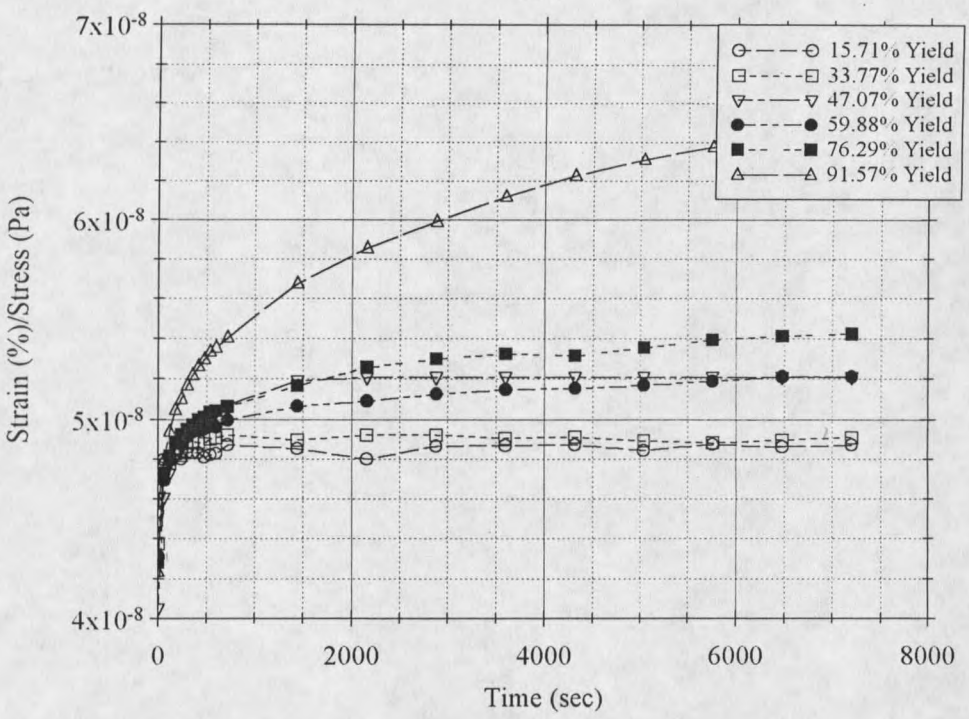


Figure 6-5. Normalized creep curves for tests conducted in the 2 direction.

CHAPTER 7

VISCOELASTIC CONSTITUTIVE MODELING BASED ON DMTA

Parameters Considered

Based on the results of the tests conducted to determine the significance of time dependent effects, the hereditary viscoelasticity model has been adopted to characterize the creep properties of PVDF. The parameters required for complete viscoelastic modeling are the creep compliance and the relaxation moduli functions for the 1 and 2 material directions. The experimental method of dynamic mechanical testing and analysis, or DMTA, described in Chapter 3 was used to accomplish this task. In this method, the complex parts of the viscoelastic functions were measured in the frequency domain, thereby avoiding the long time commitment required to evaluate the functions from traditional creep and relaxation tests. Measurements in the frequency domain, however, require a much more complex testing apparatus. Unlike creep tests, where a static load is applied and the strain recorded versus time, or relaxation tests where a constant strain is applied and the stress is recorded versus time, the dynamic tests requires a prescribed oscillatory strain at a prescribed pre-stress and temperature. The equipment and process required for this test are now described.

Testing Apparatus

The frame of the testing apparatus, shown in Figure 7-1, was constructed of 1 inch square steel tubing. The tripod was 4' 6" tall and had a square base that was 3' 5.5" wide. The small top plate was used to support a threaded steel rod that hangs vertically from a tension adjustment nut. This rod was used to provide adjustable positioning to the upper grip of the assembly. The lower grip was attached to a mechanical shaker mounted on the bottom plate of the tripod by a similar rod. The grips were positioned to be inside of a temperature chamber positioned on the center plate of the tripod. In this manner, a sample could be mounted in the grips of the apparatus such that it was inside of a temperature controlled environment, had a pre-stress controlled by the upper tension nut, and had a prescribed strain controlled by the mechanical shaker below.

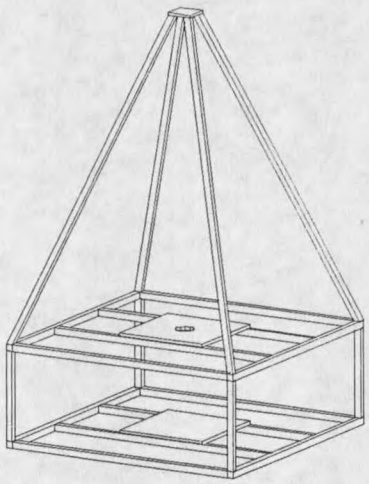


Figure 7-1. Testing apparatus support frame.

The grips, shown in Figure 6-1, were constructed of steel and feature aluminum faceplates and adjustable clamping force. The support frame, connecting rods, grips, and shaker comprised the mechanical component of the experimental setup. The arrangement of these components can be seen in Figure 7-2.

A schematic diagram showing the transducers and accompanying measurement devices of the experimental setup is shown in Figure 7-3. This equipment measured and recorded the load, displacement, and voltage of the piezoelectric sample. The temperature of the sample's environment was also monitored.

A linear voltage differential transformer, or LVDT, was mounted between the upper, stationary grip and the lower, oscillating grip to measure absolute position of the lower grip and ultimately the strain of the sample. The LVDT used for this apparatus was a Data Instruments model Fastar 1000 (50 mm maximum displacement) and used a 112 kHz excitation frequency provided by a Data Instruments model Fastar SP 200A signal processor that compensated the LVDT's output signal for phase and temperature. The processor's output was a DC voltage proportional to the change in inductance caused by the LVDT's core movement and was measured with an oscilloscope. The LVDT and processor combination was able to sense dynamic motion up to 15 kHz with less than 1°/100 Hz phase lag, provide temperature compensation to less than 0.005% of full scale per °C, and had absolute error of less than ± 0.0452% full scale. An in-line load cell was positioned on the upper threaded rod well above the temperature chamber to provide measurement of the force, and ultimately the stress applied to the sample. The load cell

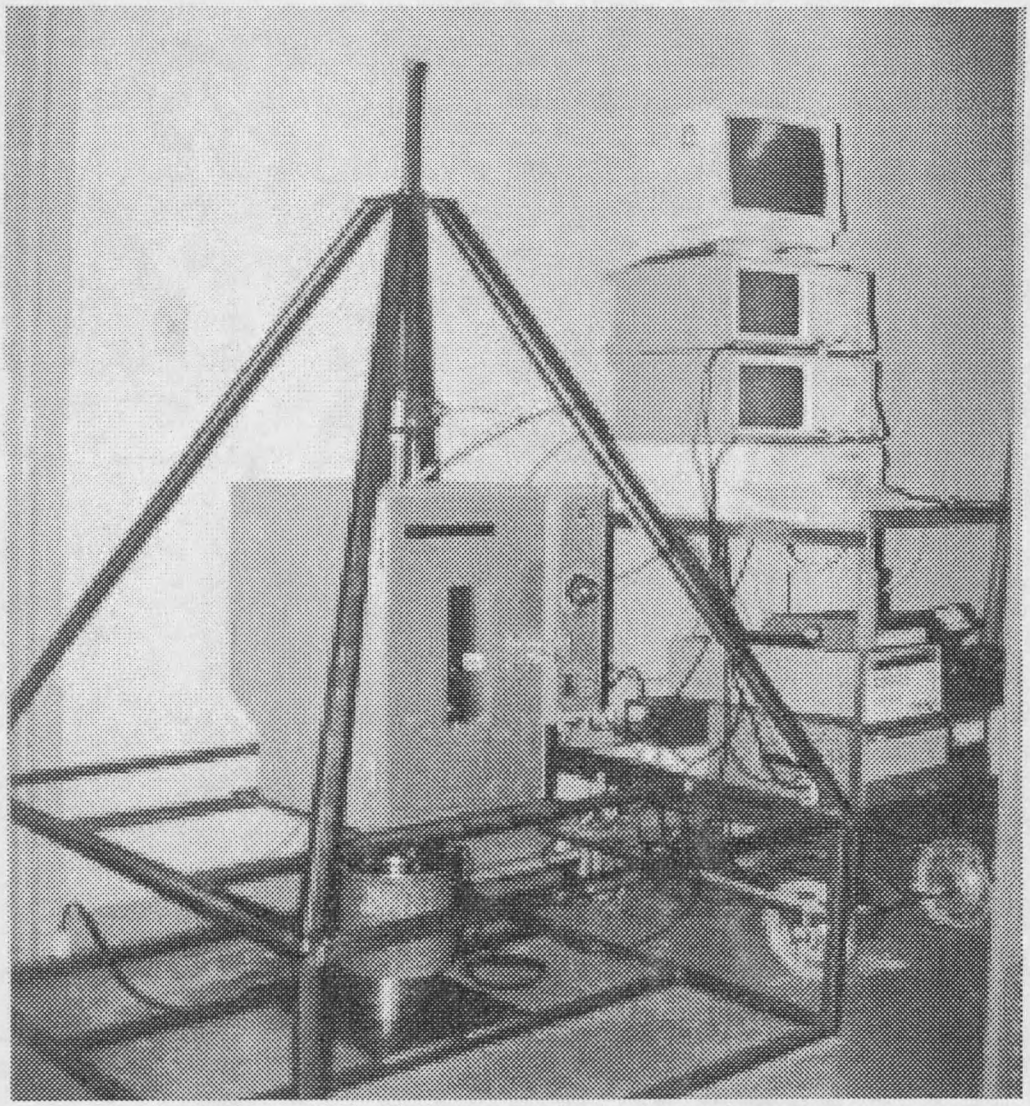


Figure 7-2. Photograph of experimental setup.

used in this apparatus was an Interface model 1210AF rated at 500 pounds maximum. The cell required a 10 VDC excitation voltage and had a static error band of ± 0.0330% full scale for temperatures between -9.4°C and 46.1°C. The output voltage was increased by 99.85 times by an external amplifier and measured by an oscilloscope. The load cell was positioned well above

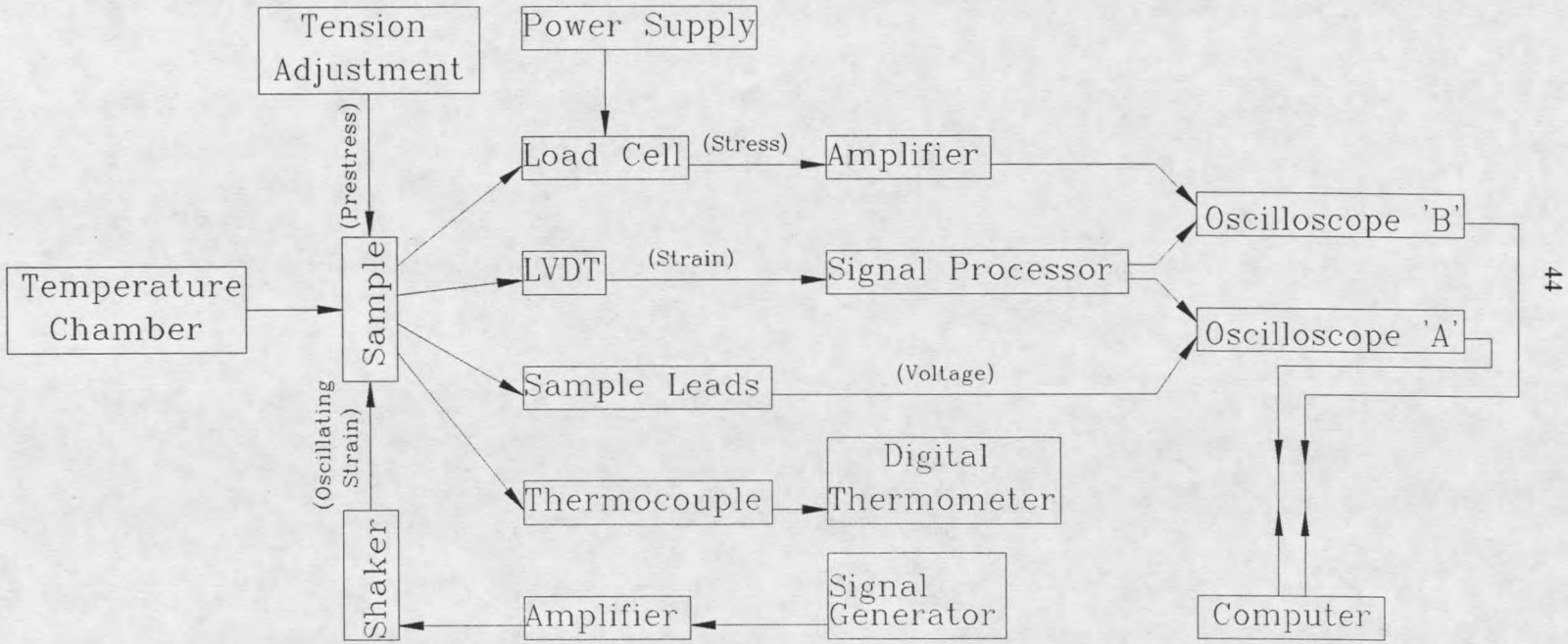


Figure 7-3. Flow chart of experimental setup.

the temperature chamber to insure minimal temperature effects on load measurements.

The temperature chamber used was an Instron model 3111 insulated chamber with a temperature range of room to 204°C. The unit featured a viewing window, circulation fan, and a locking door. The chamber also had two 70 mm holes in the top and bottom to allow the grip support rods to move freely. A type "J" thermocouple mounted inside of the temperature chamber and a Fluke model 2168A digital thermometer was used to monitor the temperature. This method was necessary because the chamber's control dial was inaccurate.

A MB Electronics model PM-50 electrodynamic vibration exciter and model 2250 power amplifier were used to provide prescribed motion to the lower grip. The shaker was capable of producing dynamic motion from 5 to 9000 Hz with a force from 0 to 50 lbs. The 400 watt amplifier powered the shaker with less than 3% total distortion from an input signal provided by a signal generator. The signal generator used in this setup was a Hewlett Packard model 894A multifunction generator and was used to prescribe the frequency and amplitude of the lower grip motion. Voltages produced from the piezoelectric sample during dynamic testing were obtained simply by attaching leads to the electrodes of the samples using conductive epoxy glue. These leads were connected directly to a 1 MΩ, 67 pF oscilloscope probe.

Two Hewlett Packard model 54504A 400 MHz digitizing oscilloscopes were used in the experimental setup to measure voltages. One oscilloscope, hereafter referred to as oscilloscope 'A', was used to measure voltages from both the LVDT and the load cell. Therefore, this oscilloscope recorded voltages proportional to the dynamic stress and

strain versus time for the testing procedure. The other oscilloscope, referred to as oscilloscope 'B', was used to measure voltages from both the LVDT and the sample leads. Thus, this oscilloscope recorded a voltage proportional to the dynamic strain and the voltage produced from the piezoelectric effect versus time. The information gathered by this oscilloscope was used to determine the piezoelectric strain coefficient properties and will be discussed in detail in the appropriate section. The waveforms produced on the oscilloscopes were then transmitted to a personal computer for storage and manipulation using the HP-IB interface standard on the 54504A model.

The 486 IBM compatible computer used in this setup was equipped with a National Instruments GPIB (General Purpose Interface Bus) communications card and NI-488.2 software for Windows 3.1 to communicate with the oscilloscopes. The computer could not only receive data recorded on the oscilloscopes, but was also used to control their operations with BASIC command language programming. This allowed the data acquisition process to be automated.

Set of Experiments

The determination of viscoelastic properties of PVDF from DMTA involved two phases, which each required distinct experimental techniques. The first step used the setup as described in 'Testing Apparatus' and determined the complex viscoelastic functions, $E'(\omega)$, $E''(\omega)$, $D'(\omega)$, and $D''(\omega)$, as well as the temperature dependent shift factor, a_T. This method determined the linear viscoelastic properties of PVDF. The second phase was used to determine the stress dependent shift factor, a_σ, for nonlinear

characterization and required only the results of the 2 hour creep tests, as previously described.

Linear characterization was accomplished by first finding the complex parts of the relaxation modulus, namely $E'(\omega)$ and $E''(\omega)$, and of the creep compliance, namely $D'(\omega)$ and $D''(\omega)$, from Equations 3-30 and 3-33. The independent variables of these equations, σ^o, ε^o, and δ, were determined for a sample subjected to strain controlled dynamic tests at constant temperature, strain amplitude, and pre-stress.

Table 7-1 shows the conditions applied to the testing program. The first row of this table shows that $D'(\omega)$ and $D''(\omega)$ were found for various levels of pre-stress between 20 % and 40 % yield. This was done to verify that DMTA measurements were taken in the linear (stress level independent) range of the material. Because the results, discussed later, were independent of the stress level in this range, it was determined that the other tests used to find the viscoelastic functions as functions frequency and temperature, could safely be conducted at 20% yield pre-stress.

Table 7-1. Test matrix for determination of viscoelastic properties from DMTA

Properties	Values Measured	Frequency (Hz)	Strain Amp. (%)	Temp. (°C)	Pre-stress % Yield
$D_1'(\omega,\sigma)$, $D_1''(\omega,\sigma)$	$\sigma^o,\varepsilon^o,\delta$	1-50	20-40	25.5	20-40
$D_1'(\omega,T)$, $D_1''(\omega,T)$	$\sigma^o,\varepsilon^o,\delta$	1-50	20	25.5-81.1	20
$D_2'(\omega,T)$, $D_2''(\omega,T)$	$\sigma^o,\varepsilon^o,\delta$	1-50	20	24.4-83.8	20

For tests conducted in the 1 direction, the samples were 2.54 cm (in the 2 direction) by 10.16 cm (in the 1 direction) and 28 μm thick. Samples for tests conducted in the 2 direction were 2.54 cm (in the 1 direction) by 10.16 cm (in the 2 direction) and had the same thickness.

For each sample, the dynamic load, displacement, and sample output voltage waveforms were recorded at 20 frequencies between 1 and 50 Hz at even increments. After the data from these waveforms was reduced, values were obtained for stress amplitude, strain amplitude, and the phase angle between stress and strain for the given range of frequencies. These measurements were taken at average constant strain amplitude of 0.070% strain amplitude and 20.31% yield average pre-stress.

One sample, then, maps out $E'(\omega)$, $E''(\omega)$, $D'(\omega)$ and $D''(\omega)$ as calculated from Equations 3-30 and 3-33 from 1 to 50 Hz. However, knowledge of these functions in this range only yields knowledge of E(t) and D(t) from 0.003175 seconds to 0.1587 seconds as given by Equations 3-34 and 3-35. To expand this range, the theory of temperature-frequency correspondence was used. For this reason, the waveforms of stress, strain, and output voltage were measured over the same frequency range, strain amplitude, and pre-stress as described previously, except at higher temperatures. For tests in the 1 direction, the response of 13 different samples dynamically tested at 13 temperatures ranging from 25.5 °C to 81.1 °C was recorded. For tests in the 2 direction, the response of 10 different samples dynamically tested at 10 different temperatures ranging from 24.4 °C to 83.8 °C was recorded. All samples tested at elevated temperatures were allowed 20 minutes under

zero pre-stress and no applied strain to reach a steady state temperature with the temperature chamber.

Data Reduction

The waveforms of load and displacement recorded for each sample (and therefore at each temperature) at each of the 20 frequencies required significant data reduction to obtain the desired quantities. The quantities needed for viscoelastic characterization were σ^o, ε^o, and δ. These values were obtained by curve fitting the waveforms to the equation

$$y = A + B * \sin(C * t + D) \qquad (7\text{-}1)$$

where y is strain or stress, and t is time. The desired values σ^o and ε^o are then twice the value of the coefficient B from their respective waveforms. The phase between stress and strain, δ, becomes the difference between the coefficient D from the stress and strain waveforms.

Computer programs written in BASIC were used to manipulate the stored data to obtain the desired values. Figure 7-4 is a flow chart showing the functions of the programs. Since the communications port of the HP digital oscilloscopes were primarily designed for printing purposes, the data received by the computer was in the form of pixel coordinates, not actual measured voltages and time. Therefore, the first objective of the computer code was to convert the stored data into usable voltage-time values. This was accomplished using information about the number of screen pixels per division and the oscilloscope settings of volts per division for each channel and the seconds per division. Once this was done, the programs converted voltage values into displacement and load

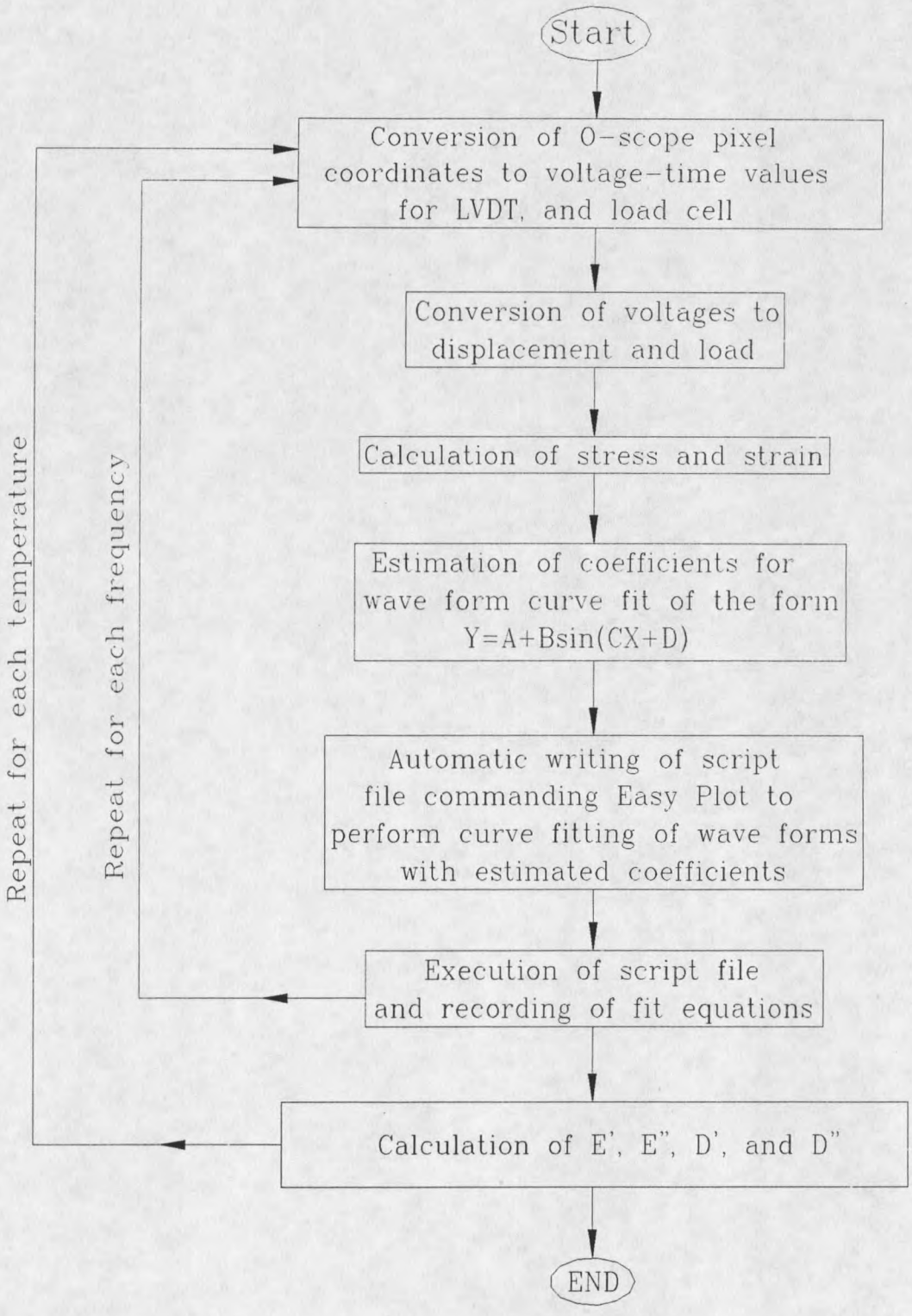


Figure 7-4. Data reduction program flowchart.

values using the correlation equations for the LVDT and the load cell, respectively. From input values for sample width, thickness, and gage length, the displacement and load data were transformed into strain and stress.

The next step of the data reduction programs was to estimate the coefficients of Equation 7-1 for each wave-form recorded for stress and strain at each frequency. This information was necessary for Easy Plot to perform its curve fitting routine. Estimation of A, B, and C coefficients were extracted from the wave-form data by calculating the average value, half of the difference of the maximum and minimum values, and the time between local maximum values, respectively. Estimation of the remaining coefficient was obtained by solving for D in Equation 7-1 using A, B, C, and a the first point of the data file. The programs then wrote a script file containing commands which instruct the Easy Plot program to automatically perform curve fitting routines on all of the wave form data files to Equation 7-1 using the estimated coefficients. The script file also commanded Easy Plot to store the results of the curve fitting to a separate data file. The programs then restructured this file into a format that could be read by Microsoft Excel, a spread sheet program. From σ^o, ε^o, and δ, an Excel template, written for this set of experiments, calculated $E'(\omega)$, $E''(\omega)$, $D'(\omega)$, and $D''(\omega)$ at 20 frequencies from 1 to 50 Hz using Equations 3-30 and 3-33. A complete listing of the programs used in this data reduction process are given in Appendix A.

In order to expand the frequency range as described in Chapter 3, the temperature dependent shift factor, a_T, was then found for the 1 direction by plotting $T/T_o E'(\omega)$ for all temperatures vs. frequency for a reference temperature of 25.5 °C. Each curve was then

shifted horizontally relative to the 25.5 °C curve to obtain the value of a_T for each temperature. These curves then produced a smooth master curve which represented $E'(\omega)$ at 25.5 °C over an expanded range of frequencies. $E''(\omega)$, $D'(\omega)$, and $D''(\omega)$ were then plotted against ωa_T using the same values of a_T that were obtained from $E'(\omega)$. This was done to insure that the same values of a_T were able to produce a smooth master curve for all of the viscoelastic functions, which is one of the requirements for the temperature-frequency correspondence principle to be valid for a particular material. The four master curves were then curve fitted by Easy Plot, so that Equations 3-34 and 3-35 could be used to determine E(t) and D(t). These functions could also be found for other temperatures by using master curves produced from different reference temperatures.

E(t) and D(t) were then found in the 2 direction by the same method that was used to find these functions in the 1 direction. These functions were also found for a reference temperature of 25.5 °C.

The first two hours of the time domain results for the 1 and 2 direction were then verified by using D(t) obtained from DMTA for each direction in Equation 3-23 for the case of constant stress and comparing the results to the respective 2 hour creep test results. The stress values used to produce four creep curves in each direction were used in Equation 3-23 for comparison.

In order to expand the range of accuracy of the linear time domain functions obtained from DMTA for the 1 direction, the nonlinear viscoelastic theory given by Equations 3-38 through 3-40 was used. Because the creep compliance obtained from

DTMA for the 2 direction matches the measured two-hour creep response curves for stress levels up to 76.29 % yield, the nonlinear theory was not applied to the 2 direction.

For the application of the nonlinear theory to the 1 direction, the stress dependent shift factor was found by horizontally shifting the compliance curves obtained from the two-hour creep tests. By shifting these curves relative to the reference stress, 56.9% yield, a master curve was produced, and values of a_T were obtained for each stress level. These values were then used with Equations 3-38 through 3-40, simplified for the case of constant stress, σ_o, to predict nonlinear creep response. For this case, Equation 3-38 reduced to

$$\varepsilon(t) = g_o D_o \sigma_o + g_1 g_2 D_1 \sigma_o \left(\frac{t}{a_\sigma}\right)^n \tag{7-2}$$

where D_1 and n were found by curve fitting $\hat{D}$ to

$$D(t) = D_o + D_1 t^n \tag{7-3}$$

The resulting nonlinear creep response, predicted by a stress level modified creep compliance obtained from DMTA, was then compared to the creep response obtained from the two-hour creep tests in the 1 direction in the nonlinear range.

Linear Results For Direction 1

DMTA testing procedures produced graphs of $E'(\omega)$, $E''(\omega)$, $D'(\omega)$, and $D''(\omega)$ from 1 to 50 Hz for 13 different temperatures in the 1 direction. Figure 7-5 shows sample results for these measurements. This figure represents the storage and loss modulus for

PVDF at 25.5 °C and 22.39% yield as measured with a strain amplitude of 0.075 %. Results for the other measured temperatures are given in Appendix B.

A curve fit representation of all storage modulus curves measured in the 1 direction at 11 different temperatures is given in Figure 7-6. The individual curves that produced this graph were used to determine the temperature dependent shift factor for the 1 direction. The master storage modulus curve and the shift factors are shown in Figures 7-7 and 7-8, respectively. The loss compliance curves for the 1 direction were also shifted by the same values of a_T. This was done not only to obtain the loss compliance function over a wider range than was measured, but also to verify the application of temperature-

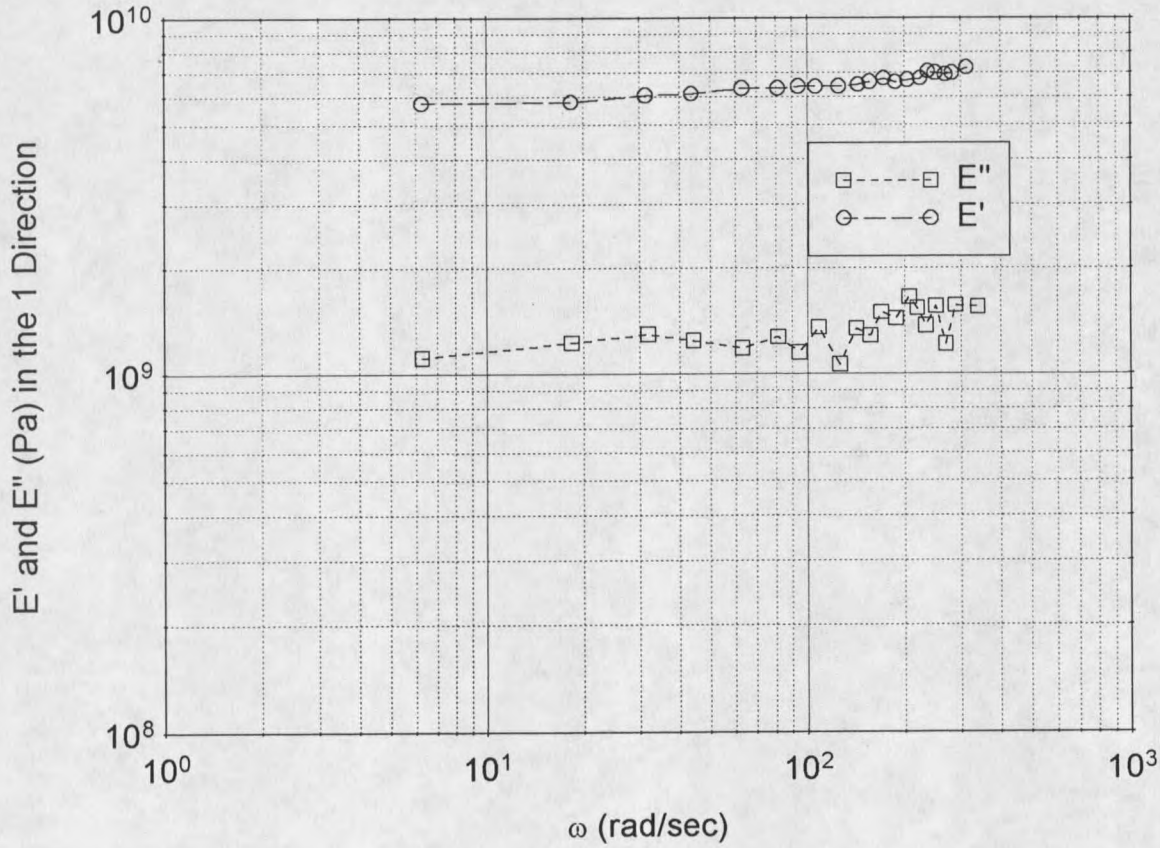


Figure 7-5. Complex modulus components in 1 direction for PVDF at 25.5 °C , 22.39 % yield, and 0.075% strain amplitude.

frequency correspondence theory to PVDF. The master loss compliance curve for the 1 direction is shown in Figure 7-9. Similar results were also obtained for the complex moduli, as well. The fact that the same values of a_T were able to produce smooth master curves for all of the complex viscoelastic functions proved that the use of temperature-frequency correspondence was valid for this material in the 1 direction.

The master curves for $E'(\omega)$, $E''(\omega)$, $D'(\omega)$, and $D''(\omega)$ in the 1 direction were then used to obtain D(t) and E(t) by substituting their respective curve fit equations in to Equations 3-34 and 3-35. The results of the curve fitting efforts to these functions are shown in detail in Appendix C. Discrete calculations of Equations 3-34 and 3-35 were performed by a short FORTRAN program, written for this set of experiments, which

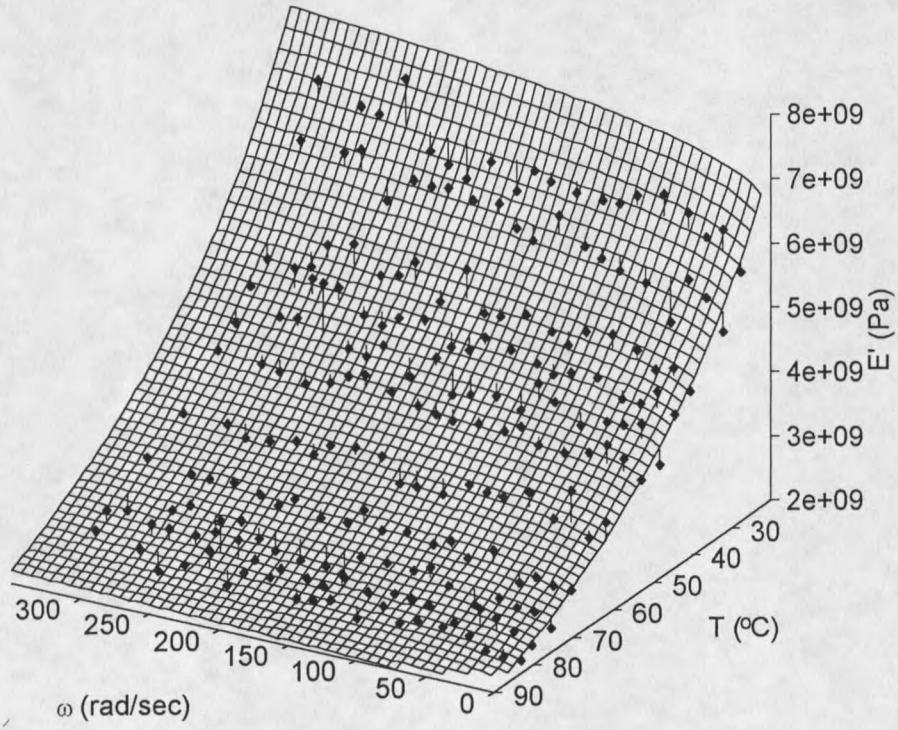


Figure 7-6. Surface fit of storage modulus for PVDF in the 1 direction.

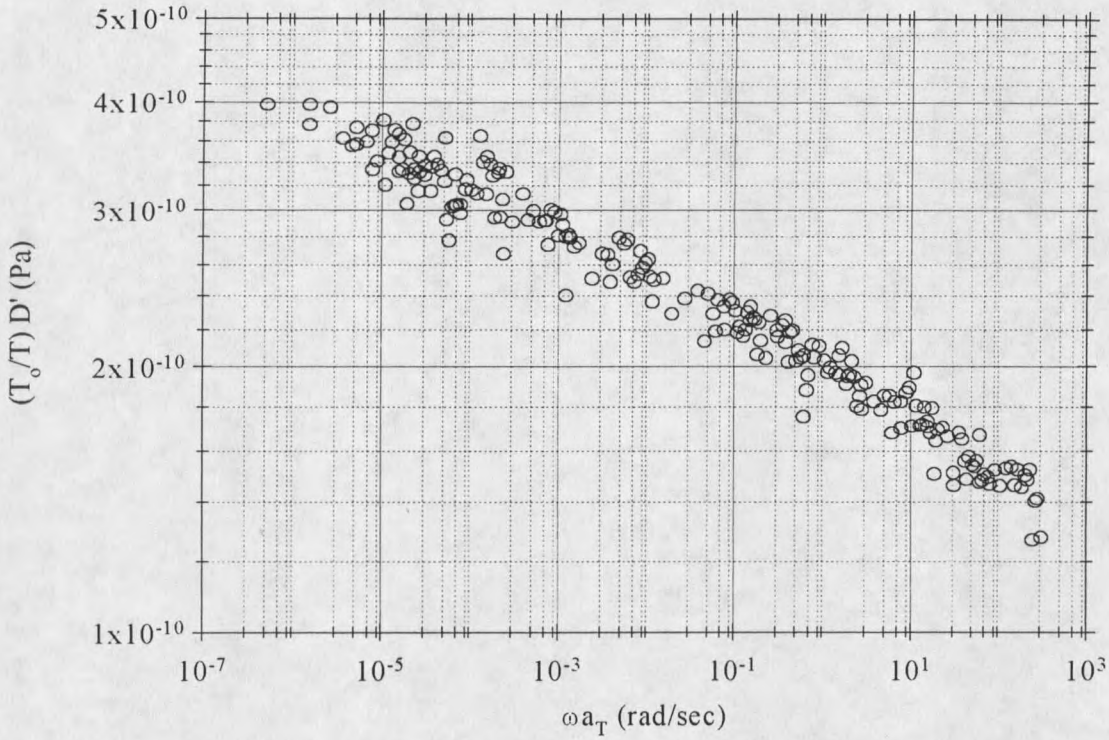


Figure 7-7. Master storage compliance curve for PVDF in the 1 direction.

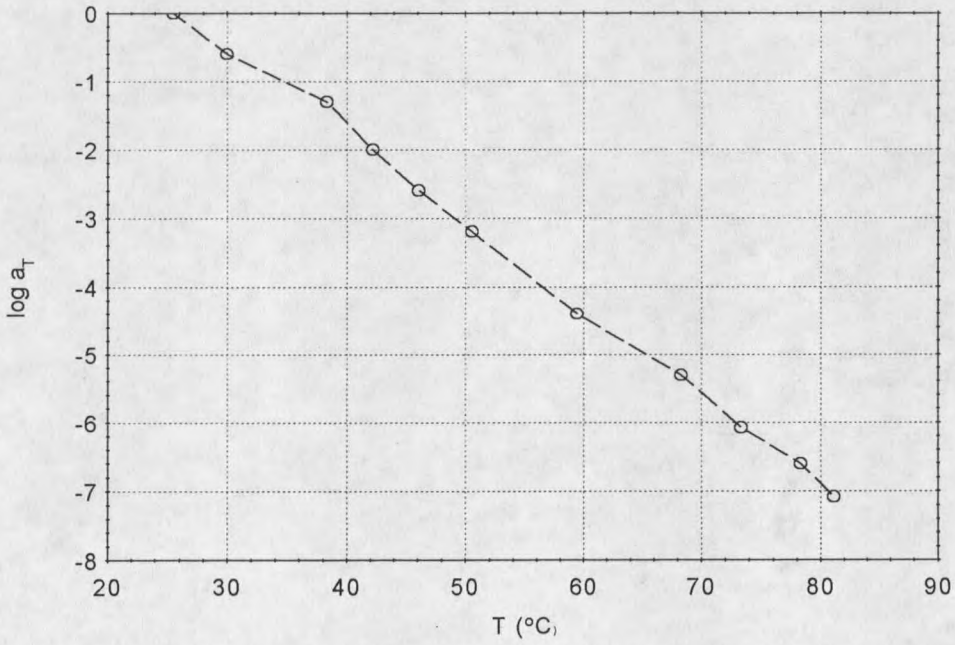


Figure 7-8. Temperature dependent shift factor for the 1 direction.

stored the resulting D(t) and E(t) data points to files. The data points representing D(t) and E(t) were then curve fit to the power law form given by Equation 7-3 to give a continuous time representations. These results can also be found in Appendix C. The first two hours of the obtained creep compliance was then multiplied by several stress values used in the two-hour creep tests and plotted against the results of the same creep curves for comparison. This was done in order to verify a portion of the creep compliance derived from DMTA. As demonstrated by Figure 7-10, the material response to constant

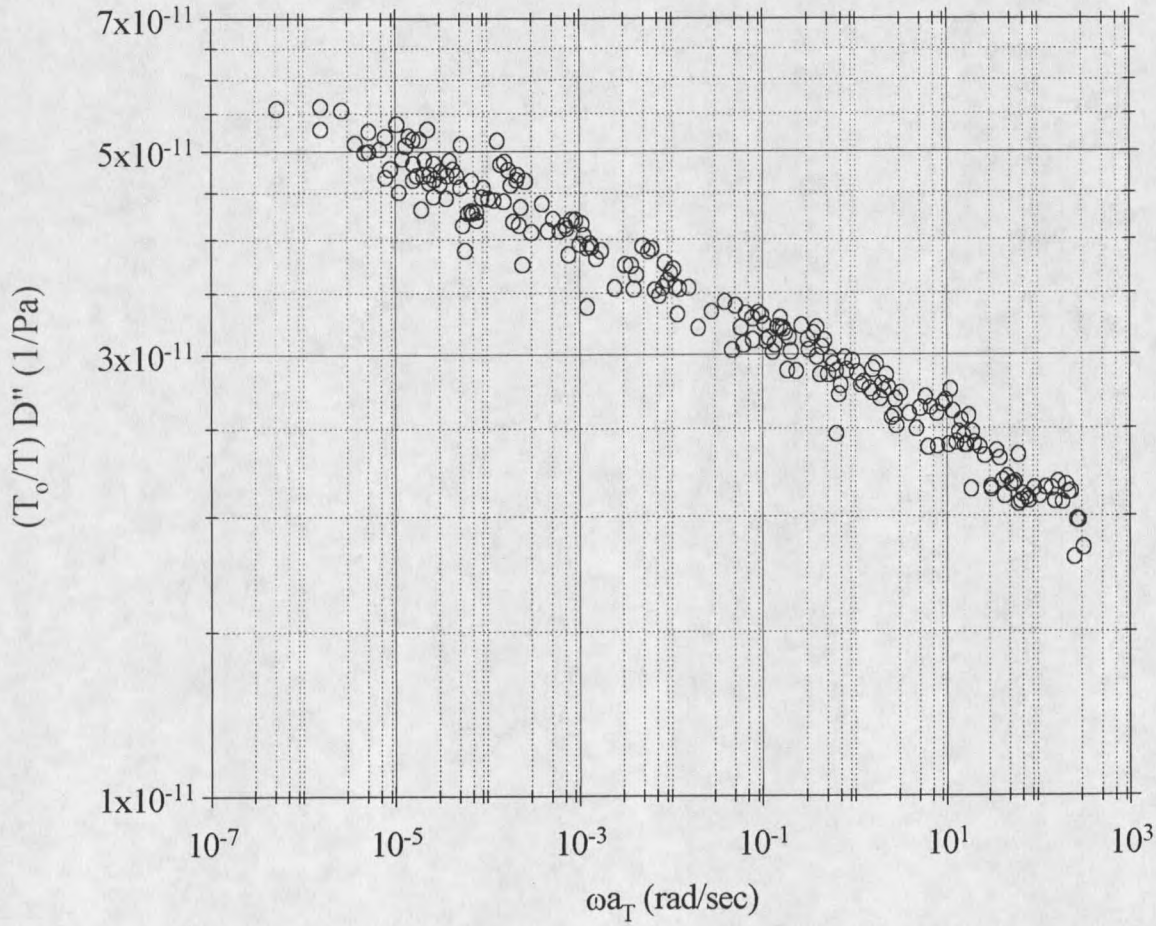


Figure 7-9. Master loss compliance curve for PVDF in the 1 direction.

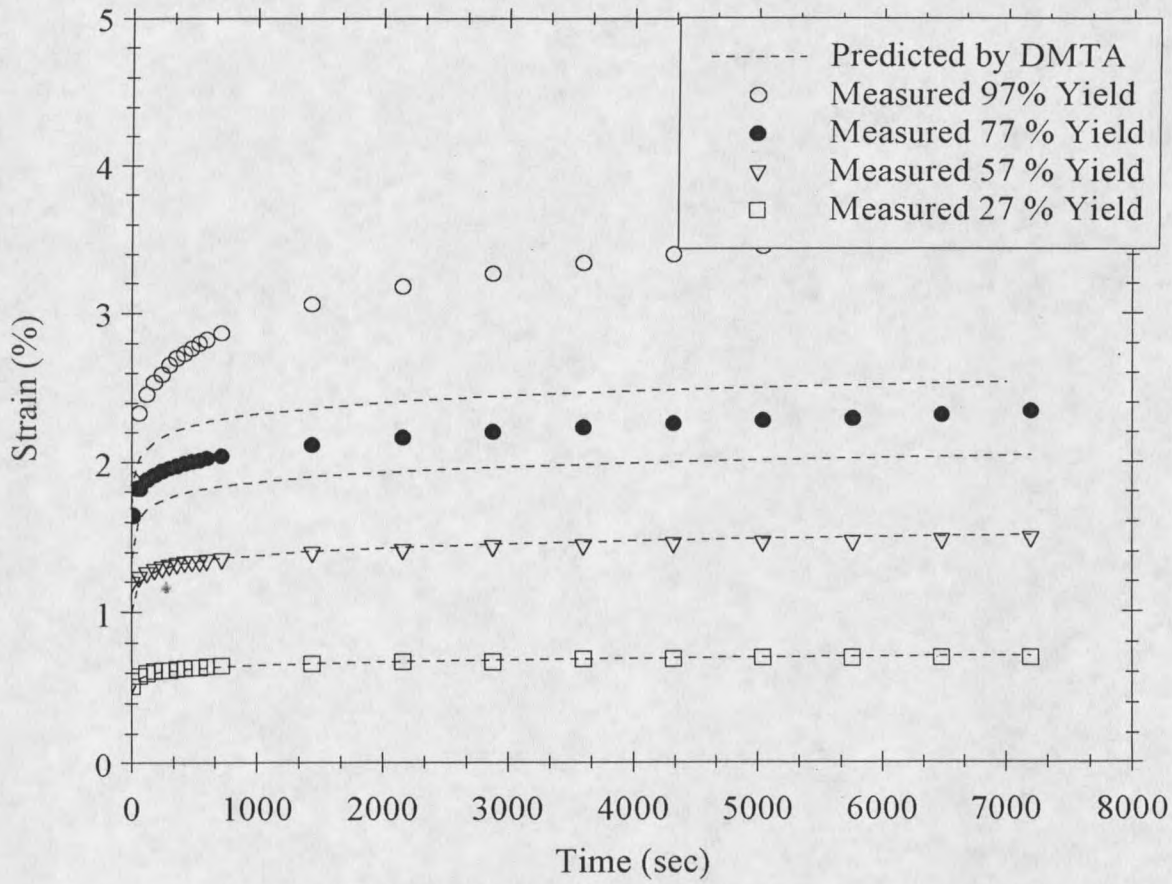


Figure 7-10. DMTA predicted creep compared with traditional creep measurements for PVDF in the 1 direction.

stress predicted by the compliance derived from DMTA is very close to the response measured by creep tests for stress levels at or below 56.9 % yield , the linear range. For stress levels beyond the linear range, the prediction using DMTA derived compliance becomes increasingly inaccurate.

Linear Results For Direction 2

DMTA testing procedures produced graphs of $E'(\omega)$, $E''(\omega)$, $D'(\omega)$, and $D''(\omega)$ from 1 to 50 Hz for 10 different temperatures in the 2 direction. Figure 7-11 shows

sample results for measurements conducted in the 2 direction. The given data was measured at 26.7 °C, 21.09 % yield, and a strain amplitude of 0.068 %. A curve fit representation of all storage modulus curves measured in the 2 direction was also obtained for 10 different temperatures is given in Figure 7-12. The master storage modulus curve and the shift factors for the 2 direction are shown in Figures 7-13 and 7-14, respectively.

The loss compliance curves for the 2 direction were also shifted by the same values of a_T and is shown in Figure 7-15. Similar results were also obtained for the complex moduli, as well. The fact that the same values of a_T were able to produce smooth master curves for all of the complex viscoelastic functions proved that the use of temperature-

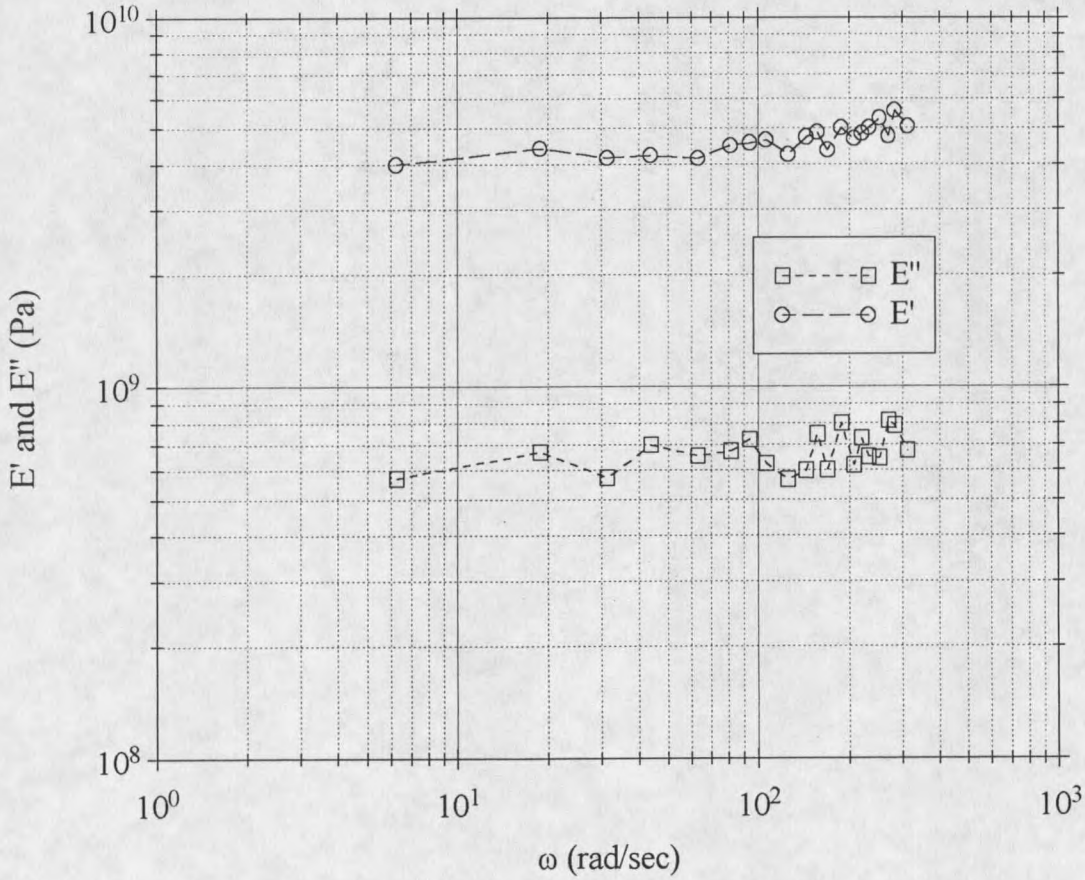


Figure 7-11. Complex modulus components in 2 direction for PVDF at 26.7°C, 21.9 % yield, and 0.068% strain amplitude.

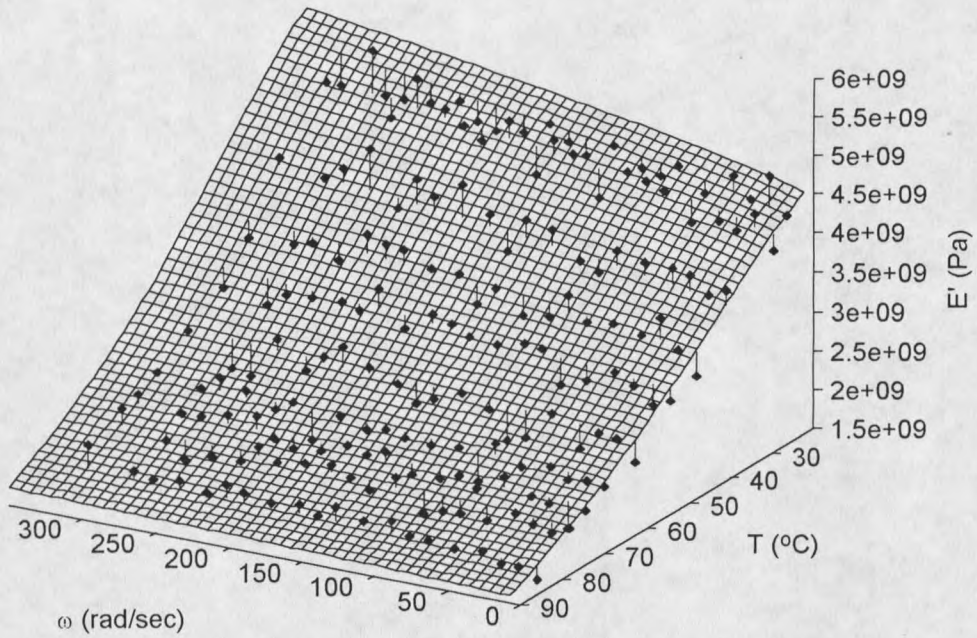


Figure 7-12. Surface fit of storage modulus for PVDF in the 2 direction.

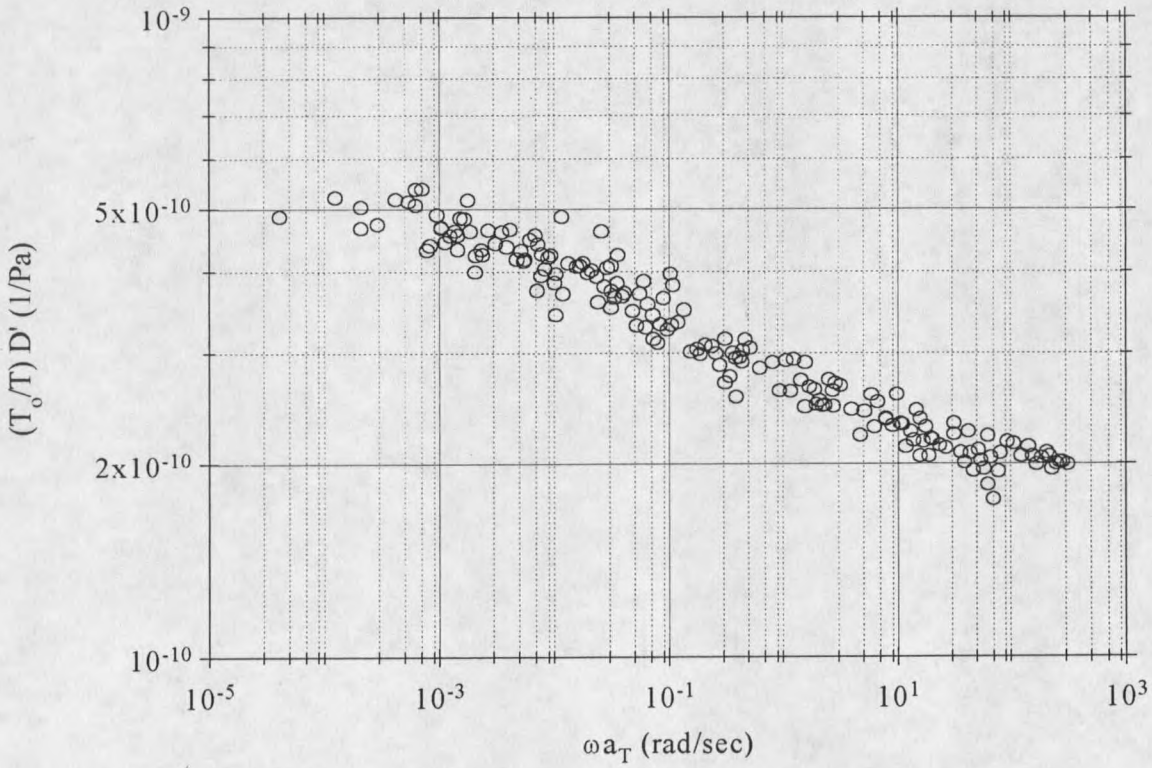


Figure 7-13. Master storage compliance curve for PVDF in the 2 direction.

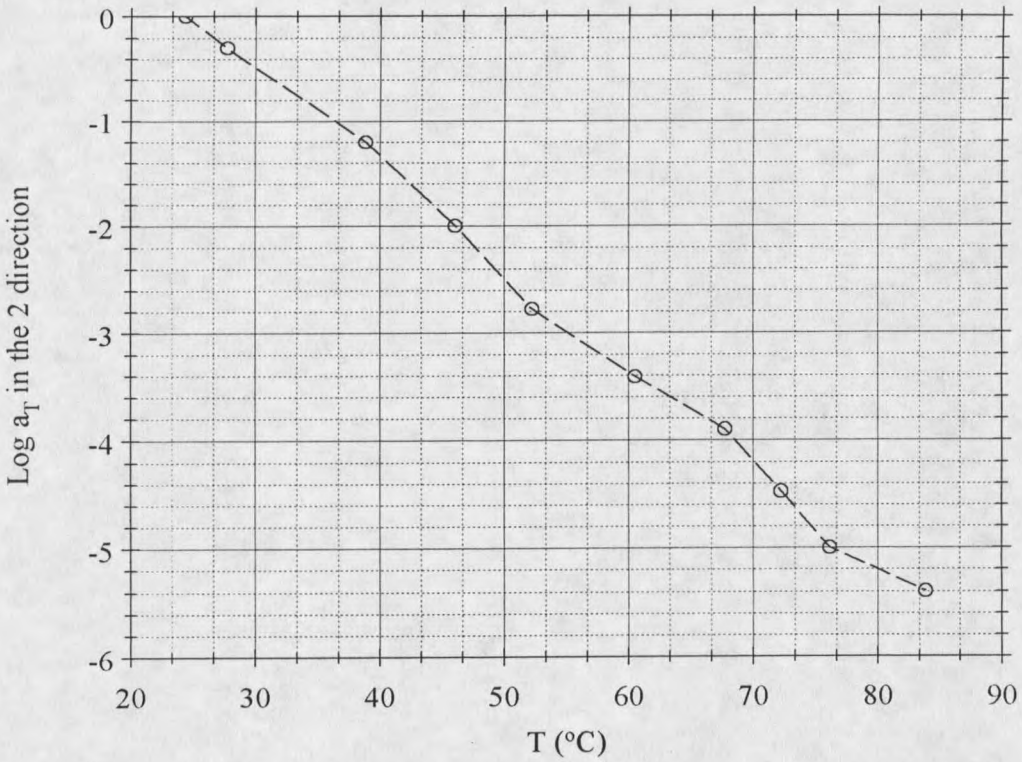


Figure 7-14. Temperature dependent shift factor for the 2 direction.

frequency correspondence was valid for this material in the 2 direction.

The master curves for $E'(\omega)$, $E''(\omega)$, $D'(\omega)$, and $D''(\omega)$ in the 2 direction were then used to obtain D(t) and E(t) by substituting their respective curve fit equations into Equations 3-30 and 3-33. The results of the curve fitting efforts to these functions are shown in detail in Appendix C. Discrete calculations of these curve fit relations into Equations 3-34 and 2-35 were performed by a short FORTRAN program which stored the resulting D(t) and E(t) data points to files. The data points representing D(t) and E(t) in the 2 direction were then curve fit to the power law form given by Equation 7-3 to give a continuous time representations. These results can also be found in Appendix C.

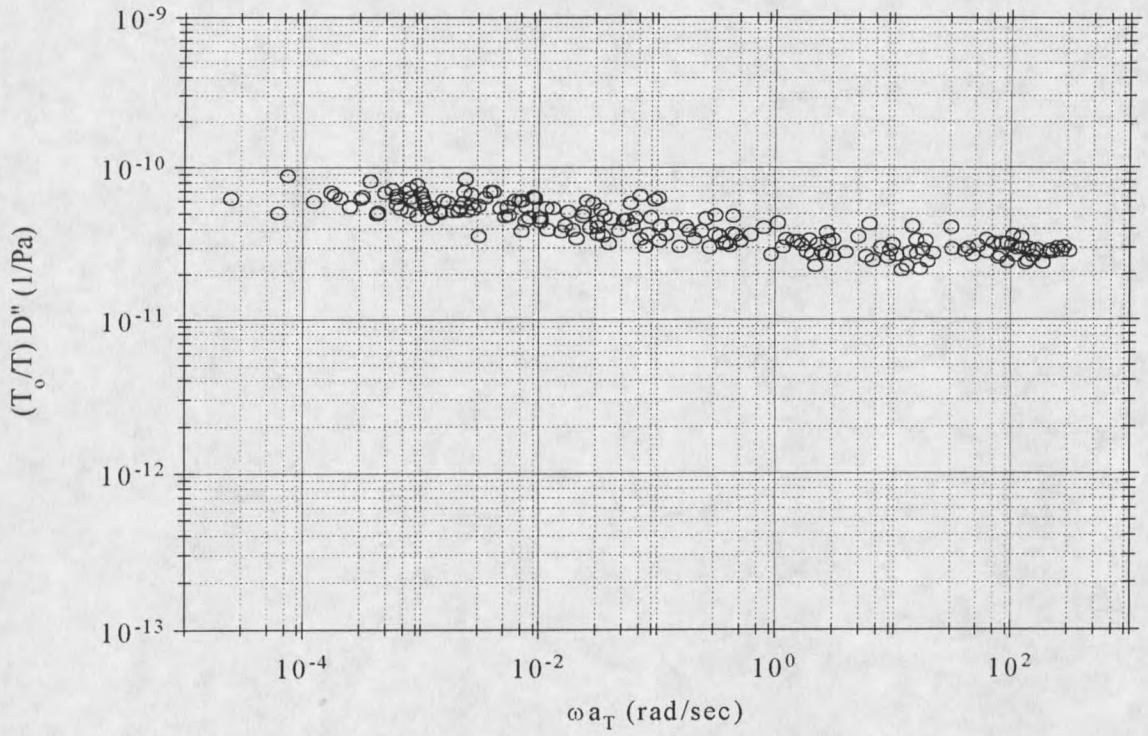


Figure 7-15. Master loss compliance curve for PVDF in the 2 direction.

The first two hours of the creep compliance obtained from DMTA for the 2 direction was then multiplied by several stress values used in the 2 hour creep tests and plotted against the results of the same creep curves for comparison. This was done to verify a portion of the creep compliance derived from DMTA. As demonstrated by Figure 7-16, the material response to constant stress predicted by the compliance derived from DMTA is very close to the response measured by creep tests for stress levels at or below 56.9 % yield, the linear range. For stress levels beyond the linear range, the prediction using DMTA derived compliance becomes increasingly inaccurate.

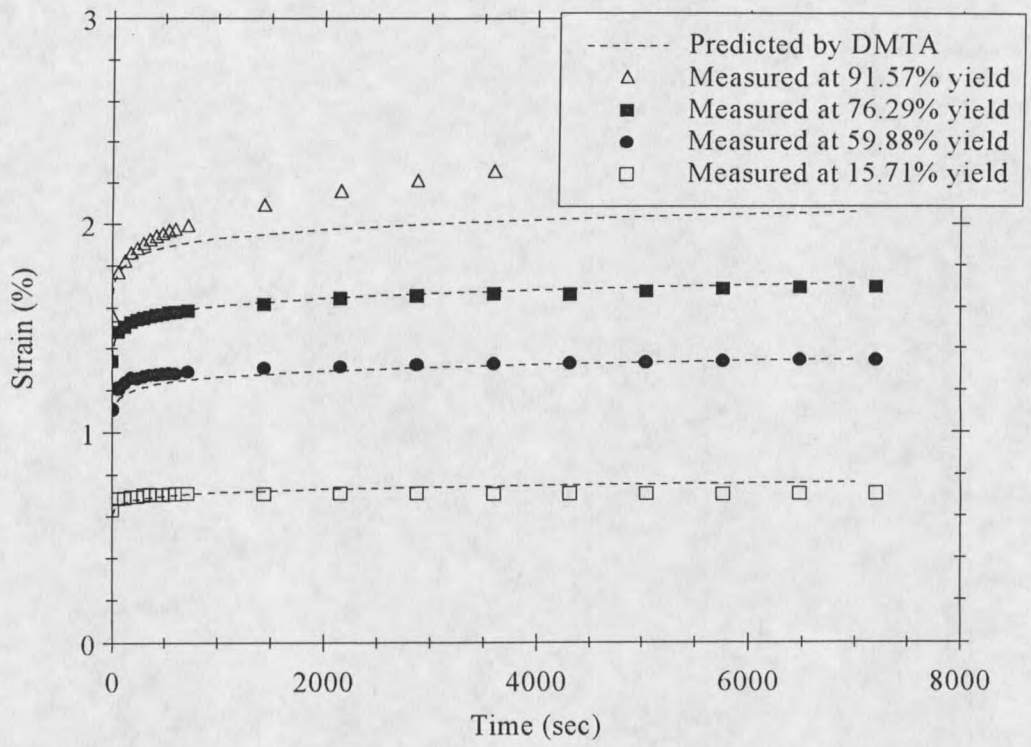


Figure 7-16. DMTA predicted creep compared with traditional creep measurements for PVDF in the 2 direction.

Nonlinear Results for Direction 1

In order to expand the range of accurate material response described by the compliance derived by DMTA beyond linearity, the nonlinear theory described by Equations 3-36 to 3-38 was utilized. For this purpose, the stress dependent shift factor, a_σ, was found in the 1 direction from the experimentally determined normalized creep curves. The corresponding compliance curves were derived from the data shown in Figure 6-3 divided by 100 to obtain D(t). The stress dependent shift factor was found for each stress level above the linear range by shifting the curves in a manner analogous to finding a_T. The reference stress was 56.9% yield. Figure 7-17 shows the stress dependent shift factors found for direction 1. The other parameters appearing in

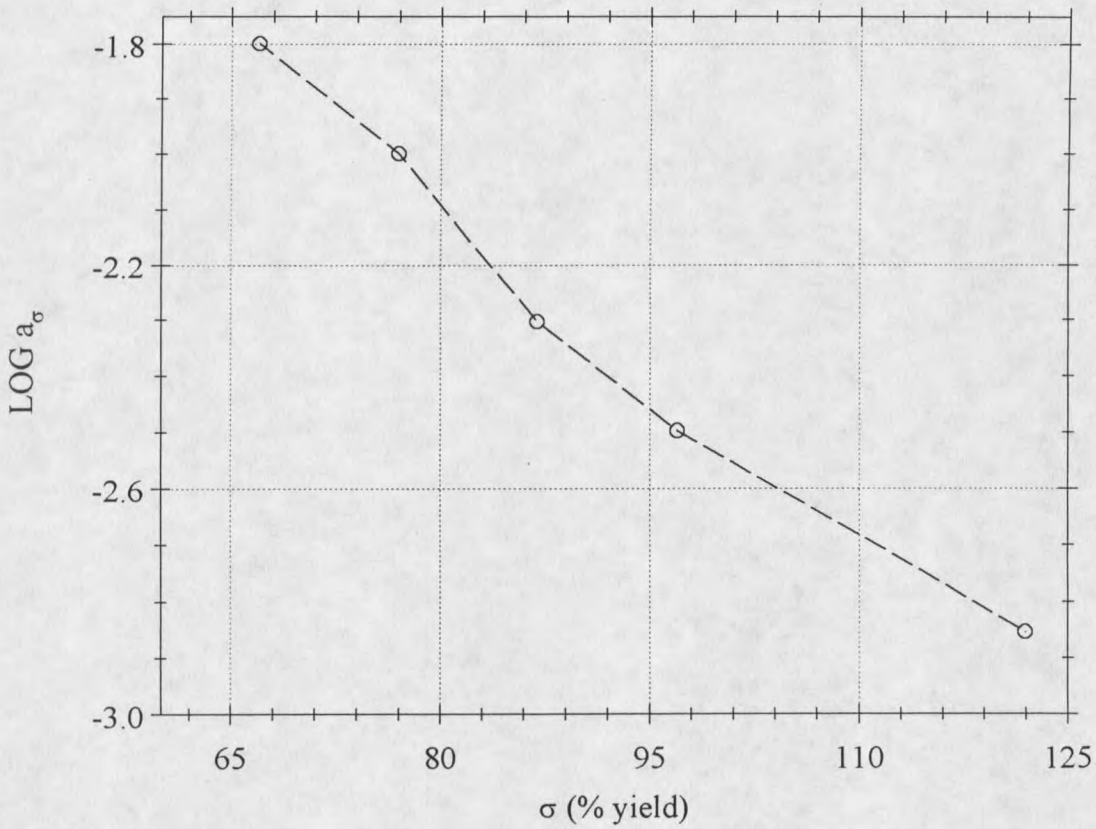


Figure 7-17. Stress dependent shift factor for direction 1.

Equations 3-38 to 3-40, namely g_o, g_1, and g_2, were found from DMTA measurements as described in [16]. In this method, the transient mean strain response is found by subtracting the transient oscillatory response from the measured total strain response. This gives the level of strain as a function of time over which the applied oscillatory strain is applied. This response leads to the development of two equations that can be used to identify g_1 and g_2 for various levels of pre-stress. Thus, g_1 and g_2 can be individually identified by considering the non-oscillatory portion of the strain response that changes with time. However, upon examination of the A coefficient of the curve fit equation given by Equation 7-1 for the measured strain, it was determined that the non-oscillatory portion of the strain response did not change with time for any level of stress up to 97% yield. It

was therefore determined that the value of these two nonlinear parameters, g_1 and g_2, were unity.

The remaining nonlinear parameter, g_o, can be extracted graphically from the compliance derived from DMTA as shown in [16]. This is accomplished by plotting the creep compliance versus t^x where x is varied until the creep compliance forms a straight line. The y intercept of this line is $D_o g_o$, where g_o can be determined by comparing $D_o g_o$ to the value of D_o obtained from creep testing for each stress level. This method resulted in a value for g_o very close to one. Thus, the nonlinear parameters g_0, g_1, and g_2 were all found to be unity for PVDF in the 1 direction.

The stress dependent shift factors were then used with Equation 7-2 to predict nonlinear creep response for stress levels outside the viscoelastic linear range using the creep compliance determined from DMTA. Figure 3-18 shows the results of these predictions together with the linear predictions and measured creep for various stress levels. As shown, the nonlinear prediction using the principle of stress-time correspondence was able to predict creep response for nonlinear stress levels much more accurately than the linear predictions. This demonstrates that the theory of stress-time correspondence is valid of PVDF.

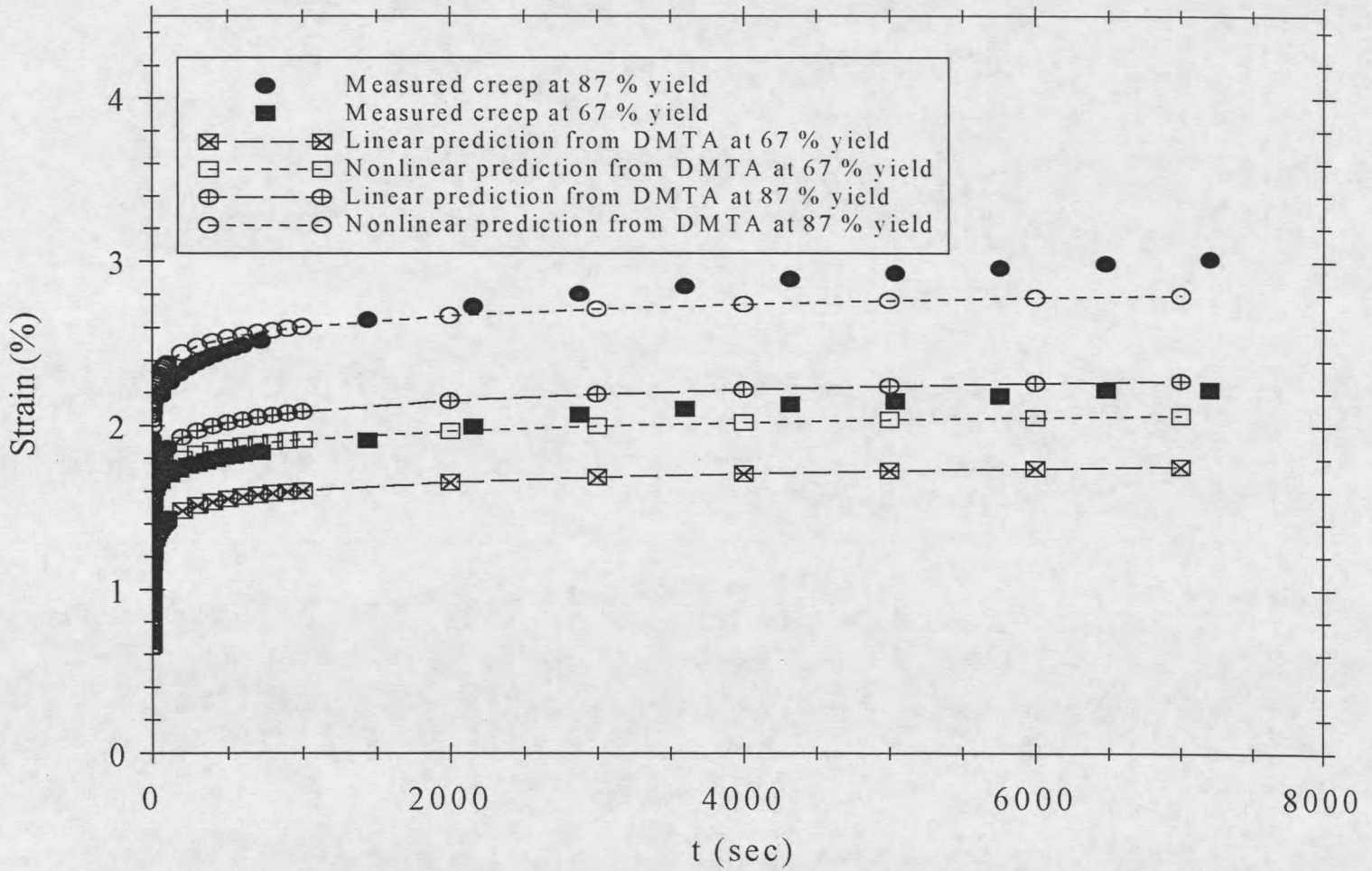


Figure 7-18. Comparison of linear and nonlinear creep predictions from DMTA with measured creep response.

CHAPTER 8

PIEZOELECTRIC STRAIN COEFFICIENTS

Parameters Considered

The properties of the piezoelectric strain coefficients were found by measuring the voltage produced from a sample that is subjected to known strain. Measurements of produced voltage were made in a manner very similar to methods used to determine the viscoelastic properties. By varying the conditions applied to the sample, the piezoelectric strain equations were found as functions of frequency, pre-stress, temperature, and time. The equipment and process required for this test are now described.

Testing Apparatus

The testing apparatus used in this set of experiments was identical to that described for determination of viscoelastic properties. The support structure, experimental setup, and flowchart showing the transducers and accompanying equipment are therefore shown in Figure 7-1 through Figure 7-3, respectively. Detailed descriptions of this setup are given in the Chapter 7. The voltage produced by the sample was measured by connecting leads to the electrodes of the samples with conductive epoxy.

Set of Experiments

For tests conducted in the 1 direction, the samples were 2.54 cm (in the 2 direction) by 10.16 cm (in the 1 direction) and 28 μm thick. 2.54 cm in the 1 direction (between the grips) was electroded over the entire width for measurement of the resulting voltage. Samples for tests conducted in the 2 direction were 2.54 cm (in the 1 direction) by 10.16 cm (in the 2 direction) and had the same thickness. These samples had 5.08 cm in the 2 direction electroded over the entire width. The difference in the electrode area between samples tested in the 1 direction and samples tested in the 2 direction is due to the electrode pattern of the full material sheet from which the samples were cut. 26-gage lead wire was attached to these electrodes with conductive silver epoxy for direct connection to the 1MΩ oscilloscope probe.

Calculation of the piezoelectric strain coefficient properties required knowledge of produced voltage amplitude, oscillatory strain amplitude, and the phase angle between the produced voltage and the strain. These quantities were found for various frequencies, pre-stresses, temperatures, and as functions of time. Table 8-1 shows the conditions applied to the various tests conducted. The first two sets of experiments were used to determine the effect of frequency and temperature on the amplitude of produced voltage under constant strain amplitude and pre-stress in the 1 and 2 directions, respectively. In these experiments, a sample was tested in a specific material direction under constant pre-stress, temperature, and strain amplitude over a sweep of 20 frequencies between 1 and 50 Hz. A new sample was then tested in the same material direction, pre-stress, strain amplitude,

Table 8-1. Test matrix for determination of piezoelectric strain coefficient properties.

Property	Values Measured	Strain Amp. (%)	Frequency (Hz)	Temp. (°C)	Pre-stress (% Yield)	Time (hours)
$d_{31}(\omega,T)$	V^o,ε^o,ϕ	0.070 %	1-50	25.5-81.1	20	—
$d_{32}(\omega,T)$	V^o,ε^o,ϕ	0.070 %	1-50	24.4-83.8	20	—
$d_{31}(\omega,\sigma)$	V^o,ε^o,ϕ	0.070 %	1-50	25.5	23-97	—
$d_{31}(t)$	V^o,ε^o,ϕ	0.070 %	30	25.5	20	48

and frequency range, but at a different temperature. Measurements were made for 13 different temperatures in the 1 material direction from 25.5 °C to 81.1 °C. For measurements in the 2 material direction, the samples were subjected to 10 different temperatures ranging from 24.4°C to 83.8°C. The third set of experiments was conducted to find the effect of pre-stress level on the amplitude of produced voltage subjected to constant strain amplitude and temperature. For this experiment, 16 different pre-stresses were applied between 23 and 97 % yield. The final experiment determined if the amplitude of produced voltage varied with time under constant strain amplitude, temperature, frequency, and pre-stress. In this experiment, the voltage waveform was recorded every 30 minutes for 48 hours with constant strain amplitude of 0.07% strain at 30 Hz and a constant 20% yield pre-stress.

Data Reduction

The waveforms of voltage and displacement recorded for each sample (and therefore each temperature for the first two sets of experiments) at each of the 20 frequencies required significant data reduction to obtain the desired quantities. The quantities needed for piezoelectric strain coefficient characterization were V^o, the maximum produced voltage peak to peak, ε^o, the maximum strain amplitude, and ϕ, the phase angle between voltage and strain. These values were obtained by curve fitting the measured waveforms to Equation 7-1 where y is voltage or strain, and t is time. The desired values V^o and ε^o are then twice the value of the coefficient B from their respective waveforms. The phase angle between voltage and strain, ϕ, becomes the difference between the coefficient D from the voltage and strain waveforms.

The computer programs, written in BASIC command language for this set of experiments, was used to store, manipulate, and curve fit the measured waveforms were the same as those described in the 'Data Reduction' section of Chapter 7 and by Figure 7-4, except for a few minor changes. These changes incorporate the necessary modifications needed to curve fit the waveforms of voltage and strain, instead of stress and strain. Also, the Excel template used to calculate $D'(\omega)$ and $D''(\omega)$ from ε^o, σ^o, and δ was changed to calculate the compensated voltage and compensated phase. These calculations were necessary because the sample produced voltage and phase read by the oscilloscope must be compensated for the sample's capacitance, and the probe's capacitance and resistance,

as shown in Figure 8-1. The actual voltage and phase, V_{act} and ϕ_{act}, are calculated from the voltage and phase as measured by the oscilloscope, V_{osc} and ϕ_{osc}, by

$$|V_{act}| = V_{osc}\sqrt{\left(1+\frac{C_p}{C_s}\right)^2+\left(\frac{1}{\omega R_p C_s}\right)^2} \tag{8-1}$$

$$\phi_{act} = \phi_{osc} - \tan^{-1}\left[\frac{\frac{1}{\omega R_p C_s}}{1+\frac{C_p}{C_s}}\right] \tag{8-2}$$

where C_p is the probe's capacitance, C_s is the sample capacitance, and R_p is the probe's resistance. Thus, V_{act} and ϕ_{act} were found as functions of frequency at each temperature. Having determined V_{act}, and ϕ_{act}, the measured waveforms were reduced to the desired quantities.

The piezoelectric strain constant was then calculated at various conditions using a special case of Equation 3-2. If the resistance of the produced voltage measuring

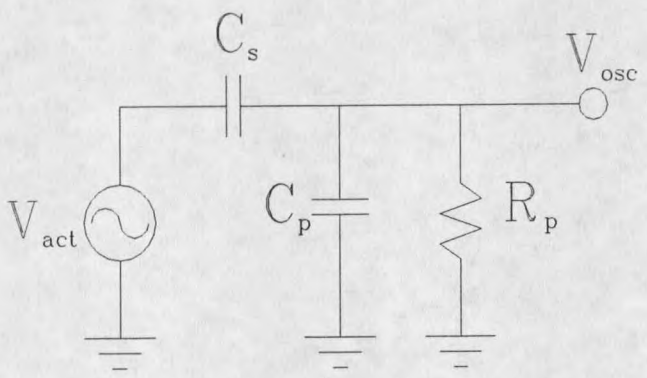


Figure 8-1. Sample produced voltage measuring circuit.

equipment is assumed to be infinite, the electric flux density can be assumed to be zero. With this condition and the case of uniaxially applied strain, Equation 3-2 becomes

$$0 = e_o e_{R_{33}} E_3 + d_{3x} Y_{xx} \varepsilon_{xx} \qquad 8\text{-}3$$

where x is the material direction, 1 or 2, the stress was replaced by the instantaneous Young's modulus, Y_x, multiplied by the applied strain in the direction in question. Also, e_{33} was replaced by the permittivity of free space (8.85×10^{-12} C/(Nm^2)) multiplied by the relative permittivity of the material, e_R. The relative permittivity was given by the material manufacturer, AMP, as 12. Replacing the electric field, E_3, by the compensated voltage amplitude, V_{act}°, divided by the sample thickness, z, the piezoelectric strain constant was then calculated as

$$d_{3x} = \frac{e_o e_{R_{33}} V_{act}^{\circ}}{z Y_{xx} \varepsilon_{xx}^{\circ}} \qquad 8\text{-}4$$

Results

The values of the terms needed to calculate the compensated voltage and phase from Equations 8-1 and 8-2 were measured with a Hewlett Packard LCR meter, model 4262A. The capacitance of the samples and of the probe and its connecting cable were measured at 1 kHz excitation. The average capacitance of samples constructed for testing in the 1 direction was 1.98 nF, whereas samples constructed for testing in the 2 direction had an average capacitance of 3.82 nF due to differences in average electrode size. The capacitance and resistance of the probe and connecting cable were measured to be 67.1 pF and 1.015 MΩ, respectively.

Figure 8-2 shows the compensated and uncompensated voltage and phase angle (between voltage and strain) for a sample tested at 25.5 °C and 22.39% yield as measured with a strain amplitude of 0.075 %. This figure shows quite clearly that the compensated voltage and phase angle do not depend on frequency.. The average produced voltage was calculated to be 31.4 V peak to peak and the average phase angle was found to be zero within a small experimental error. Figure 8-3 shows the compensated and uncompensated voltage and phase angle for a sample in the 2 direction measured at 26.7 °C, 21.09 % yield, and with a strain amplitude of 0.068 %. These results also show the compensated voltage and phase angle are independent of frequency with an average voltage of 3.42 V p-p and a zero average phase angle. Note that both the measured and compensated voltages for the samples tested in the 2 direction are multiplied by 10 in this figure for clarity. The results shown are typical of the measurements taken at room temperature and 20% yield pre-stress.

Similar measurements were then taken at elevated temperatures for both the 1 and 2 material directions. Appendix D provides the voltage and phase angle results for the other temperatures tested in both material directions. Figure 8-4 summarizes the results of these measurements. This figure shows the produced voltage, normalized with respect to the strain amplitude and averaged over the measured frequencies, for each of the measured temperatures has nearly the same value. Thus, the produced voltage is independent of temperature in the measured range. Because the piezoelectric strain coefficient, calculated using Equation 8-4, is a function of the voltage amplitude and the applied strain amplitude

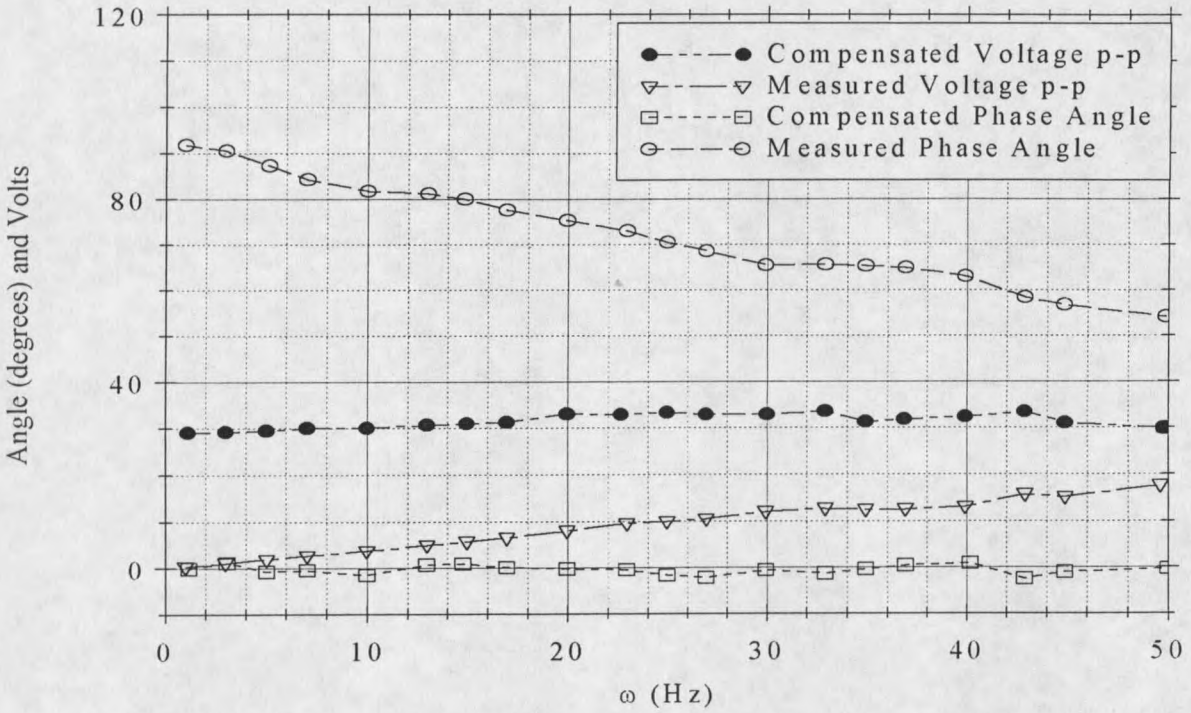


Figure 8-2. Voltage produced from tests conducted in the 1 direction.

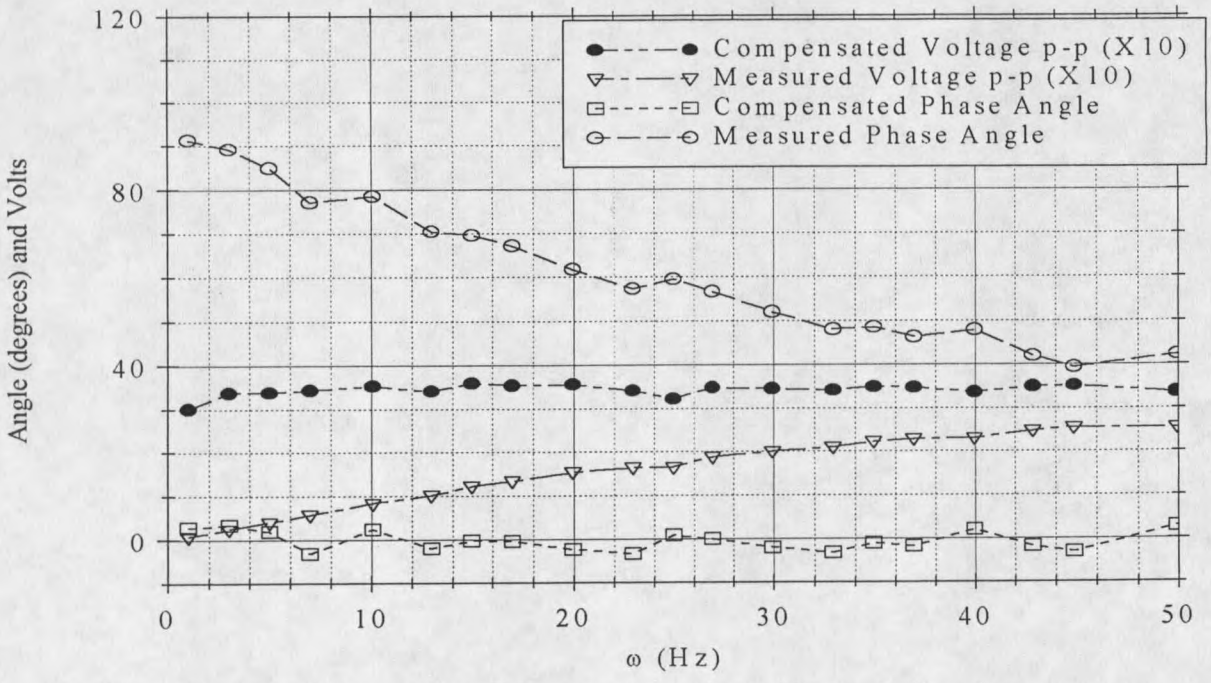


Figure 8-3. Voltage produced from tests conducted in the 2 direction.

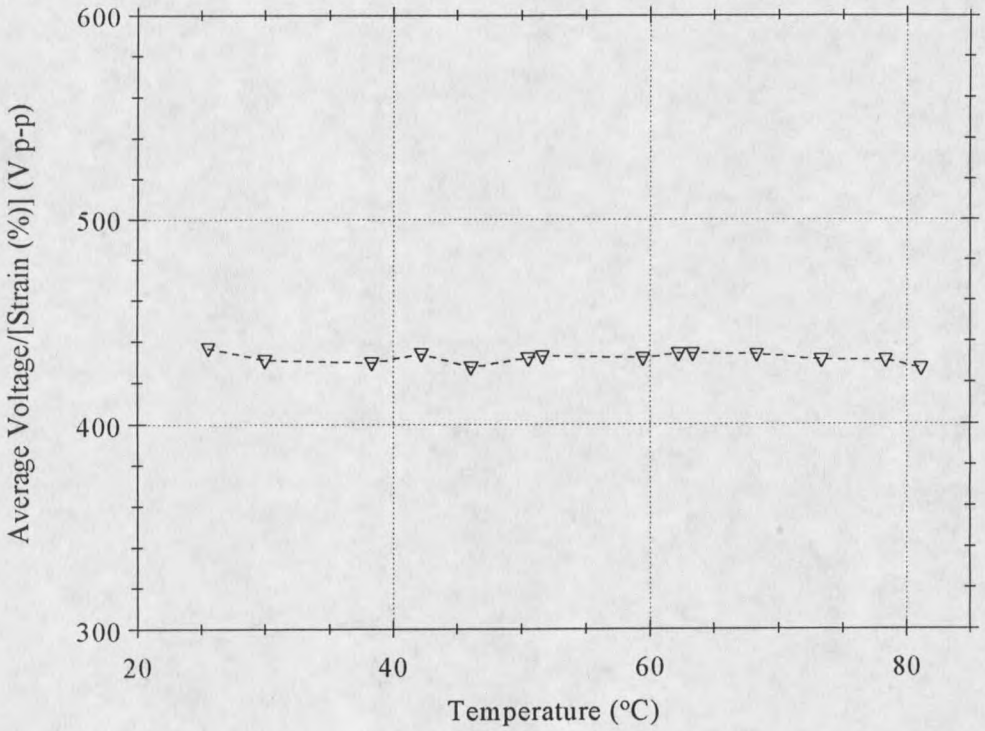


Figure 8-4. Average normalized produced voltage amplitude in the 1 direction for various temperatures at constant pre-stress, strain amplitude, and frequency range.

only, the piezoelectric strain coefficient is also not a function of temperature in the measured range.

In order to determine if the piezoelectric strain coefficient was a function of pre-stress, measurements of samples subjected to constant strain amplitude, temperature, and frequency range for various pre-stress levels were taken. Figure 8-5 summarizes the results of this set of tests. This figure shows the produced voltage amplitude averaged over the measured range of frequencies for each of the measured pre-stresses. As demonstrated in the figure, the level of pre-stress did not significantly affect the amplitude of produced voltage, and respectively the value of the piezoelectric strain coefficient.

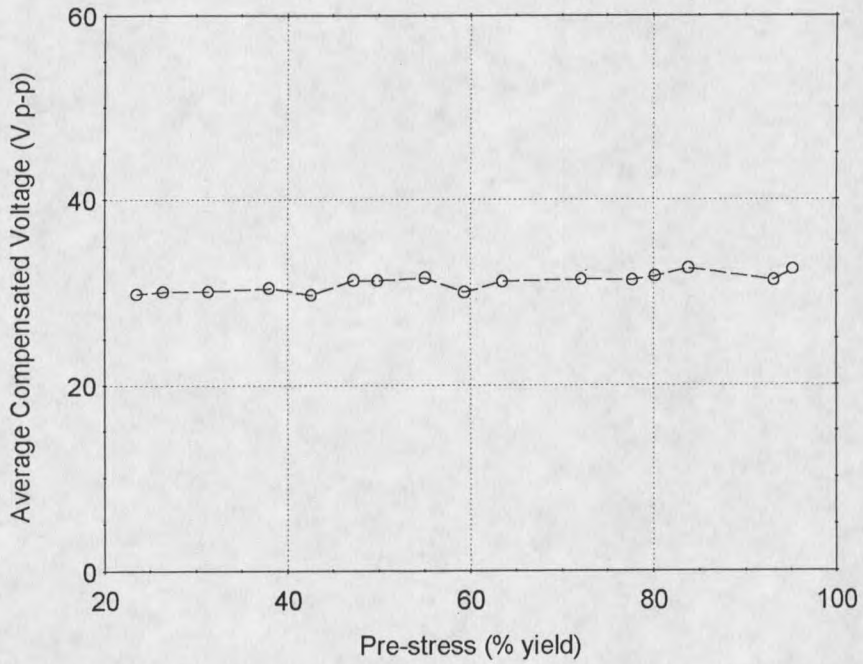


Figure 8-5. Average produced voltage amplitude in the 1 direction for various pre-stress values at constant temperature, strain amplitude, and frequency range.

The final test conducted was used to determine the time dependence of the piezoelectric strain coefficient. The results of this test indicate that the produced voltage from constant strain amplitude, frequency, temperature, and pre-stress does not vary significantly with time, as illustrated by Figure 8-6.

In summary, the tests conducted to determine the dependence of the piezoelectric strain coefficient show that this coefficient is not a function of frequency, temperature, pre-stress level, or time *in the applied parameter ranges*. For this reason, the coefficients d_{31} and d_{32} were calculated using the averages of voltage amplitude and strain amplitude

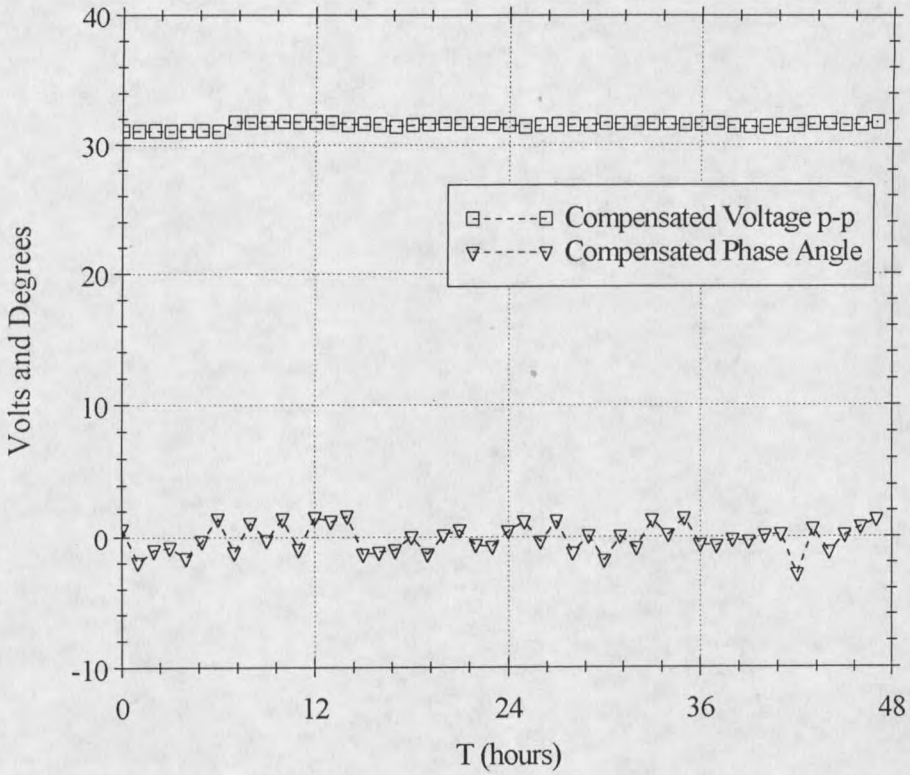


Figure 8-6. Produced voltage amplitude in the 1 direction for various time values at constant temperature, strain amplitude, frequency, and pre-stress.

over all of the tests listed above to obtain the most accurate values possible. Using these overall average values, the coefficients d_{31} and d_{32} were calculated from Equation 8-4 to be 26.24×10^{-12} ($C/m^2/N/m^2$) or (m/m/V/m) and 2.61×10^{-12} ($C/m^2/N/m^2$), respectively.

CHAPTER 9

DISCUSSION AND CONCLUSIONS

Instantaneous Elastic Properties

The results of the set of experiments conducted to determine the instantaneous elastic properties of PVDF are shown in Table 9-1. The Young's modulus values agree quite well with other published values. Values found [17] for Young's modulus values Y_1 and Y_2 using a Rheovibron mechanical spectrometer were 2.56×10^9 Pa and 2.61×10^9 Pa, respectively. This reference lists a single Poisson's ratio of 0.392 while reference 3 lists a Poisson's ratio ν_{21} value of 0.34, which shows that the obtained values for this parameter are reasonable. Other values are near the average of values published by other sources [3, 4].

In addition to the benefit of knowing the instantaneous elastic properties, an important conclusion can be drawn from the results of this set of experiments. This is the fact that the mechanical properties of stretched and poled PVDF thin films are anisotropic. Although the values listed in Table 9-1 do not suggest a high degree of anisotropic behavior, the stress-strain diagrams shown in Figures 5-1 and 5-3 show a high degree of anisotropy. Therefore, it was concluded that other experiments required tests to be conducted for each preferred material direction.

Table 9-1. Instantaneous elastic properties of PVDF.

Property	Symbol	Value	Units
Young's Modulus	Y_1 Y_2	$2.7x10^9$ $2.5x10^9$	Pa Pa
Yield Stress	σ_{Y1} σ_{Y2}	$4.5x10^7$ $3.9x10^7$	Pa Pa
Yield Strain	ε_{Y1} ε_{Y2}	1.8 1.4	% %
Ultimate Stress	σ_{U1} σ_{U2}	$3.5x10^8$ $5.0x10^7$	Pa Pa
Ultimate Strain	ε_{U1} ε_{U2}	16.9 2.5	% %
Poisson's Ratio	ν_{12} ν_{21}	0.326 0.348	

Significance of Time Dependent Effects

The results of the tests outlines in Chapter 6 clearly show the mechanical response of PVDF in thin film form is time dependent. Both the magnitude of initial response and the rate of creep measured in tests conducted in the 1 direction compare very well to the creep curve given by [3]. The results again show the anisotropic behavior of PVDF in that the time dependency of the 2 direction is much less than the time dependency in the 1 direction. These tests also provide information about the linear range of viscoelastic theory. The linear range for material direction 1 was determined to be up to 56.9% yield, whereas the linear range found for material direction 2 was up to 76.3% yield. The conclusions drawn form the results of this set of tests were that simple elastic modeling of this material is insufficient, and further testing was required to fully model the time dependency of PVDF.

Viscoelastic Constitutive Modeling Based on DMTA

The results of the set of experiments described in Chapter 7 show that the time dependent behavior of PVDF can successfully be described by the theory of viscoelasticity. The complete response of the material can be described by the relaxation modulus or the creep compliance for a particular material direction. Table 9-2 shows these experimentally determined functions for their known time ranges. These functions could also be found for any temperature between 25.5 °C and 81.1 °C in the 1 direction and between 24.4 °C and 83.8 °C in the 2 direction from the obtained data. Comparison of the first two hours of the creep compliance in both directions obtained by DMTA with the creep compliance found for both directions from static creep tests show that these functions are accurate.

Table 9-2. Summary of results of viscoelastic characterization at room temperature.

Function	Symbol	Curve Fit Relation	Units	Range (sec)
Creep Compliance	$D_1(t)$	= 3.514e-10 + 5.018e-11 · t ^ 0.107	Pa^{-1}	.0032<t<1.915e6
	$D_2(t)$	= 3.206e-10 + 1.112e-10 · t ^ 0.085	Pa^{-1}	.0032<t<4.001e4
Relaxation Modulus	$E_1(t)$	= 8.467e+8 + 3.303e+9 · t ^ -0.098	Pa	.0032<t<1.915e6
	$E_2(t)$	= 8.895e+8 + 3.976e+9 · t ^ -0.065	Pa	.0032<t<4.001e4

These functions, along with the values of instantaneous Poisson's ratios can be used to replace s_{11}, s_{12}, and s_{22} in the compliance matrix of Equation 3-9 as described in Chapter 3. This matrix will be critical in understanding the passive damping characteristics of the actuator described in Chapter 1.

For these tests, it was also demonstrated that the theory of temperature-frequency correspondence was valid for this material. The results also indicate that Schapery's nonlinear viscoelastic theory and the stress-time correspondence principle works comparatively well [17, 18, 19] for this material to describe nonlinear behavior.

Piezoelectric Strain Coefficients

From results of the set of experiments described in Chapter 8, it was also concluded that the terms appearing in the piezoelectric strain matrix are independent of the parameters tested in the range considered. Specifically, these coefficients are independent of frequency from 1 to 50 Hz, of temperature from 24.4 °C to 83.8 °C, of pre-stress from 23 to 97 % yield, and of time up to 48 hours at room temperature. Averages over all of the tests were therefore used to calculate the coefficient values. The piezoelectric strain coefficients d_{31} and d_{32} were found to be 26.24×10^{-12} ($C/m^2/N/m^2$) and 2.61×10^{-12} ($C/m^2/N/m^2$), respectively.

These values compare very well with the d_{31} and d_{32} values provided by the manufacturer, which are 23×10^{-12} ($C/m^2/N/m^2$) and 3×10^{-12} ($C/m^2/N/m^2$), respectively. The remaining coefficient, d_{33}, could not be found in the same manner as was used to find d_{31} and d_{32}. This would require an applied strain in the 3 material direction and measurement of the produced voltage in the 3 direction. Because of the thickness of the film, this procedure would require a very accurate prescribed strain with an amplitude of only a few microns. This could not be achieved with the current hardware and transducers. Also, very specialized sample grips would have to be constructed that could apply the prescribed strain in the 3 direction. Alternatively, an electric field could be applied in the 3 direction,

and the resulting change in thickness measured to find the desired coefficient. However, this would also require real time measurement of the sample thickness, which is not possible with the current hardware and transducers. For these reasons, d_{33} was not measured. If the assumption is made that this coefficient is also not a function of frequency, temperature, pre-stress, and time in the applied ranges as d_{31} and d_{32} are, then it can be considered constant and the value provided by the manufacturer, -33×10^{-12} ($C/m^2/N/m^2$), can be used.

Future Work

There are two recommendations by the author for the continued research of the material properties of PVDF. First, the shear modulus, G_{12}, should be found as a function of time. This would conclude the characterization necessary to complete the compliance matrix for orthotropic materials in the case of plane stress. Because the direct shear modulus is very difficult to measure [4], this process would require a unique experimental setup with precise transducers. A method for determining shear properties of PVDF by observing shear resonances induced through direct electrical coupling has been outlined [13] and may prove useful in this endeavor.

Also, a mirostructural study of the material's properties would be helpful in understanding the highly anisotropic behavior of PVDF. This process could make possible better understanding of the phenomenology behind the observed macro-scale properties.

REFERENCES

1. Sessler, G. M., "Polymeric Electrets" in *Electrical Properties of Polymers* (D. A. Seanor, Ed.), Academic Press, 1982, pp. 241-284

2. Dunn, P. and Carr, S. "A Historical Perspective on the Occurrence of Piezoelectricity in Materials", *MRS Bulletin*, February, 1989.

3. AMP SENSORS, technical product report, Valley Forge, PA 19482

4. Broadhurst, M., Davis, G., McKinney, J., "Piezoelectricity and Pyroelectricity in Polyvinylidene Fluoride - A Model", *Journal of Applied Physics*, Vol. 49, No. 10, October 1978, pp. 4992-4997.

5. Halvorsen, D., "Putting Piezo Polymer Film to Work", *Machine Design*, July 25, 1994, pp. 47-51.

6. G.E. Johnson, L. C. Blyler, G.R. Crane, and C. Gieniewski, "Thermal Piezoelectric Stability of Poled Uniaxially and Biaxially-Oriented Polyvinylidene Fluoride", *Ferroelectrics*, Vol. 32, No. 43, 1981.

7. Ikeda, Takuro "Fundamentals of Piezoelectricity", Oxford Science Publications, 1990.

8. Williams, J. G., "Stress Analysis of Polymers", 2nd Edition, John Wiley & Sons, New York, 1980

9. Rabotnov, Yu. N."Creep Problems in Structural Members",Wiley Interscience, 1969.

10. Ferry, John D.,"Viscoelastic Properties of Polymers", John Wiley & Sons, Third ed., 1980.

11. Flugge, Wilhelm, "Viscoelasticity", Blaisdell Publishing, Waltham, Massachusetts, 1967.

12. McCrum, N.G., Buckley, C.P., Bucknall, C.B., "Principles of Polymer Engineering", Oxford University Press, New York, 1988.

13. Strganac, T., Letton, A., Payne, D., and Biskup, B., "Characterization of Nonlinear Viscoelastic Behavior Using a Dynamic Mechanical Approach", *AIAA Journal*, Vol. 33, No. 5, May 1995, pp. 904-910.

14. Schapery, R. A., "On the Characterization of Nonlinear Viscoelastic Materials", *Polymer Engineering and Science*, July, 1969, Vol. 9, No. 4, pp. 295-310.

15. Schapery, R. A., "An Engineering Theory of Nonlinear Viscoelasticity with Applications", *Int. Journal of Solid Structures*, 1966, Vol. 2, pp. 407-425.

16. Golden, H., and Strganac, T., "A Test and Analysis Protocol to Rapidly Characterize Nonlinear Viscoelastic Properties of Balloon Materials" *AIAA Journal* 96-0572, 34th Aerospace Sciences Meeting and Exhibit, Reno, NV, January 15-18.

17. Kepler, R.G., Anderson, R.A., "Piezoelectricity and Pyroelectricity in Polyvinylidene Fluoride", *Journal of Applied Physics*, Vol. 49, No. 8, August 1978, pp. 4490-4494.

18. Payne, D., Biskup, B., Letton, A., and Strganac, T., "Viscoelastic Characterization of thin-film Materials Using a Dynamic Mechanical Approach", *AIAA Journal* 94-0641, 32nd Aerospace Sciences Meeting and Exhibit, Reno, NV, January 10-13.

19. Strganac, T., Williams, K., Farrow, D., Rock, N., and Letton, A., "Characterization of Polymer Films Retrieved for NASA's Long Duration Exposure Facility" *Journal of Spacecraft and Rockets* Vol. 32, No. 2, pp. 502-50.

APPENDICES

APPENDIX A

DATA REDUCTION PROGRAMS

Figure A-1. Program #1

This program:

1. Opens and reads data files containing waveforms in pixel coordinate form.
2. Converts pixel coordinates to voltage and time values.
3. Converts voltages into load and displacement.
4. Converts load and displacement into stress and strain.
5. Saves values to data files.

```
2 CLS
3 off1 = 0
4 INPUT "Enter directory name to manipulate (d:\re\in\**):",
FILE$
6 INPUT "Enter the sample width (in.) : ", w
8 INPUT "Enter the sample gage length (in.) : ", l
20 FOR f = 1 TO 20
23    FOR ab = 1 TO 2
24       flag = 0: n = 1
25       GOSUB 4000
38       DIM times1(4000), coord1(4000), coord2(4000),
TIMES2(4000)
40       INPUT #1, TIMES$, COORD$
50       IF TIMES$ = "IN;IP 0" THEN 2000
60       TIMES$ = MID$(TIMES$, 4, 5)
65       IF flag = 0 THEN times1(n) = VAL(TIMES$)
68       IF flag = 1 THEN TIMES2(n) = VAL(TIMES$)
80       COORD$ = LEFT$(COORD$, 4)
90       IF flag = 0 THEN coord1(n) = VAL(COORD$)
100      IF flag = 1 THEN coord2(n) = VAL(COORD$)
200      REM PRINT times1(n), coord1(n), TIMES2(n),
coord2(n), times1(n) - TIMES2(n)
210      n = n + 1
220      GOTO 40
2000     IF flag = 1 THEN 3000
2002     FOR t = 1 TO 14
2005        INPUT #1, I$
2010     NEXT t
2012     flag = 1
2015     REM PRINT
"*************************************************"
2017     n = 0
2020     GOTO 60
3000     CLOSE #1
3005     OPEN "O", #1, "d:\re\out\" + FILE$ + "\" + p$ + aob$
+ ".OUT"
3010     FOR I = 1 TO n - 3
3012        REM transform numbers into time and mvolts
```

```
3015        times1(I) = times1(I) * msd * 10 / 450
3020        coord1(I) = ((coord1(I) - 4080) * mvd1 * 4 /
4080) + off1
3040        coord2(I) = ((coord2(I) - 4080) * mvd2 * 4 /
4080) + off2
3045        REM transform mvolts into displacement (in.) and
load(lbs.)
3050        coord1(I) = .099 * coord1(I) / 1000
3055        IF ab = 1 THEN coord2(I) = (24.48 * coord2(I) /
100 - .98654 - .4675)
3058        IF ab = 2 THEN coord2(I) = coord2(I) / 1000
3060        REM transform disp. and load into
strain(in/100in)and stress(psi*10^3)
3065        coord1(I) = (coord1(I) / 1) * 100
3070        IF ab = 1 THEN coord2(I) = (coord2(I) / (w *
.0011023)) / 1000
3080        WRITE #1, times1(I), coord1(I), coord2(I)
3090     NEXT I
3095     CLOSE #1
3100   NEXT ab
3105 NEXT f
3200 END
4000 REM REMOVE FIRST BLOCK AND INPUT SCOPE SETTINGS
4002 IF ab = 1 THEN aob$ = "a"
4004 IF ab = 2 THEN aob$ = "b"
4006 k$ = STR$(f)
4008 p$ = RIGHT$(k$, LEN(k$) - 1)
4010 OPEN "I", #1, "d:\re\in\" + FILE$ + "\" + p$ + aob$ +
".TXT"
4020 INPUT #1, d$
4025 REM PRINT d$
4030 IF d$ = "LB" THEN 4050
4035 GOTO 4020
4050 INPUT #1, a$
4055 INPUT #1, a$
4060 INPUT #1, a$
4062 INPUT #1, a$
4064 a$ = LEFT$(a$, 22)
4066 a$ = RIGHT$(a$, 6)
4068 msd = VAL(a$)
4070 INPUT #1, a$
4075 INPUT #1, a$
4080 INPUT #1, a$
4085 INPUT #1, a$
4090 INPUT #1, a$
4092 INPUT #1, a$
4094 a$ = LEFT$(a$, 21)
4096 a$ = RIGHT$(a$, 5)
4098 mvd1 = VAL(a$)
4100 INPUT #1, a$
```

```
4102 INPUT #1, a$
4104 INPUT #1, b$
4106 b$ = LEFT$(b$, 21)
4108 b$ = RIGHT$(b$, 5)
4110 mvd2 = VAL(b$)
4112 IF ab = 2 AND mvd2 = 5 THEN mvd2 = 5000
4114 IF ab = 2 AND mvd2 = 1 THEN mvd2 = 1000
4116 INPUT #1, a$
4118 IF a$ = "IN;IP 0" THEN 5000
4120 GOTO 4116
5000 IF msd = 1 THEN msd = 1000
5002 PRINT f, msd, mvd1, mvd2
5005 FOR u = 1 TO 9
5010   INPUT #1, a$
5015 NEXT u
5020 RETURN
```

Figure A-2. Program #2

This program:

1. Opens and reads the data file created by program1.
2. Estimates curve fit coefficient from waveform data points.
3. Writes Easy Plot script file which performs curve fitting routine using the estimated coefficients.
4. Saves the results of curve fitting routine to a data file.

```
2 PI = 3.14159
□
4 CLS : PRINT : PRINT

6 PRINT "ENTER THE DIRECTORY THAT THE DATA IS IN"
8 PRINT " (d:\RE\OUT\xxxx\1A.OUT)"
10 INPUT DIP$
11 DIP$ = RIGHT$(DIP$, LEN(DIP$))
12 DIM T(500), C(2, 500)

14 OPEN "d:\RE\EP\" + DIP$ + "\A.EP" FOR OUTPUT AS #1
16 OPEN "d:\RE\EP\" + DIP$ + "\B.EP" FOR OUTPUT AS #2
18 FOR O = 1 TO 20: REM FOR 20 FREQUENCIES IN EACH SAMPLE
20 FOR P = 1 TO 2: REM FOR 2 FILES FOR EACH FREQUENCY
22 SCREEN 12: CLS : col = 1
24 REM READ DATA FILE
26 IF P = 1 THEN E$ = "A"
28 IF P = 2 THEN E$ = "B"
30 FILE$ = RIGHT$(STR$(O), LEN(STR$(O)) - 1) + E$
32 PRINT "   FILE= "; FILE$
35 OPEN "I", #3, "d:\RE\OUT\" + DIP$ + "\" + FILE$ + ".OUT"
40 FOR I = 1 TO 498
50    INPUT #3, T(I), C(1, I), C(2, I)
60 NEXT I
70 CLOSE #3
80 FOR R = 1 TO 2: REM FOR 2 CURVES IN EACH FILE

100 REM CALCULATE INITIAL GUESS FOR A....THE AVERAGE
105 AVE = 0
110 FOR I = 1 TO 498
120    AVE = AVE + C(R, I)
130 NEXT I
140 AVE = AVE / 498
150 A = AVE
162 A = INT(A * 100) / 100

800 REM CALCULATE INITIAL GUESS FOR B...THE AMPLITUDE
810 MAX = C(R, 1)
```

```
820 MIN = C(R, 1)
830 FOR I = 1 TO 498
840  IF C(R, I) > MAX THEN MAX = C(R, I)
850  IF C(R, I) < MIN THEN MIN = C(R, I)
860 NEXT I
870 AMP = (MAX - MIN) - .4 * (MAX - MIN)
880 B = AMP / 2
892 B = INT(B * 100) / 100
895 GOSUB 7000

900 REM CALCULATE INITIAL GUESS FOR C...THE FREQUENCY
905 IF O = 1 THEN C = .36
910 IF O = 2 THEN C = 1.08
915 IF O = 3 THEN C = 1.8
920 IF O = 4 THEN C = 2.52
925 IF O = 5 THEN C = 3.6
930 IF O = 6 THEN C = 4.68
935 IF O = 7 THEN C = 5.4
940 IF O = 8 THEN C = 6.12
945 IF O = 9 THEN C = 7.2
950 IF O = 10 THEN C = 8.28
955 IF O = 11 THEN C = 9
960 IF O = 12 THEN C = 9.72
965 IF O = 13 THEN C = 10.8
970 IF O = 14 THEN C = 11.88
975 IF O = 15 THEN C = 12.6
980 IF O = 16 THEN C = 13.32
985 IF O = 17 THEN C = 14.4
990 IF O = 18 THEN C = 15.48
994 IF O = 19 THEN C = 16.2
996 IF O = 20 THEN C = 18

2000 REM CALCULATE INITIAL GUESS FOR D....THE PHASE
2010 AVE2 = 0
2020 FOR I = 1 TO 5
2030   AVE2 = AVE2 + C(R, I)
2040 NEXT I
2042 SLOPE = 1
2044 IF C(R, 6) < C(R, 1) THEN SLOPE = -1
2050 AVE2 = AVE2 / 5
2060 ARG = (AVE2 - A) / B
2062 S = 1
2063 IF ARG < 0 THEN
2064    ARG = -ARG
2066    S = -1
2068 END IF
2070 IF ARG > 1 THEN PRINT ARG: ARG = .999
2075 D = PI / 2 - (1 - ARG) ^ .5 * (1.57072 + -.21211 * ARG
+ .07426 * ARG ^ 2 + -.01872 * ARG ^ 3)
2080 D = S * D * 180 / PI
```

```
2082 PRINT "SLOPE= "; SLOPE
2085 IF SLOPE = -1 THEN D = 180 - D
2095 D = INT(D * 100) / 100
2098 PRINT
3000 PRINT "   INITIAL GUESSES FOR CURVE "; R
3005 IF D < 0 THEN D = 360 + D
3010 PRINT A, B, C, D
5550 PRINT "A="; A, "B="; B, "C="; C, "D="; D
5575 IF R = 1 THEN A1 = A: B1 = B: C1 = C: D1 = D
5577 IF R = 1 THEN PRINT : PRINT : PRINT : PRINT : PRINT :
PRINT
5580 NEXT R
5585 G$ = "/FO " + CHR$(34) + "d:\RE\OUT\" + DIP$ + "\" +
FILE$ + ".OUT" + CHR$(34)
5590 IF P = 1 THEN
5592    PRINT #1, G$
5594 ELSE
5596    PRINT #2, G$
5598 END IF
5600 G$ = "/ET G " + CHR$(34) + FILE$ + CHR$(34)
5605 IF P = 1 THEN
5607    PRINT #1, G$
5610 ELSE
5612    PRINT #2, G$
5614 END IF
5620 G$ = "/OA N"
5625 IF P = 1 THEN
5630    PRINT #1, G$
5632 ELSE
5634    PRINT #2, G$
5638 END IF
5640 G$ = "/SM"
5645 IF P = 1 THEN
5650    PRINT #1, G$
5652 ELSE
5654    PRINT #2, G$
5656 END IF
5660 G$ = "/SD"
5665 IF P = 1 THEN
5670    PRINT #1, G$
5672 ELSE
5674    PRINT #2, G$
5676 END IF
5680 G$ = "/SR A"
5685 IF P = 1 THEN
5690    PRINT #1, G$
5692 ELSE
5694    PRINT #2, G$
5696 END IF
```

```
5700 G$ = "/TC 2 " + CHR$(34) + "Y=A+B*SIN(C*X+D)" +
CHR$(34) + " " + STR$(A1) + " " + STR$(B1) + " " + STR$(C1)
+ " " + STR$(D1) + " " + CHR$(34) + "d:\RE\EP\" + DIP$ + "\"
+ FILE$ + RIGHT$(STR$(1), 1) + ".FIT" + CHR$(34)
5705 IF P = 1 THEN
5710    PRINT #1, G$
5712 ELSE
5715    PRINT #2, G$
5717 END IF
5720 G$ = "/TC 2 " + CHR$(34) + "Y=A+B*SIN(C*X+D)" +
CHR$(34) + " " + STR$(A) + " " + STR$(B) + " " + STR$(C) + "
" + STR$(D) + " " + CHR$(34) + "d:\RE\EP\" + DIP$ + "\" +
FILE$ + RIGHT$(STR$(2), 1) + ".FIT" + CHR$(34)
5725 IF P = 1 THEN
5730    PRINT #1, G$
5732 ELSE
5735    PRINT #2, G$
5737 END IF
5740 G$ = "/FC"
5745 IF P = 1 THEN
5750    PRINT #1, G$
5752 ELSE
5755    PRINT #2, G$
5757 END IF
5780 FOR Y = 1 TO 100000: NEXT Y
5880 NEXT P
5890 NEXT O
5895 CLOSE #1
5897 CLOSE #2
5900 END

7000 REM PLOT THE DATA
7020 FOR N = 1 TO 497
7100   FR = T(498) / 650
7110   IF B > 1 THEN FY = 120 / (5 * B): GOTO 7130
7120   FY = 120
7130   LINE (T(N) / FR, 450 - (C(R, N) * FY + 100))-(T(N +
1) / FR, 450 - (C(R, N + 1) * FY + 100)), col
7150 NEXT N
7160 col = col + 2
7200 RETURN
```

Figure A-3. Program #3

This program:

1. Opens and reads the data file created by program 2.
2. Reformats the file to one that can be read by Excel.
3. Saves the data file.

```
3 CLS : DIM A1(30), A2(30), B1(30), B2(30), C1(30), C2(30),
D1(30), D2(30)
5 INPUT "enter the directory (d:\re\ep\XX\1a.fit)", SN$
6 INPUT "enter file suffix (a or b):", AOB$
8 OPEN "d:\RE\EXCEL\" + SN$ + "\" + AOB$ + ".EXL" FOR OUTPUT
AS #2
10 FOR f = 1 TO 20
15    FOR R = 1 TO 2
18       fwn$ = STR$(f)
20       FBN$ = RIGHT$(fwn$, LEN(fwn$) - 1)
22       G$ = "d:\RE\EP\" + SN$ + "\" + FBN$ + AOB$ +
RIGHT$(STR$(R), 1) + ".FIT"
25       OPEN "I", #1, G$
30       INPUT #1, A$
32       INPUT #1, A$
40       INPUT #1, A$
100      INPUT #1, A$
110      INPUT #1, B$
120      INPUT #1, C$
130      INPUT #1, D$
140      A$ = RIGHT$(A$, LEN(A$) - 4)
150      A$ = LEFT$(A$, 22)
155      A = VAL(A$)
160      A = INT(A * 1000) / 1000
165      B$ = RIGHT$(B$, LEN(B$) - 4)
170      B$ = LEFT$(B$, 22)
175      B = VAL(B$)
180      B = INT(B * 1000) / 1000
185      C$ = RIGHT$(C$, LEN(C$) - 4)
190      C$ = LEFT$(C$, 22)
195      C = VAL(C$)
200      C = INT(C * 1000) / 1000
205      D$ = RIGHT$(D$, LEN(D$) - 4)
210      D$ = LEFT$(D$, 22)
215      D = VAL(D$)
220      D = INT(D * 1000) / 1000
250      PRINT A, B, C, D
255      IF B < 0 THEN B = -B: D = D + 180
```

```
260       IF D > 360 THEN D = D - 360
265       IF R = 2 AND D2 > D AND AOB$ = "A" THEN D = D + 360
270       IF R = 2 AND D2 < D AND AOB$ = "B" THEN D2 = D2 +
360
285       IF R = 1 THEN A2 = A: B2 = B: C2 = C: D2 = D
290       CLOSE #1
300     NEXT R
350     WRITE #2, A, B, C, D, A2, B2, C2, D2
800   NEXT f
890   CLOSE #2
900 END
```

APPENDIX B

REPRESENTATIVE SET OF VISCOELASTIC FUNCTION PLOTS

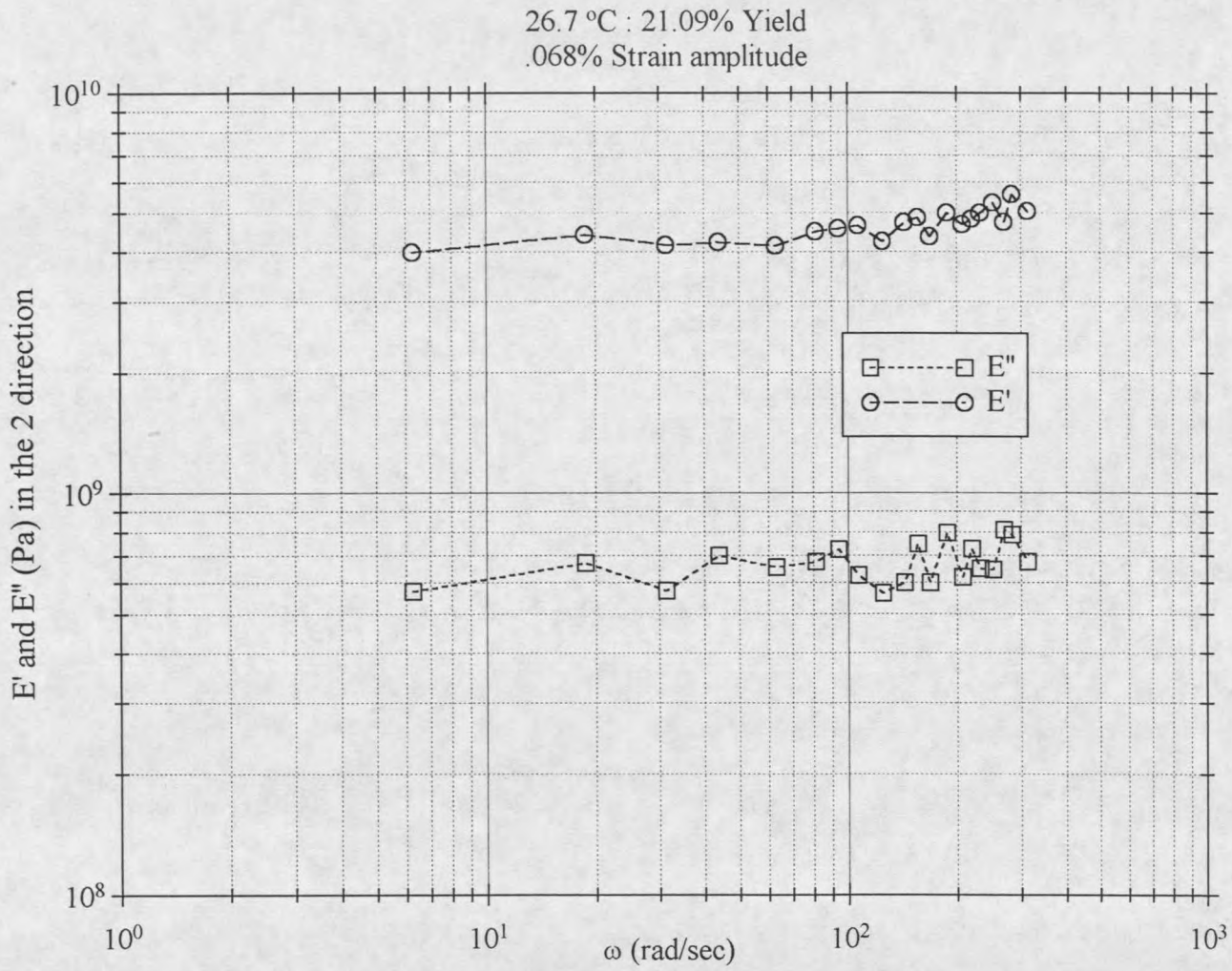


Figure B-1. Two of the complex function in the 2 direction for the conditions shown.

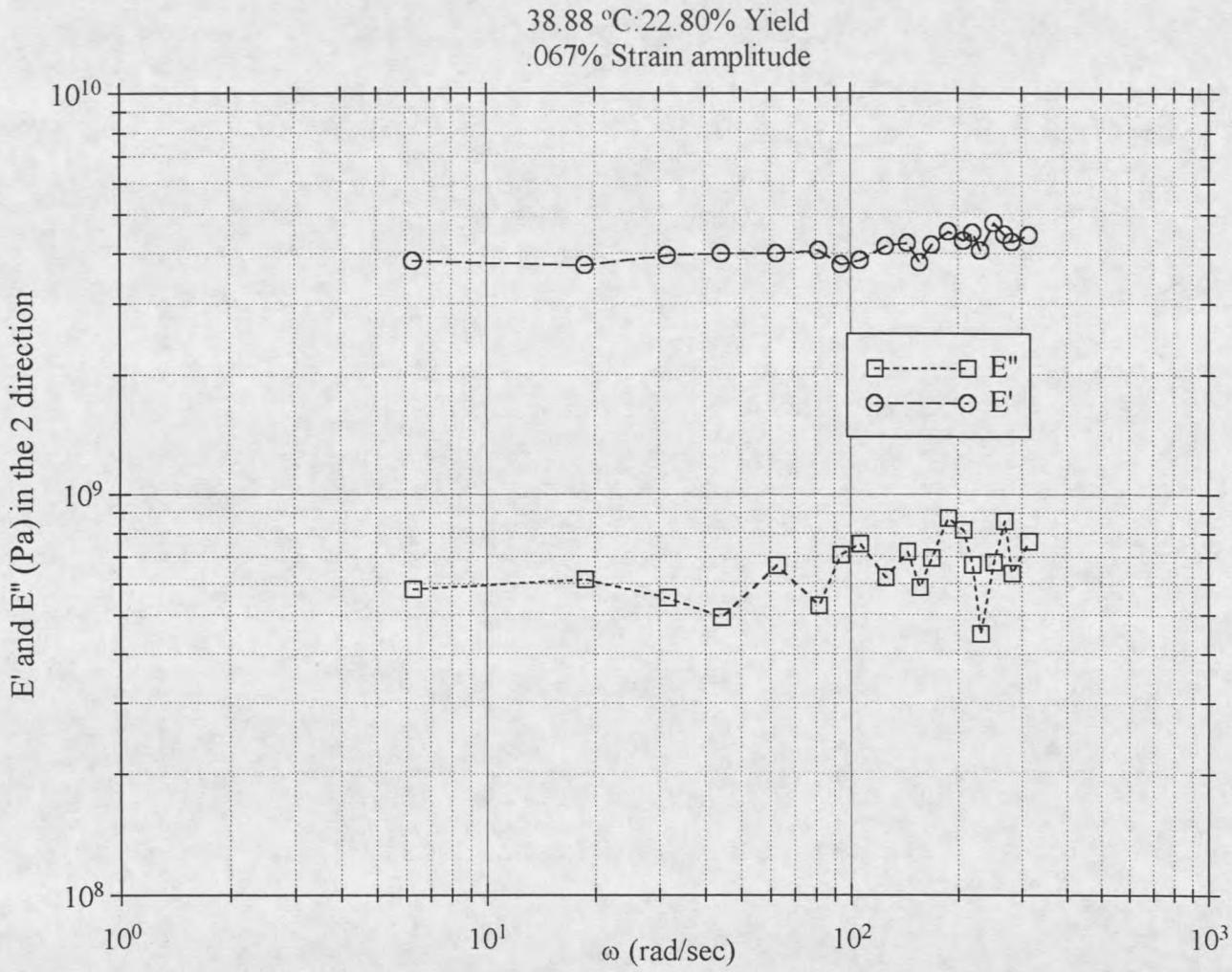


Figure B-2. Two of the complex function in the 2 direction for the conditions shown.

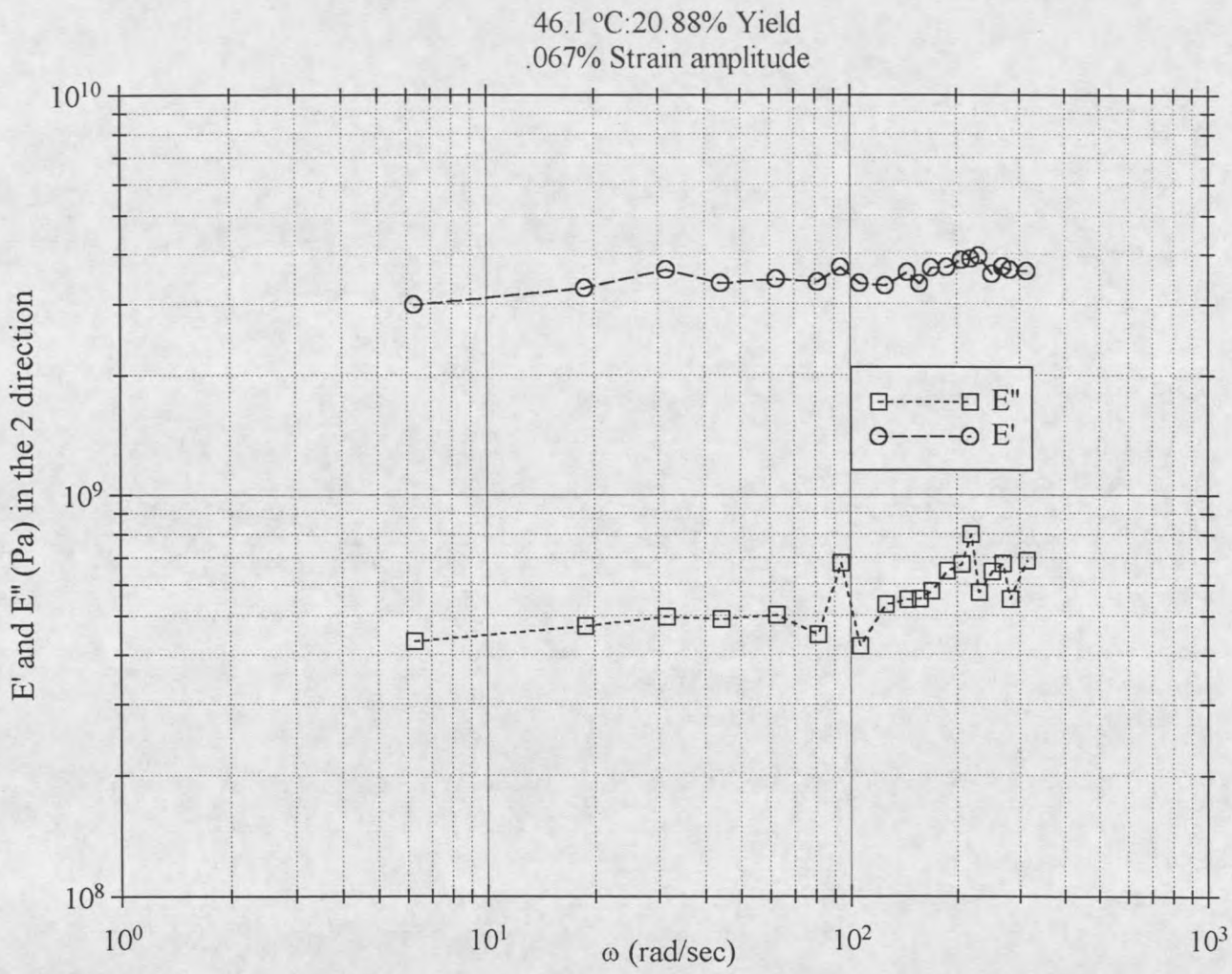


Figure B-3. Two of the complex function in the 2 direction for the conditions shown.

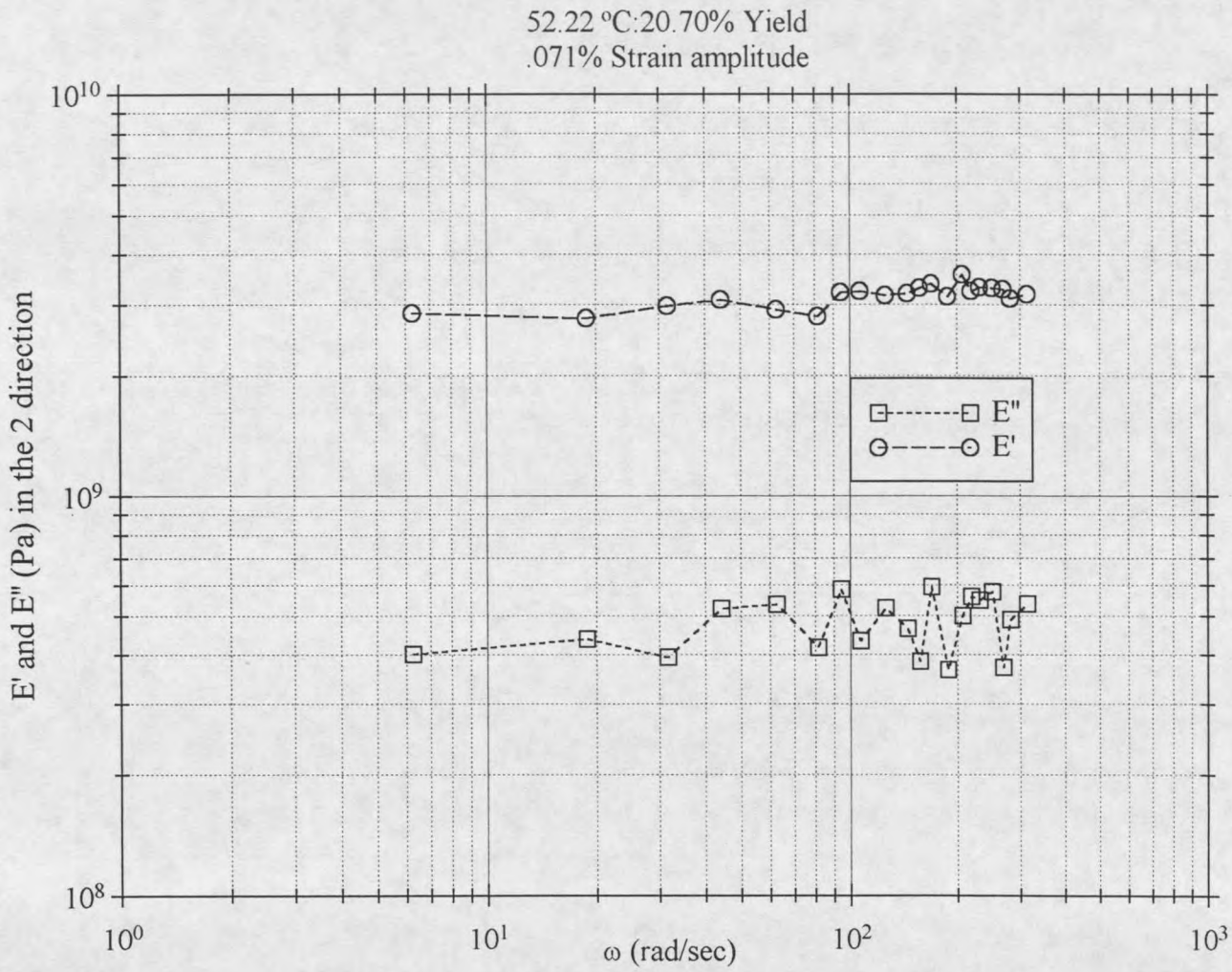


Figure B-4. Two of the complex function in the 2 direction for the conditions shown.

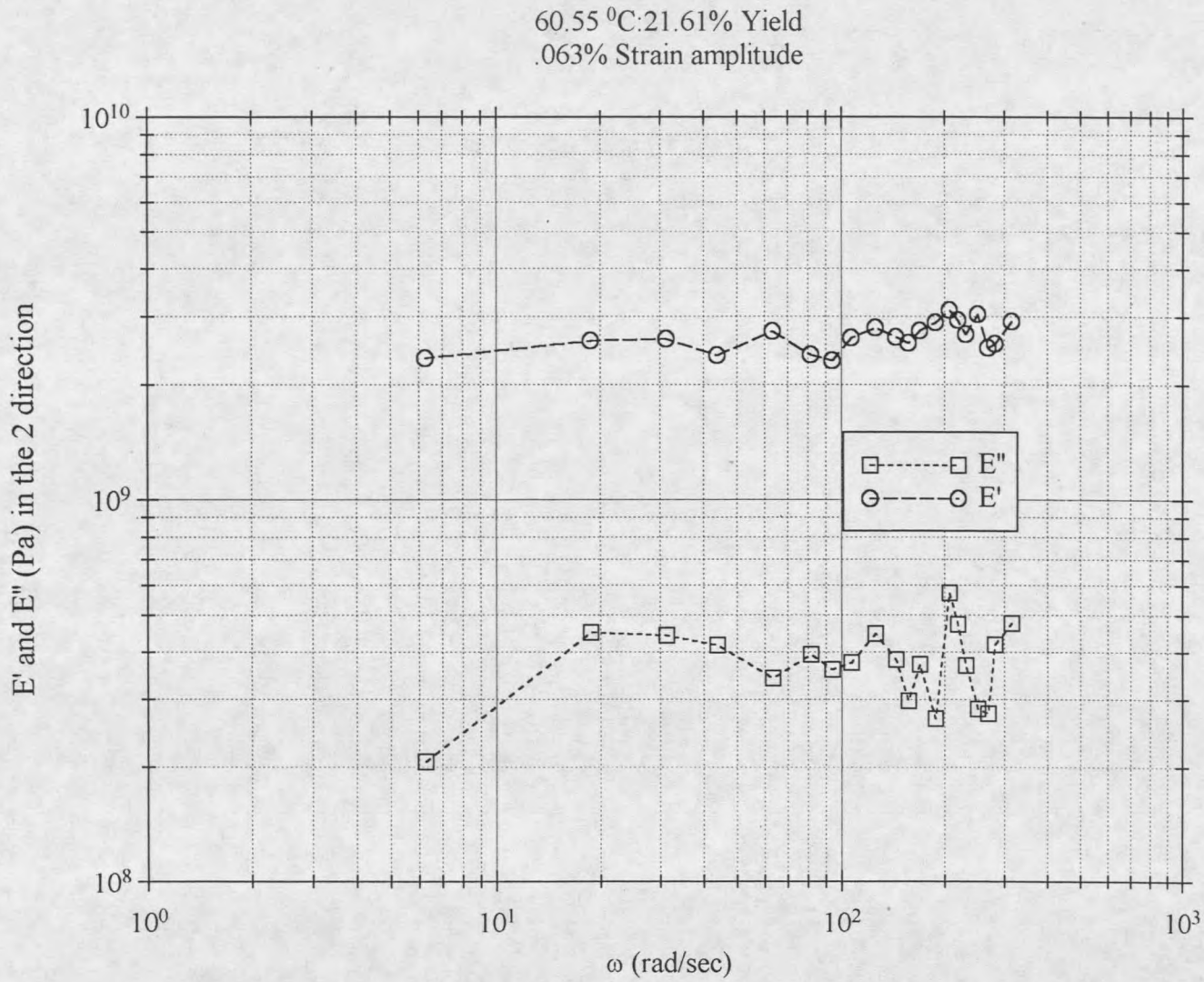


Figure B-5. Two of the complex function in the 2 direction for the conditions shown.

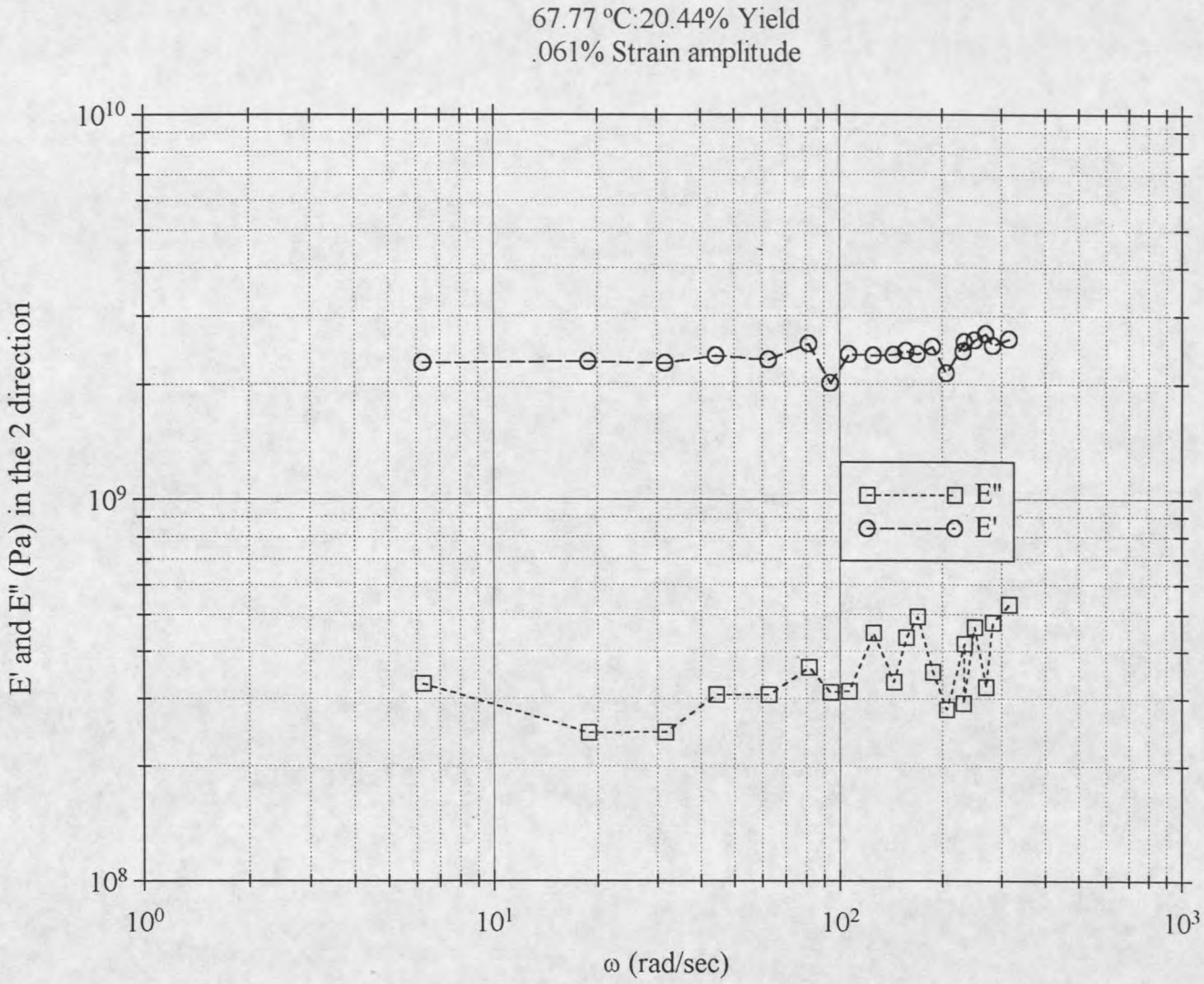


Figure B-6. Two of the complex function in the 2 direction for the conditions shown.

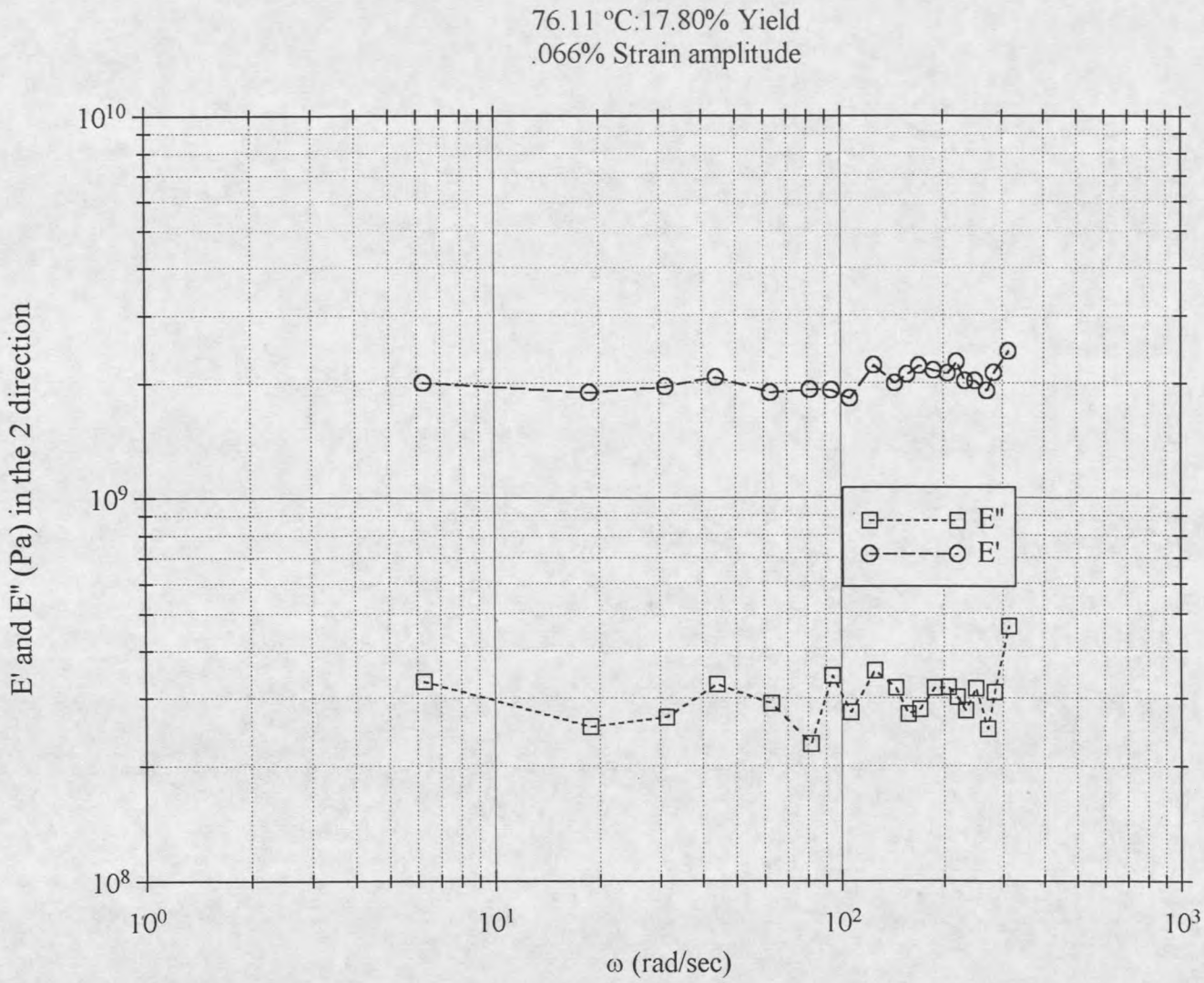


Figure B-7. Two of the complex function in the 2 direction for the conditions shown.

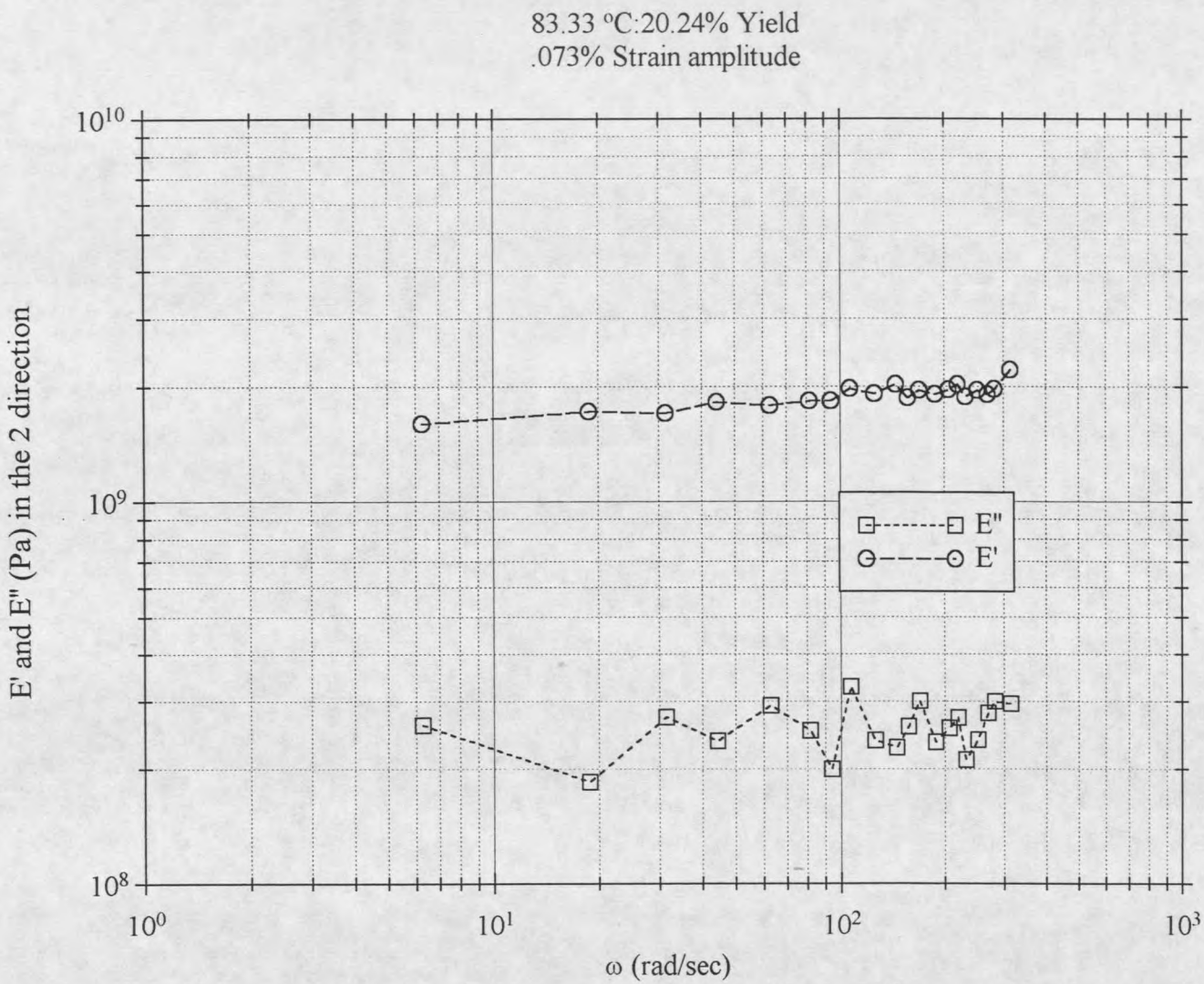


Figure B-8. Two of the complex function in the 2 direction for the conditions shown.

APPENDIX C

CURVE FIT RESULTS

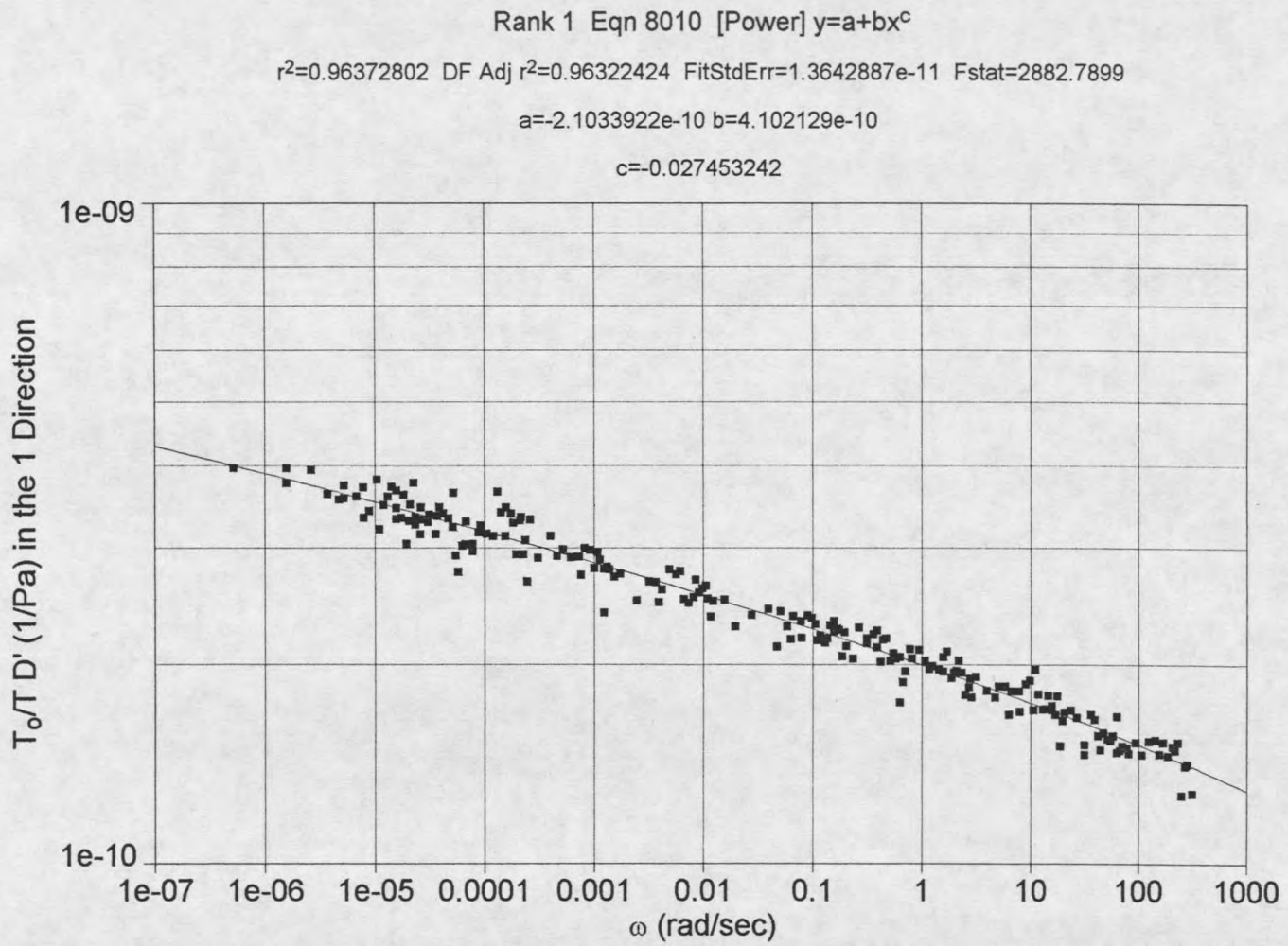


Figure C-1. Master storage compliance curve for material direction 1.

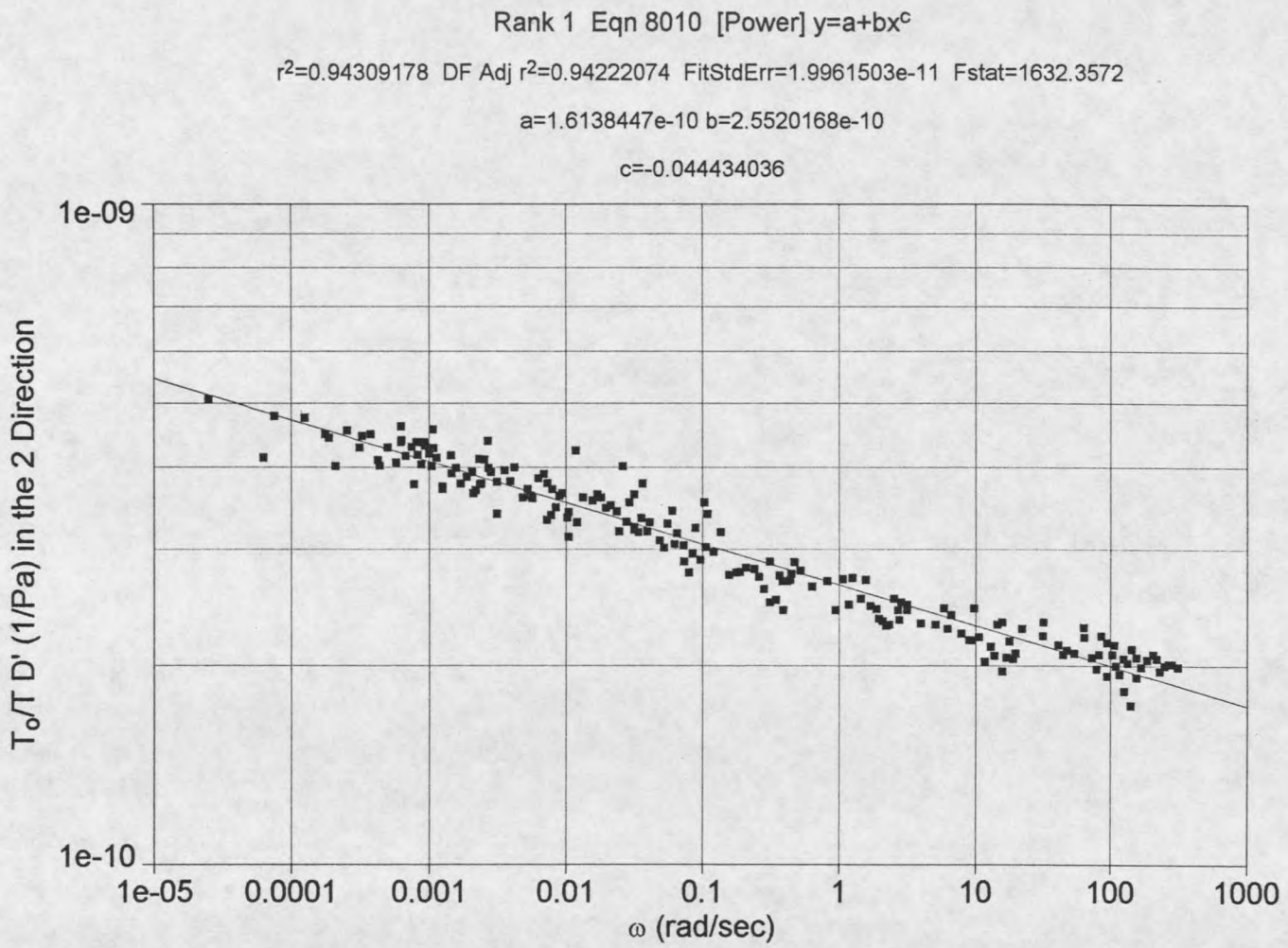


Figure C-2. Master storage compliance curve for material direction 2.

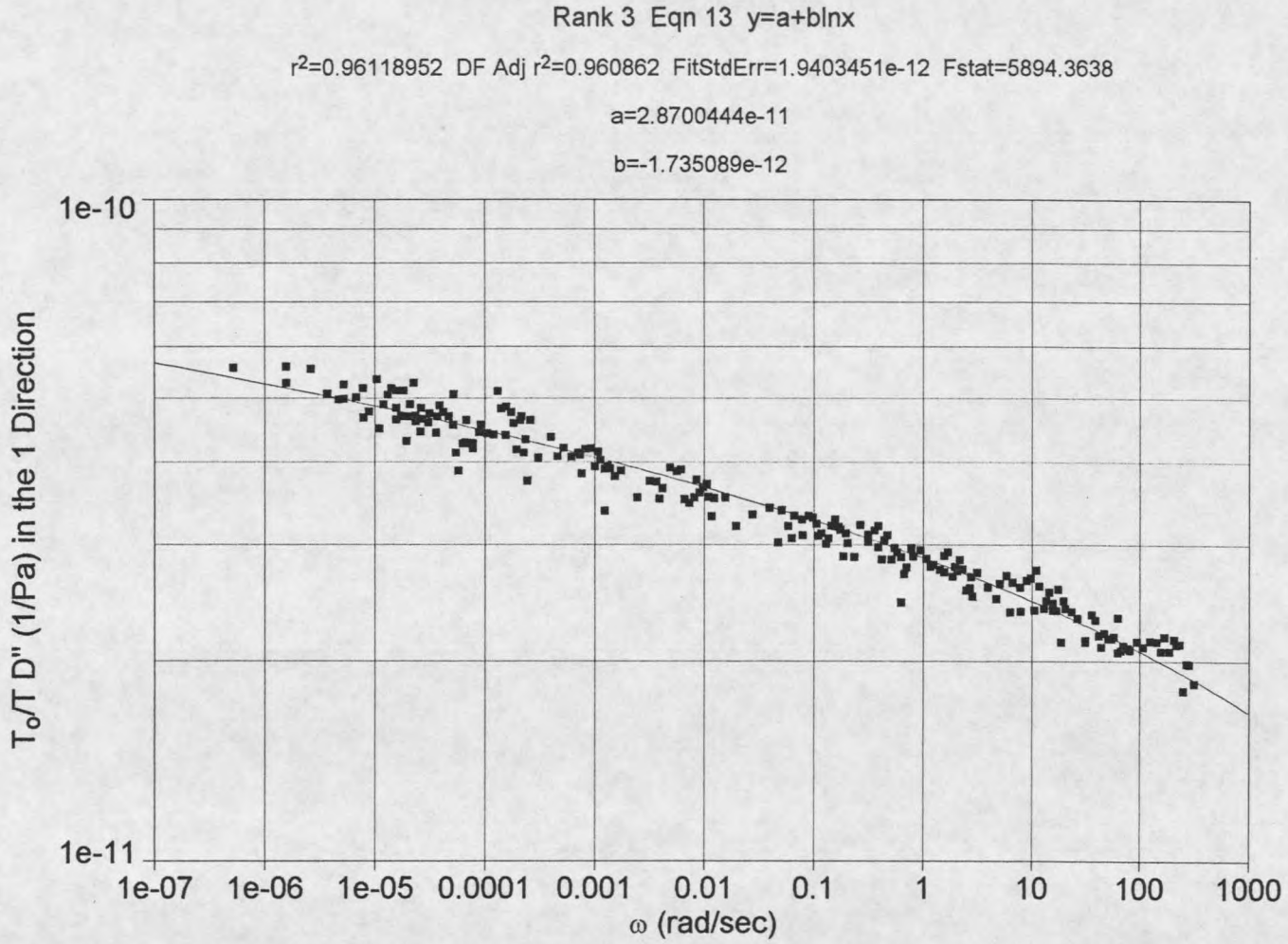


Figure C-3. Master loss compliance curve for material direction 1.

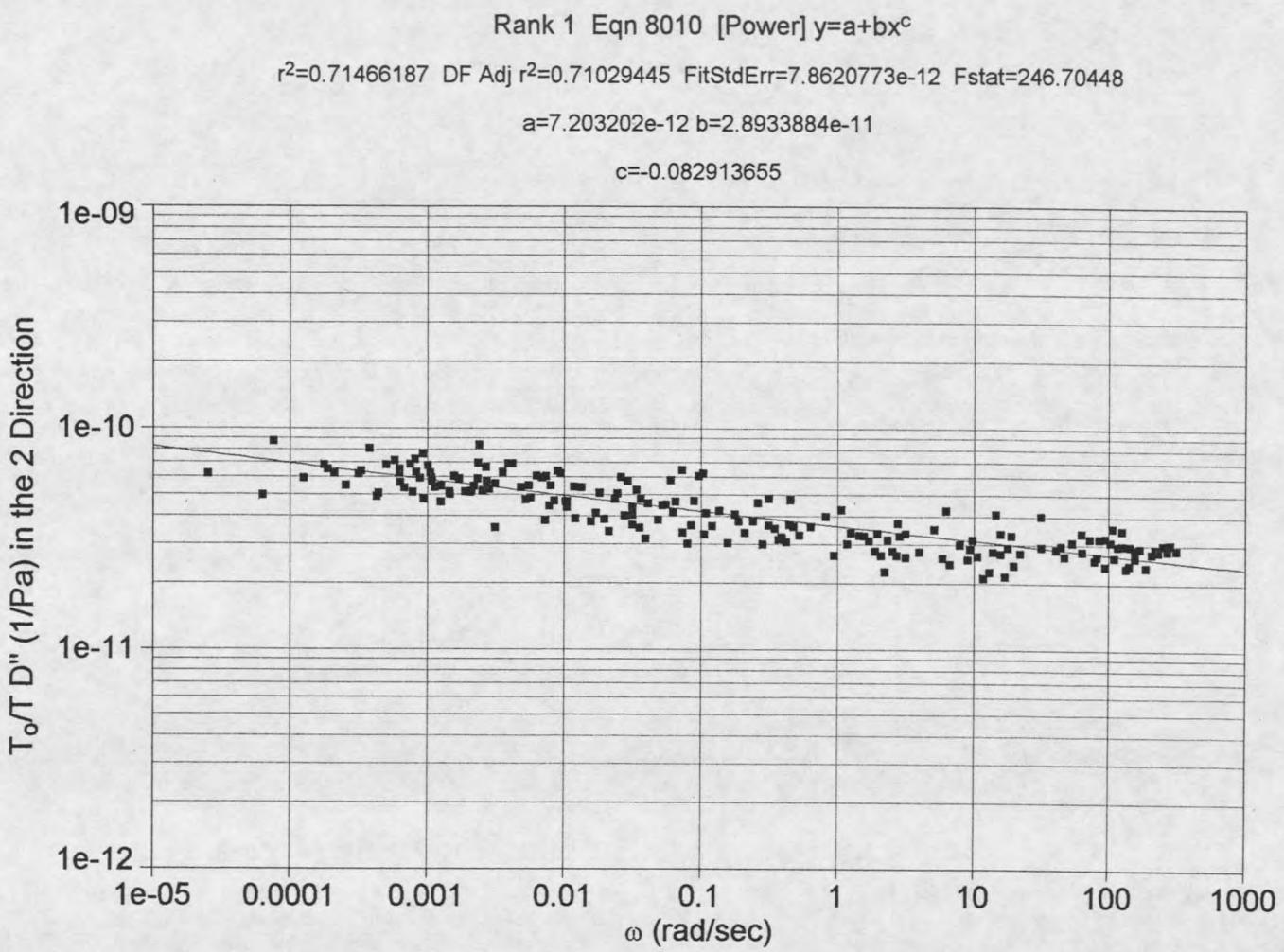


Figure C-4. Master loss compliance curve for material direction 2.

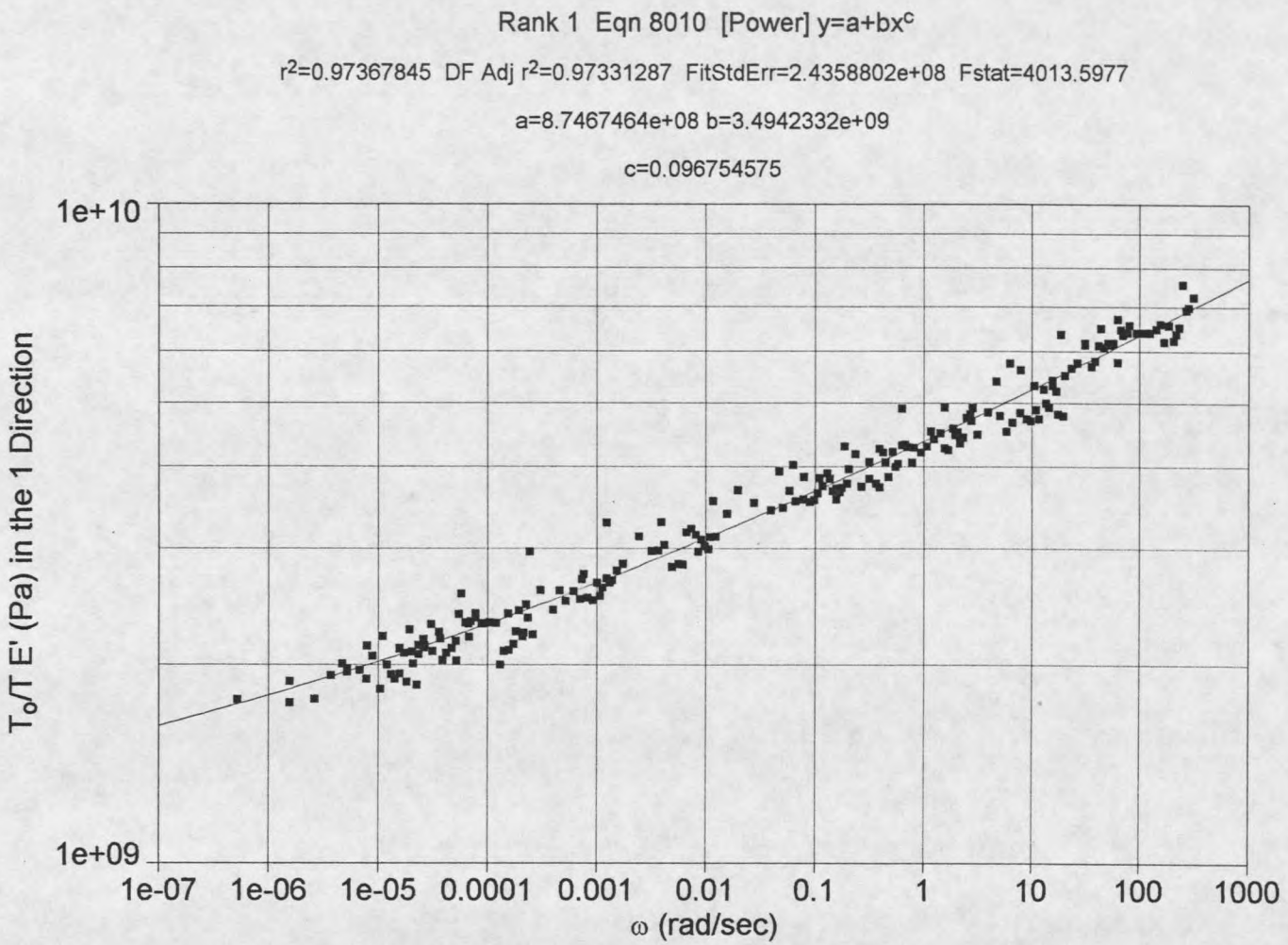


Figure C-5. Master storage modulus curve for material direction 1.

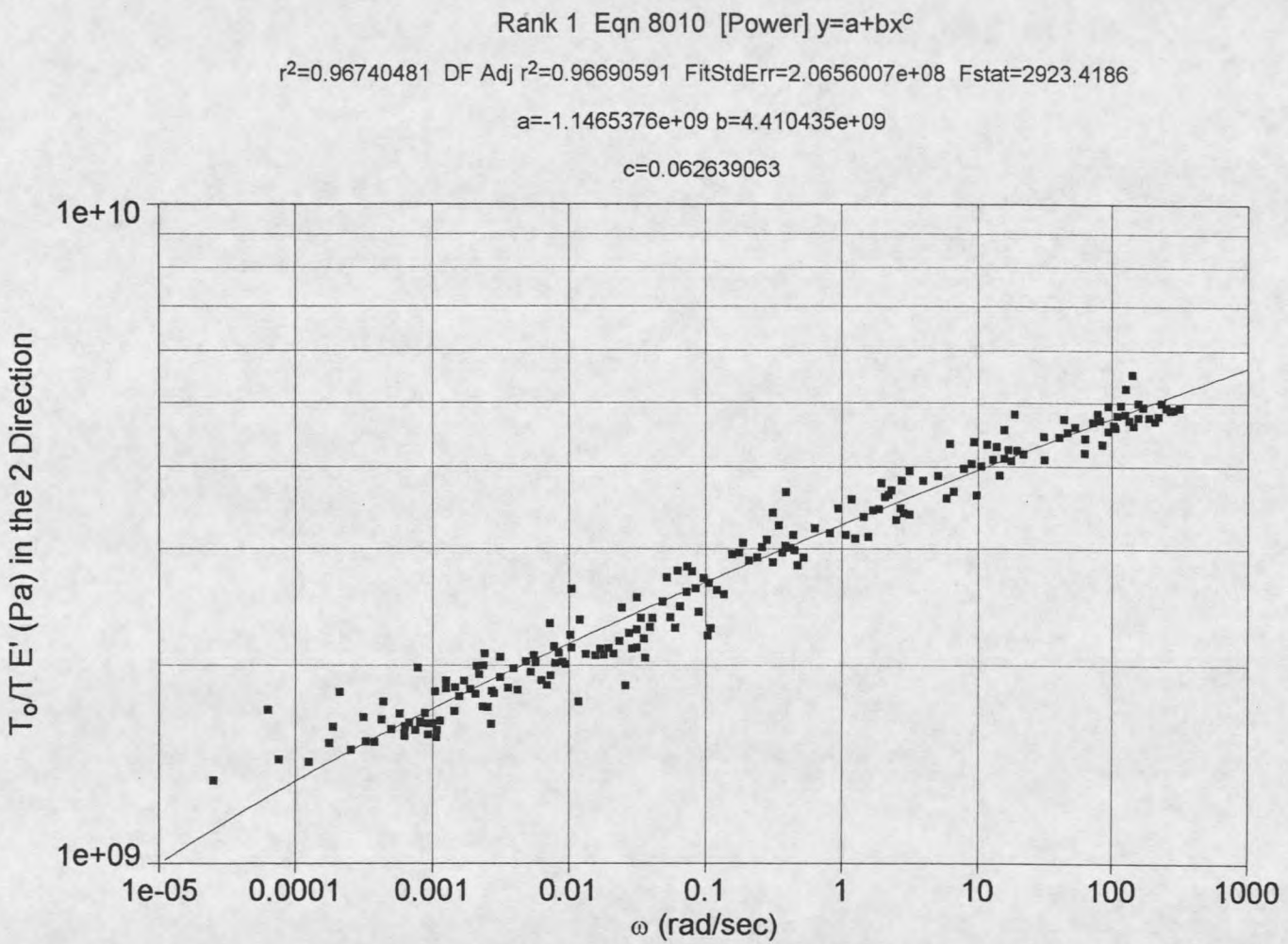


Figure C-6. Master storage modulus curve for material direction 2.

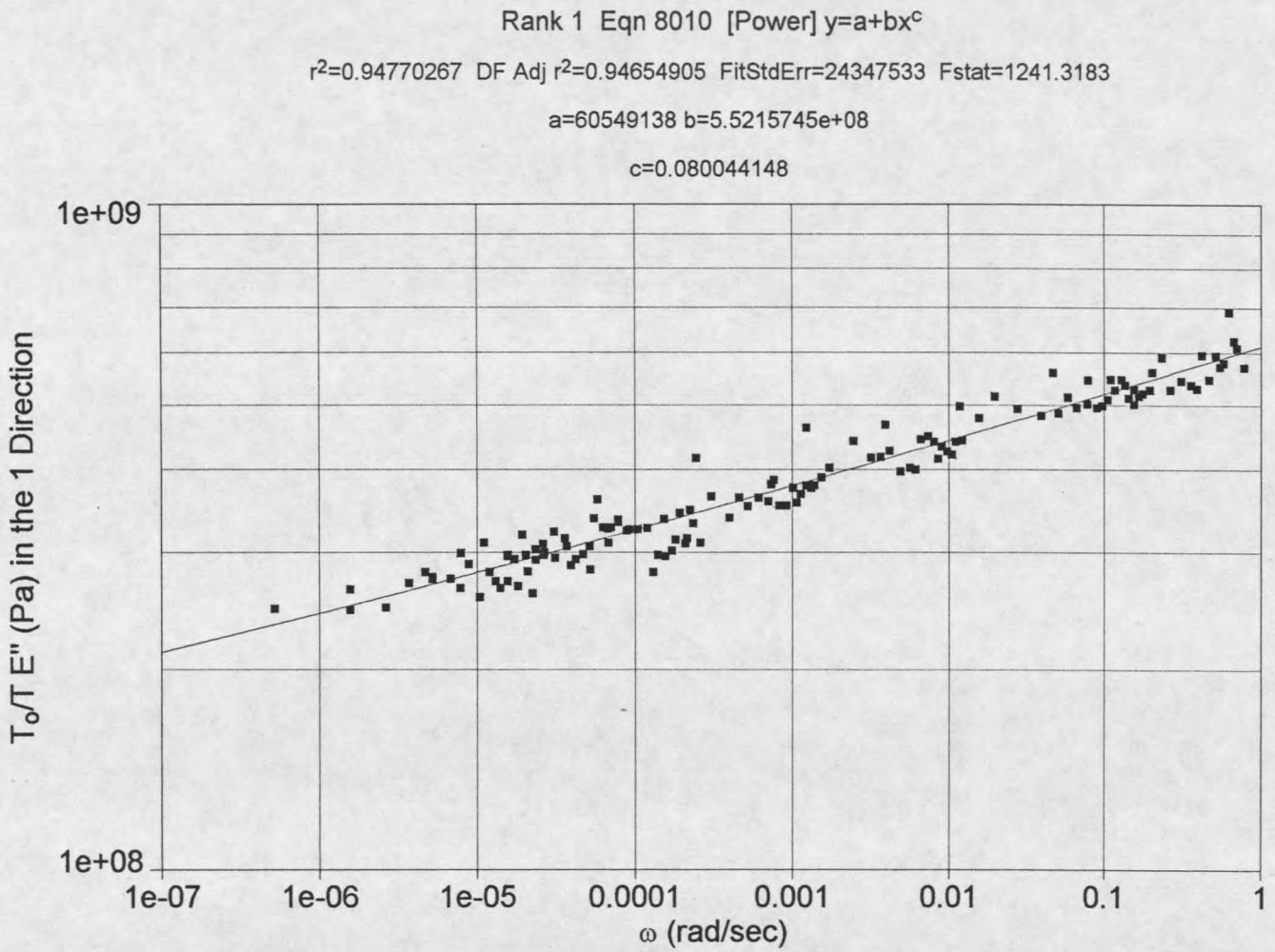


Figure C-7. Master loss modulus curve for material direction 1.

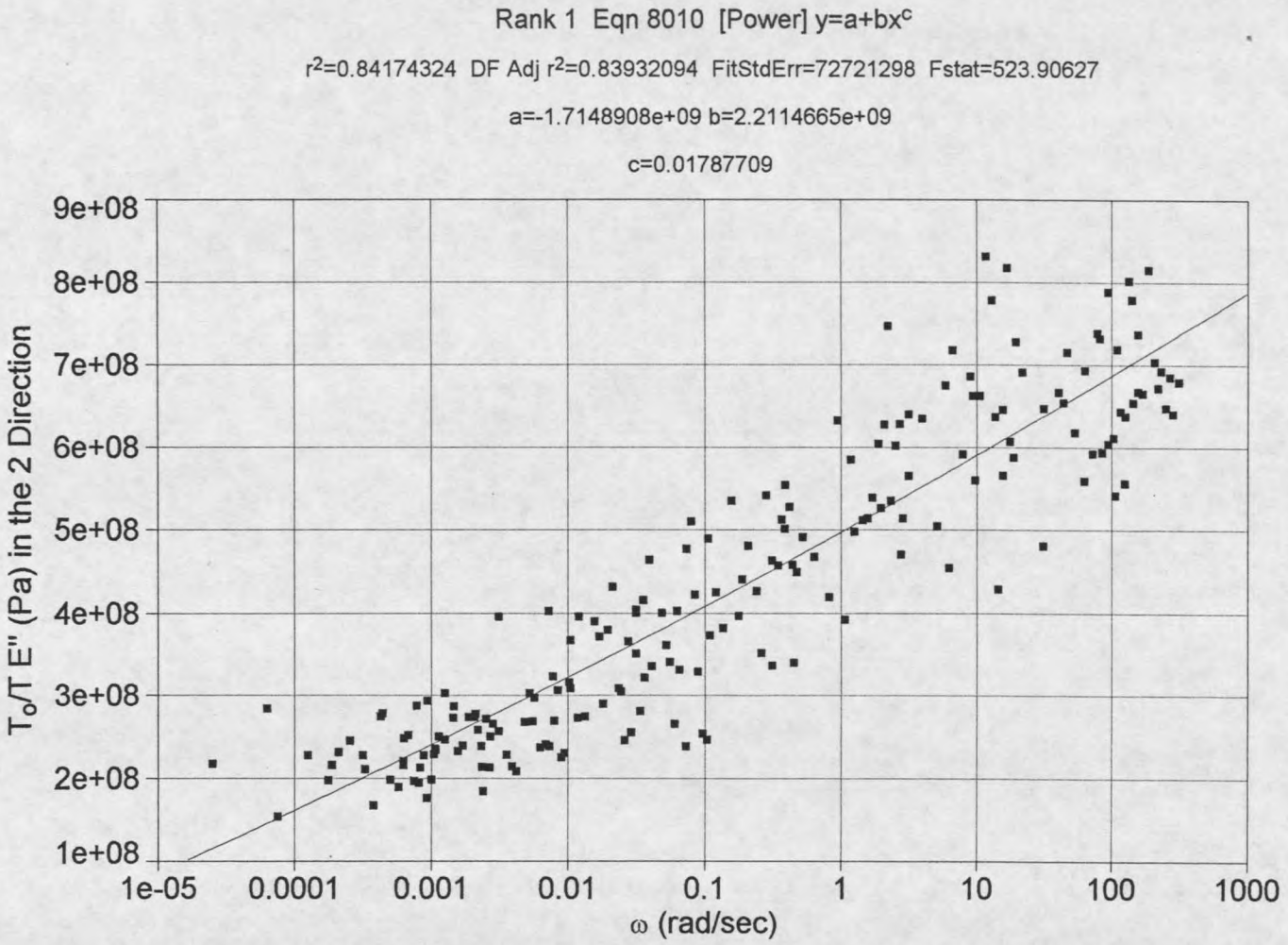


Figure C-8. Master loss modulus curve for material direction 2.

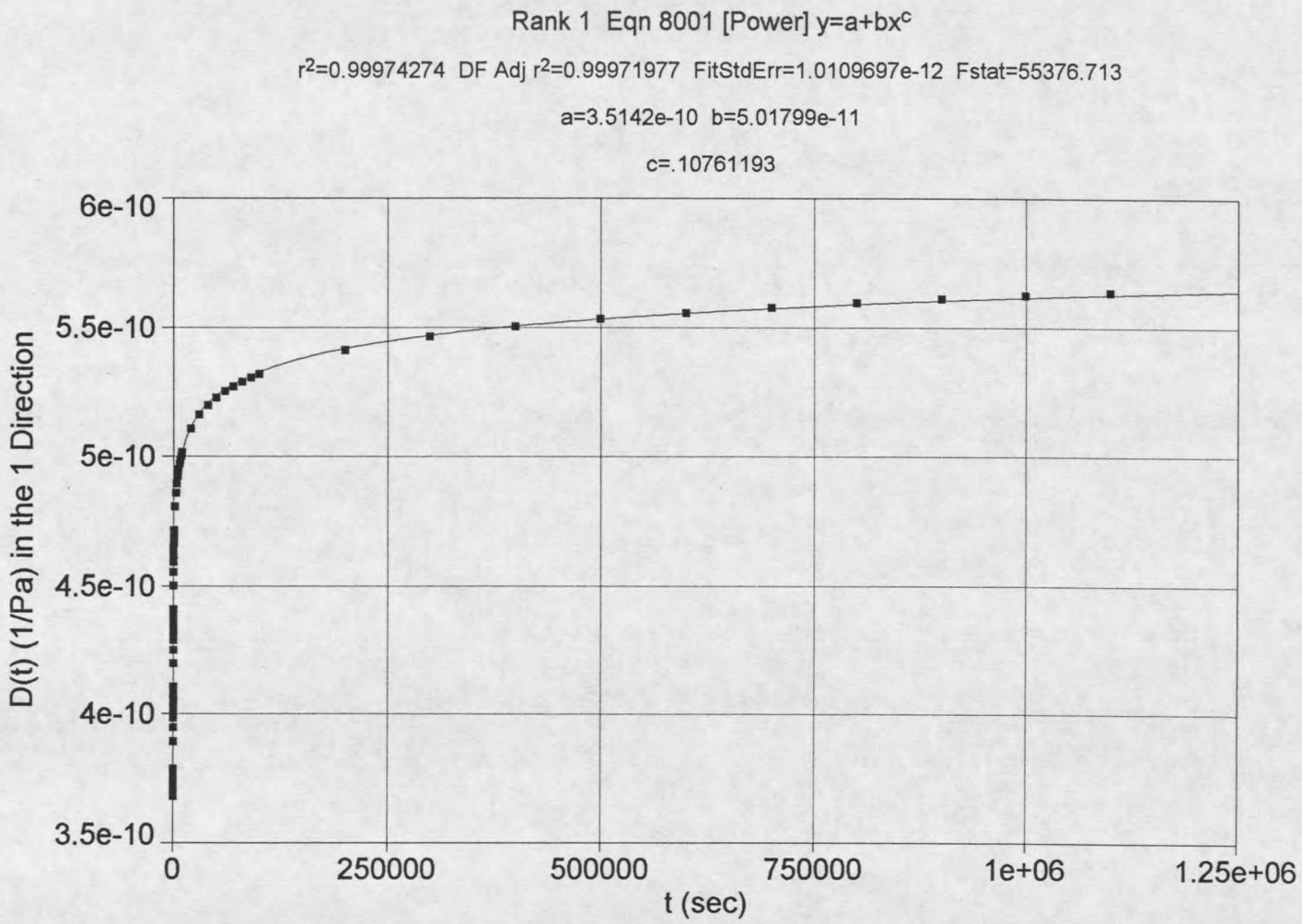


Figure C-9. Creep compliance curve for material direction 1.

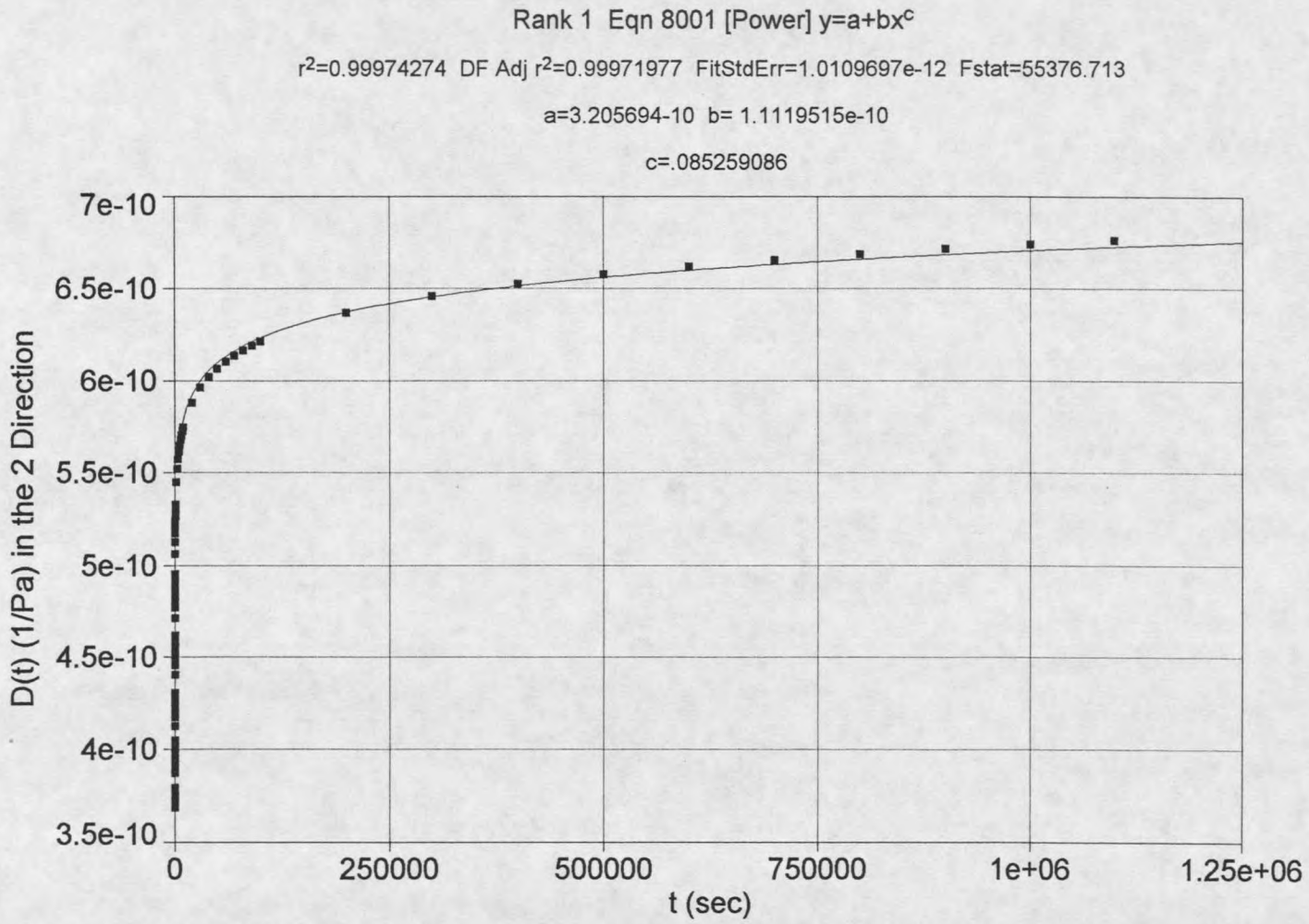


Figure C-10. Creep compliance curve for material direction 2.

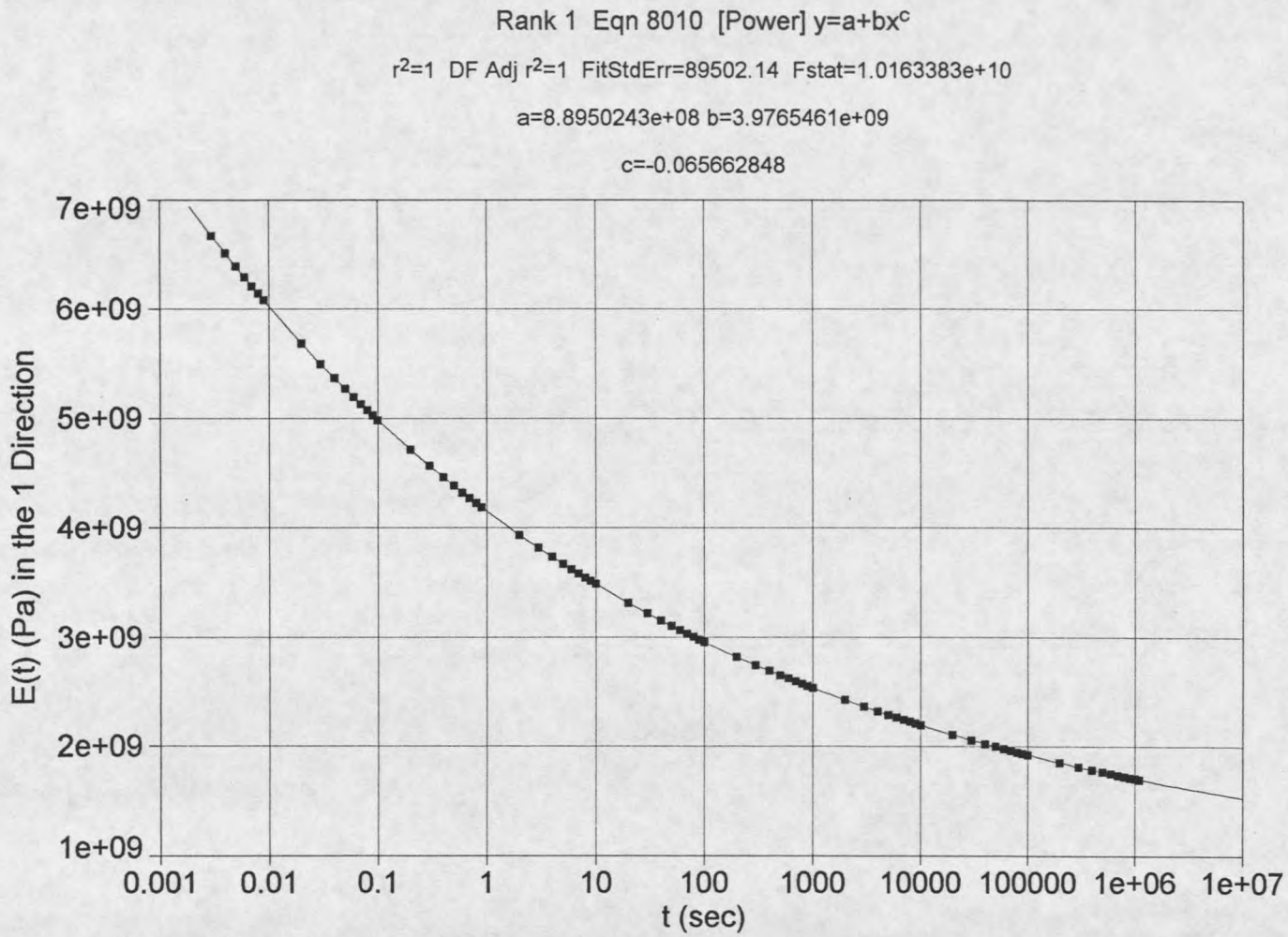


Figure C-11. Relaxation modulus curve for material direction 1.

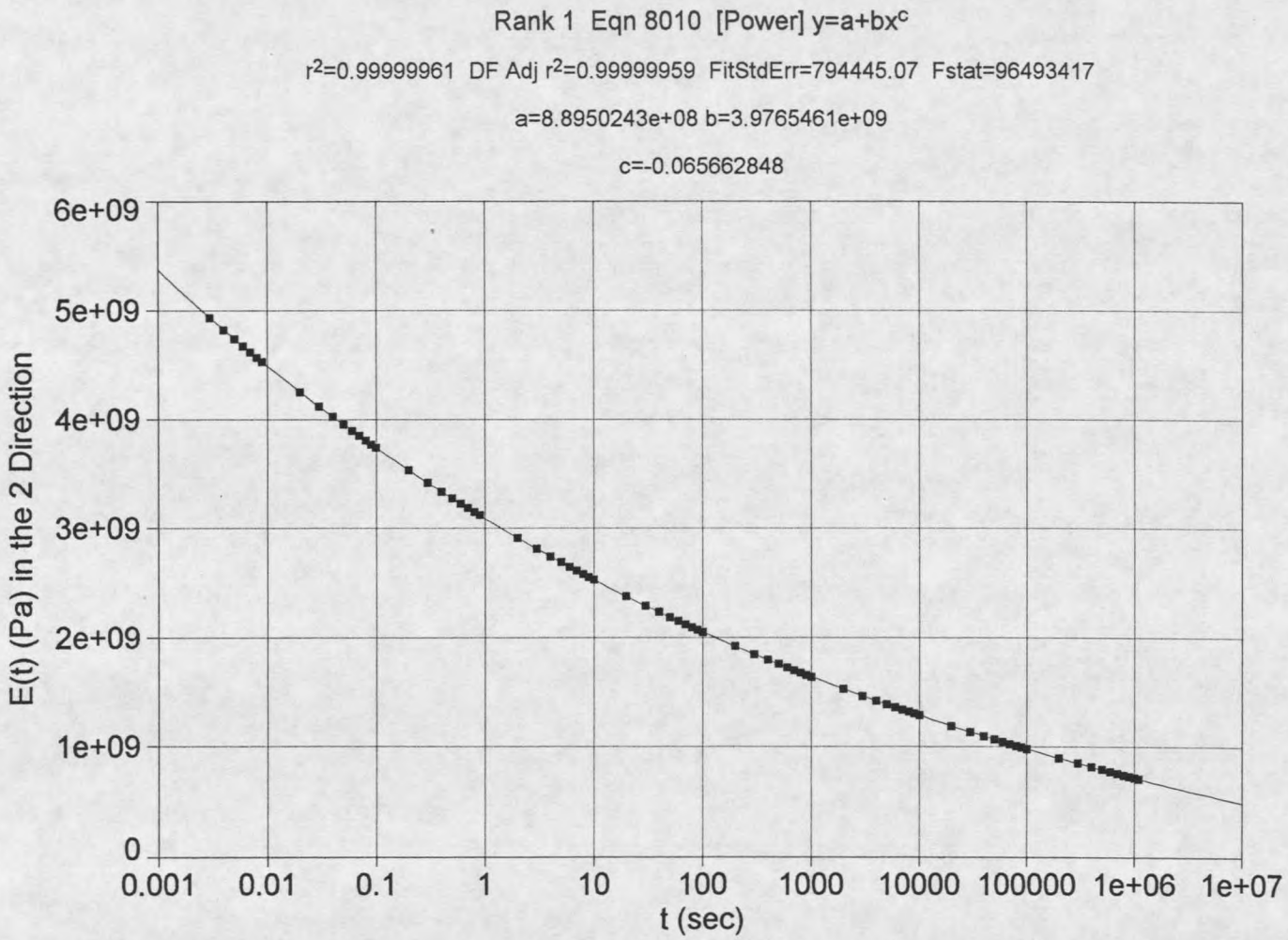


Figure C-12. Relaxation modulus curve for material direction 2.

APPENDIX D

REPRESENTATIVE SET OF PRODUCED VOLTAGE PLOTS

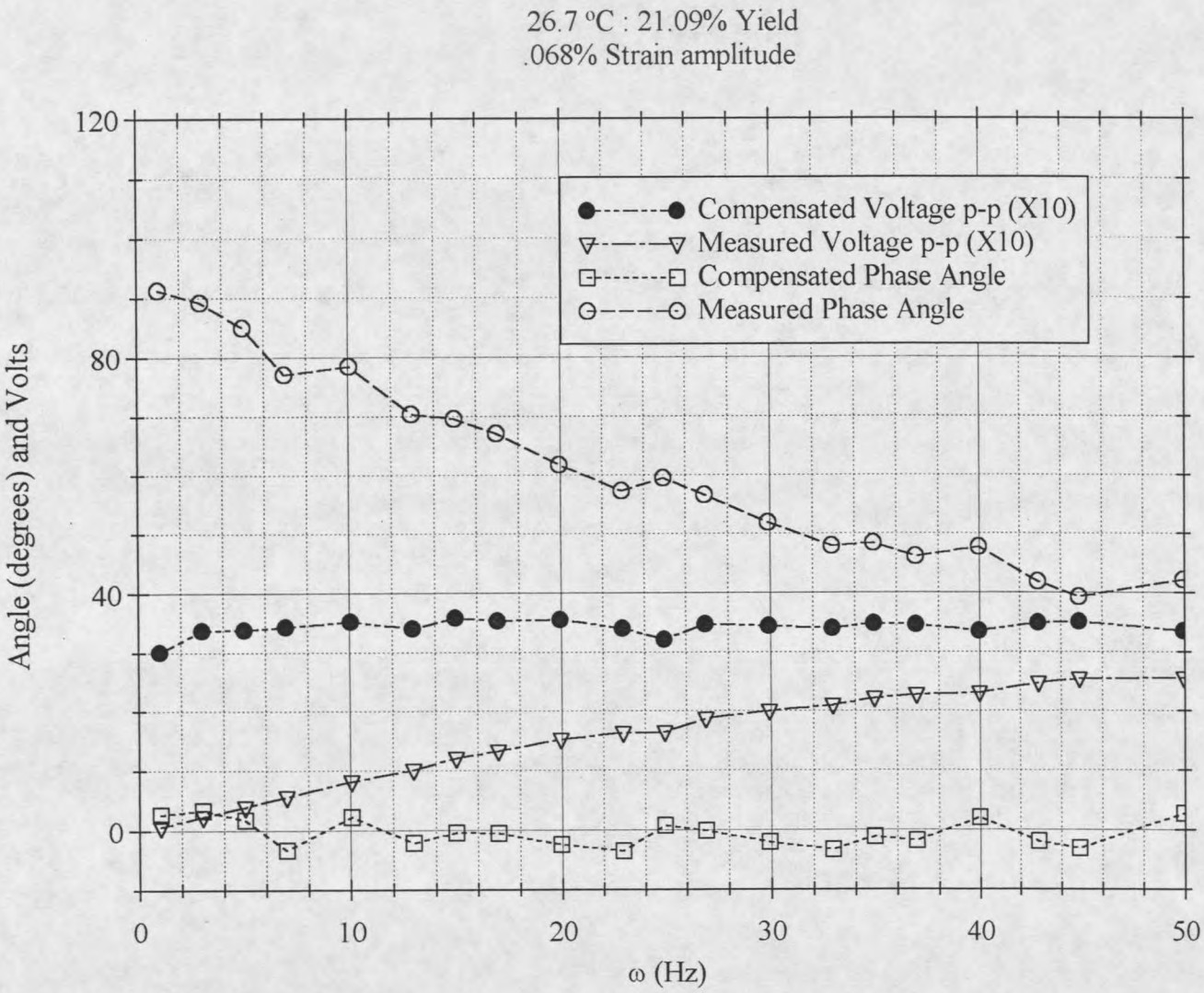


Figure D-1. Produced voltage during DMTA testing in the 2 direction for the conditions shown.

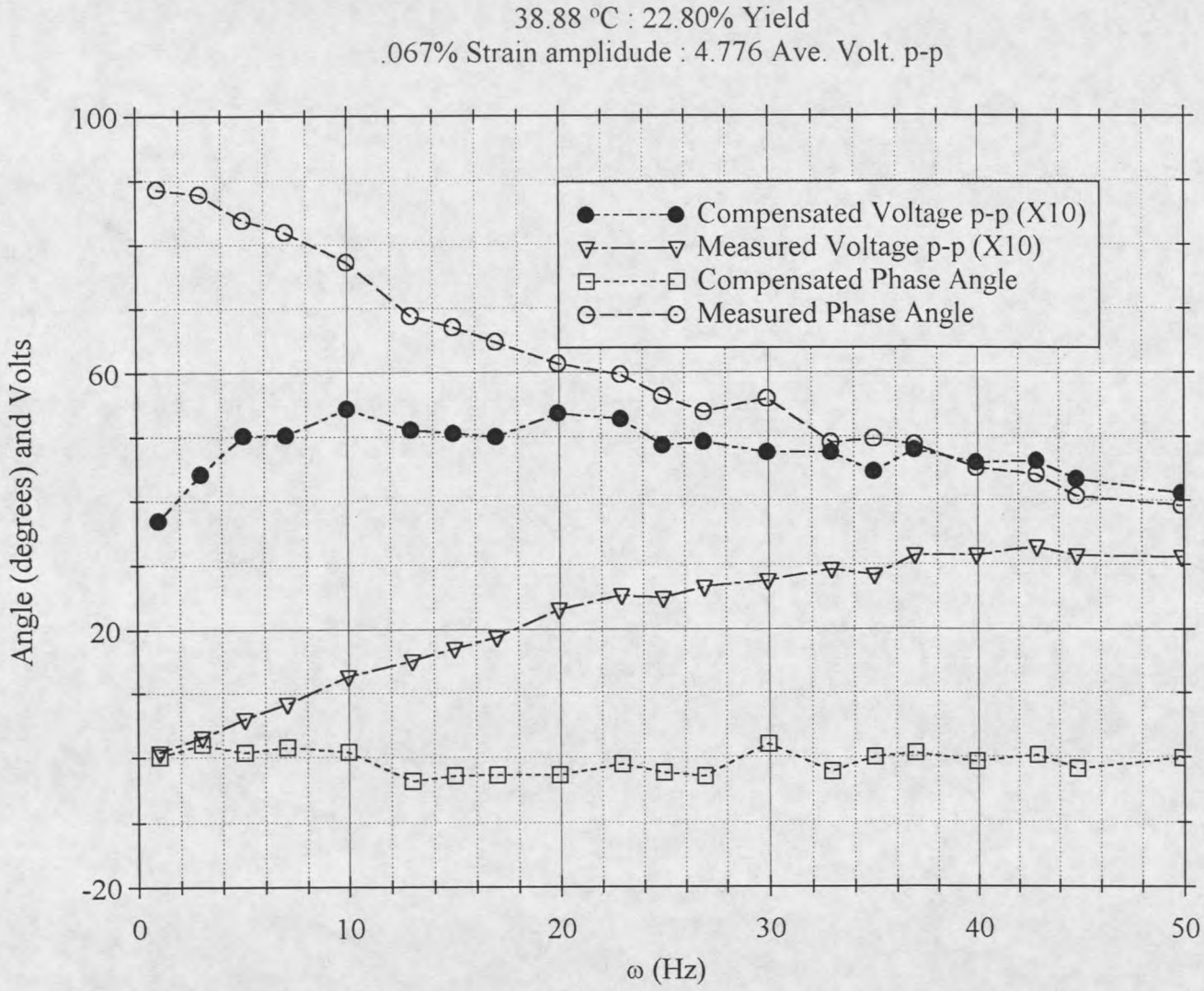


Figure D-2. Produced voltage during DMTA testing in the 2 direction for the conditions shown.

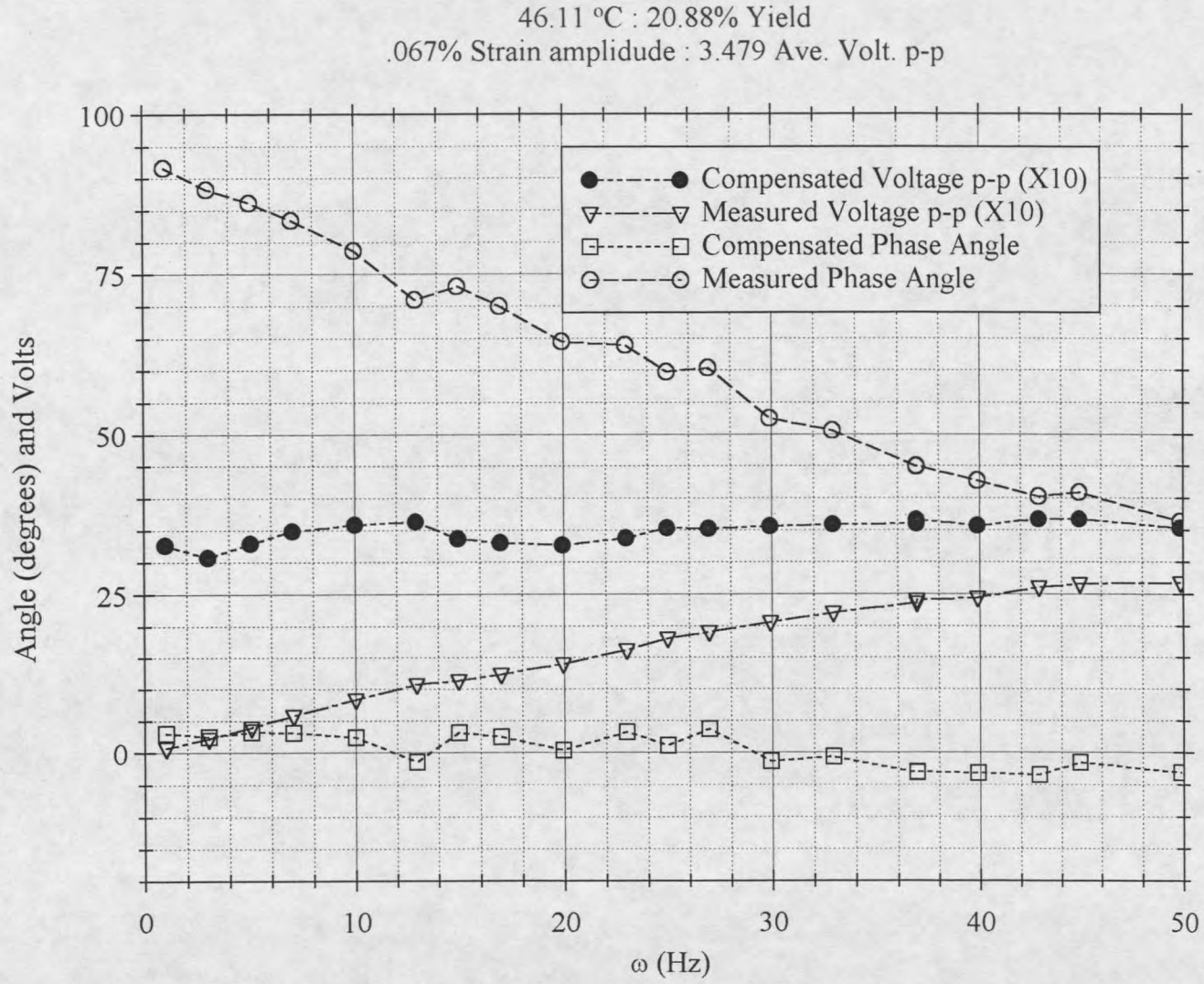


Figure D-3. Produced voltage during DMTA testing in the 2 direction for the conditions shown.

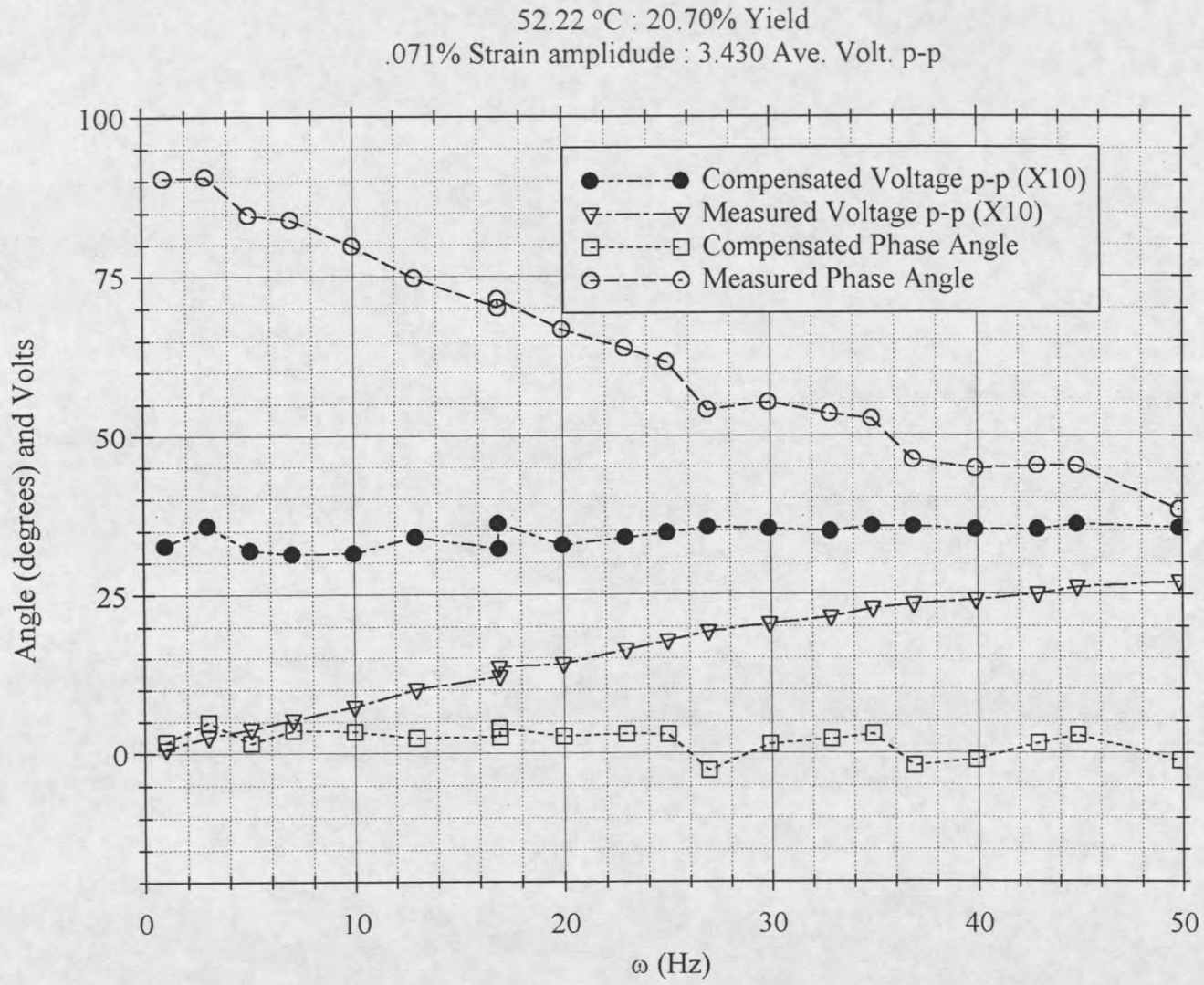


Figure D-4. Produced voltage during DMTA testing in the 2 direction for the conditions shown.

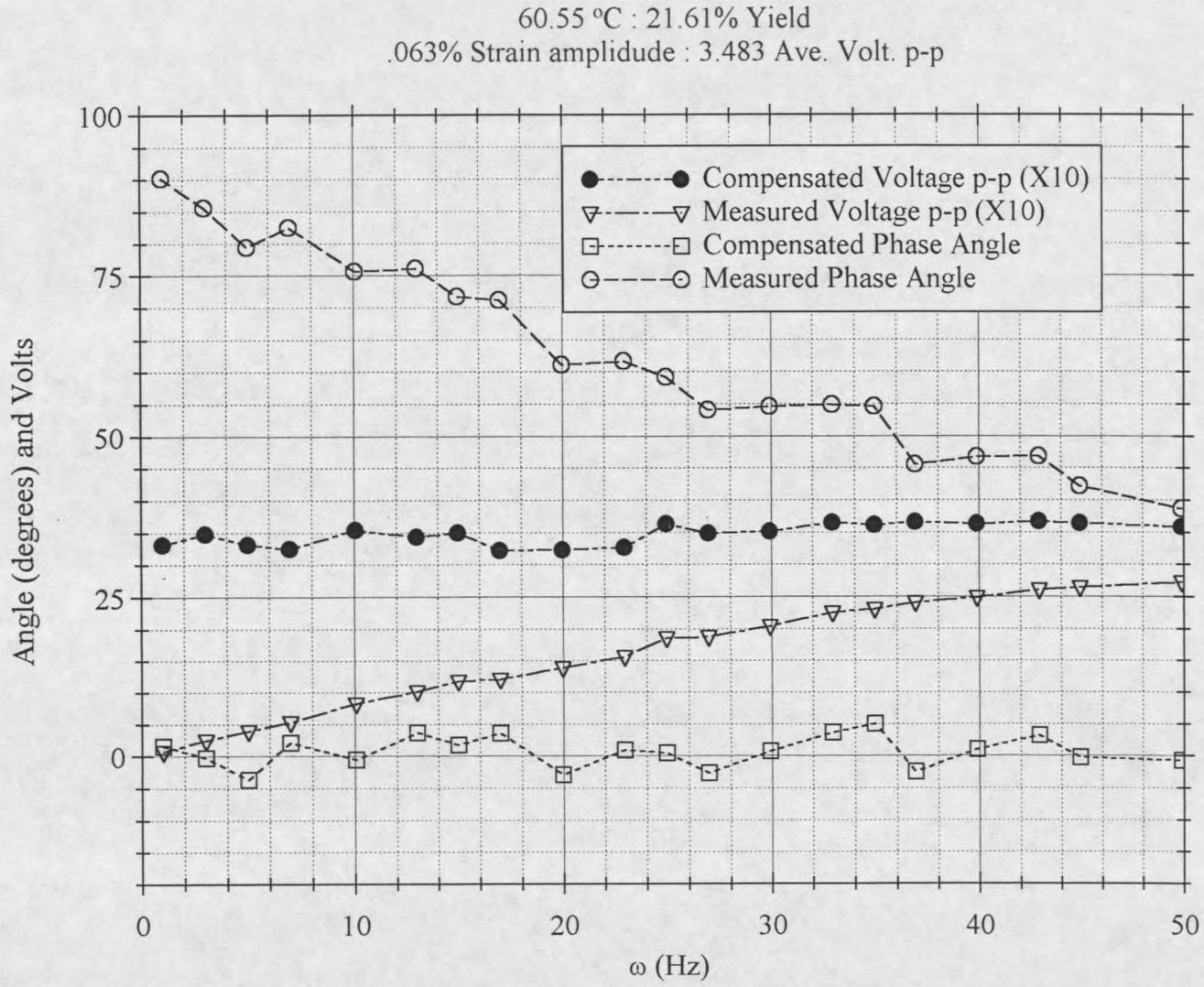


Figure D-5. Produced voltage during DMTA testing in the 2 direction for the conditions shown.

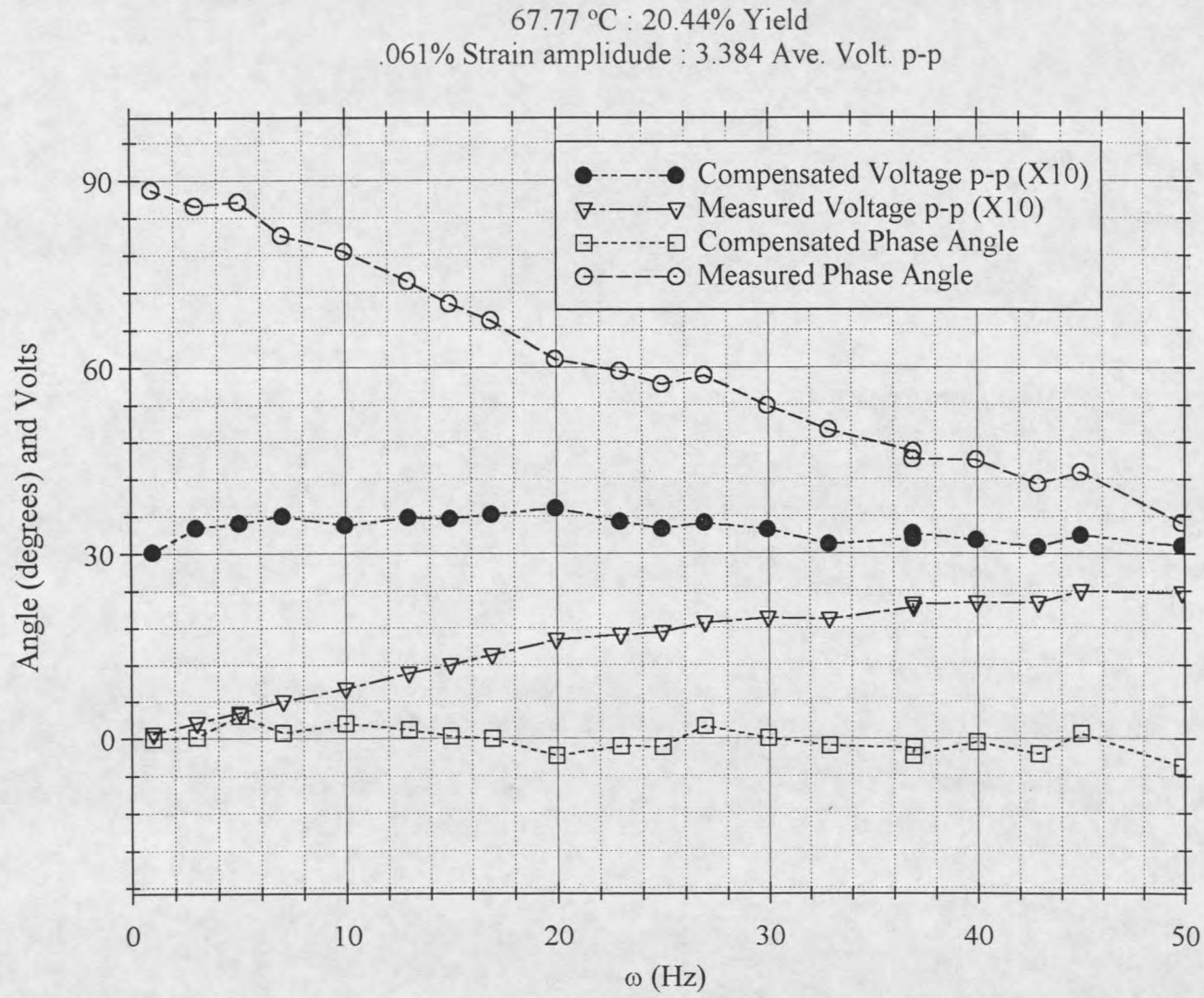


Figure D-6. Produced voltage during DMTA testing in the 2 direction for the conditions shown.

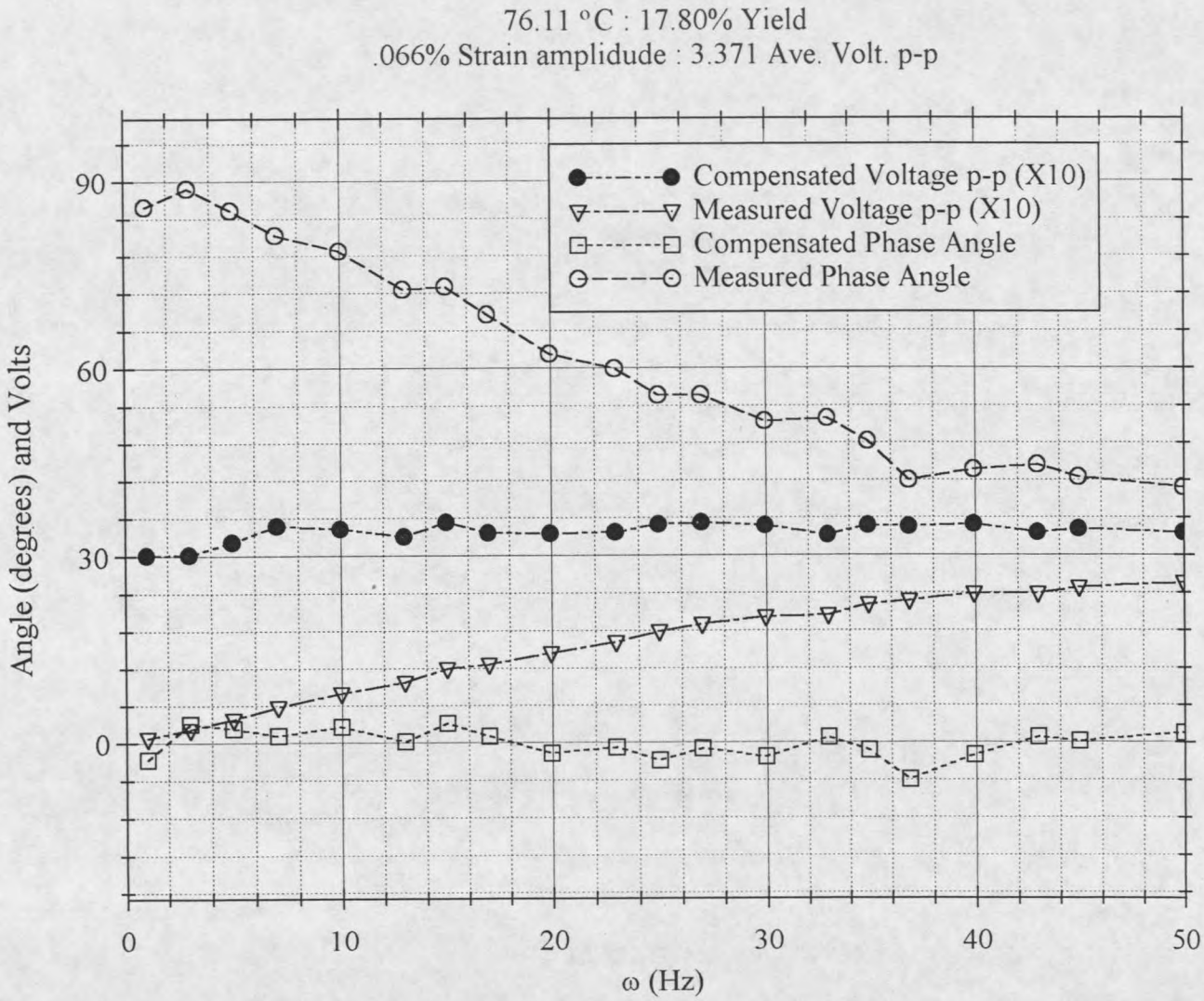


Figure D-7. Produced voltage during DMTA testing in the 2 direction for the conditions shown.

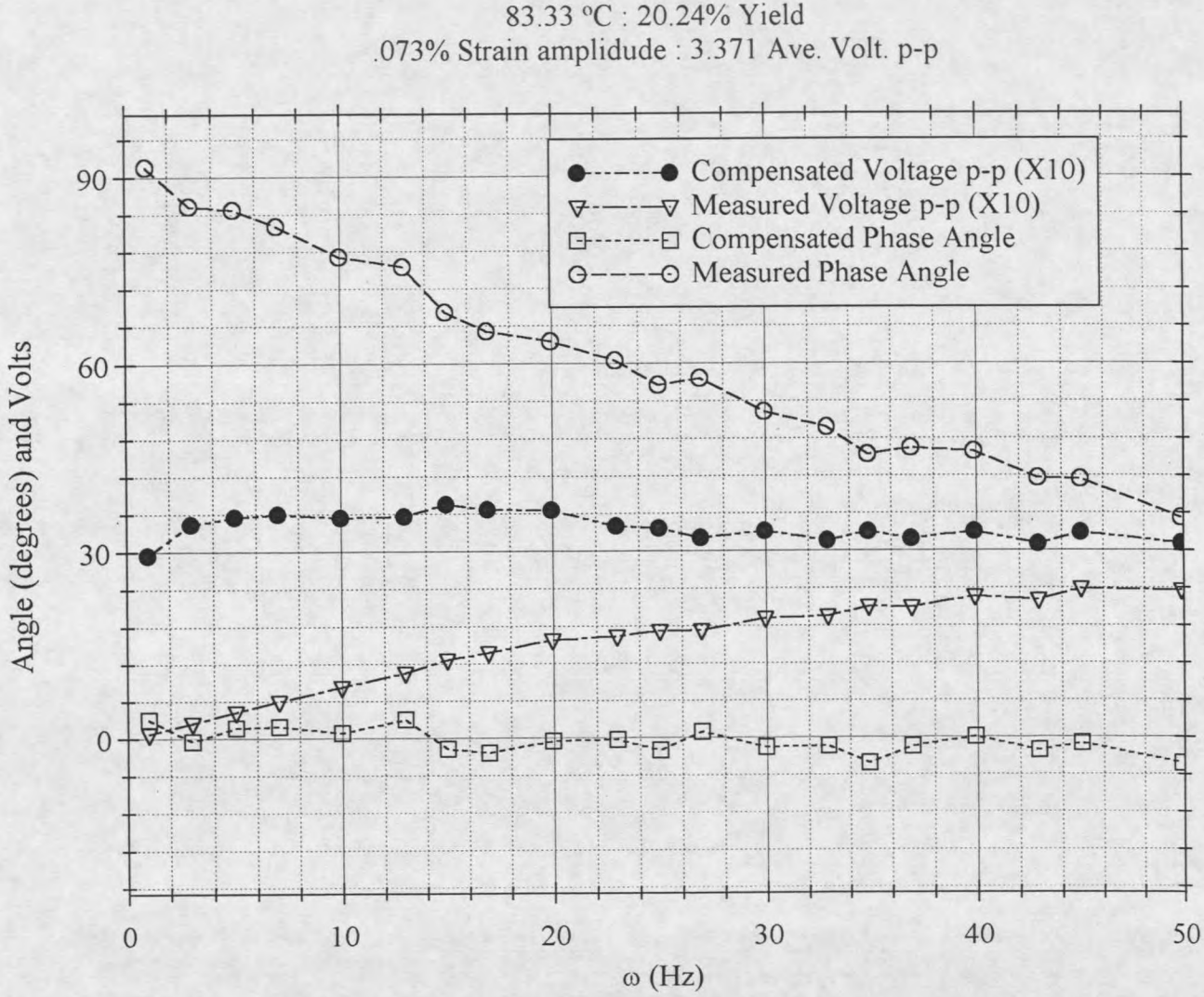


Figure D-8. Produced voltage during DMTA testing in the 2 direction for the conditions shown.

MONTANA STATE UNIVERSITY LIBRARIES
3 1762 10237064 8